CONTENT

CONTENT

AGRICULTURAL PLASTER FROM RESIDUAL OF INDUSTRIAL AND MINING PROCESSES, A CHEAP AND ECOLOGICAL CORRECT POSSIBILITY. EXAMPLE FROM MINAS GERAIS, BRAZIL.

Alexandre Sylvio COSTA[1], Adolf Heinrich HORN[2*]

[1] Federal University of Valleys of Jequitinhonha and Mucuri. Mucuri Campus, Rua Cruzeiro, Jardim São Paulo, Cep 39803371 - Teófilo Otoni, MG, Brazil. Phone: +55(33) 35226037; alexandre.costa@ufvjm.edu.br

[2] Federal University of Minas Gerais. Institute of Geosciences, Research Center Prof. Manoel Teixeira da Costa. Avenida Antônio Carlos, 6627. Pampulha. Cep 31270901 - Belo Horizonte, MG, Brasil; hahorn@ufmg.br

* corresponding author

Abstract: Industrial and mining processes produce a wide spectra of residual which are harm- or stressful or for the environment. At Minas Gerais, these materials are widely produced in metal mining and processing, cellulose production and in the recovering of industrial waste like batteries, etc. On the other hand, agricultural plaster produced from these materials is a very important material for the correction of soil and the enhancement of plant growing. Tropical and subtropical sols are often rich in Fe, Al, Si and salts due to environmental conditions and irrigation management. This work aimed to evaluate the production and the action of Ecogypsum® produced from the chemical reaction of hydrolyzed and recycled sulfuric acid from different industrial sources with mining calcitic limestone or industrial $Ca(OH)_2$, in reducing these damages in the salty soil and in the development of corn plants. For the tests, soil samples with added NaCl solution were treated with the Ecogypsum® and the plant weight production compared with the poor salty or not salted soil samples. The results indicate that the presence of Ecogypsum® in the soil increased the germination of corn seeds in the presence of higher concentrations of NaCl and enhanced the forming sodium sulfate, reducing the possibility of sodium absorption by the seeds and roots. Corn plants responded positively to the presence of Ecogypsum® in the neutralization of sodium in the soil. This methodology is cheap and easy to applicate on typical soils from tropical to subtropical environments to enhance of agricultural production in.

Keywords: Mining waste, industrial waste, soil conditioner, Ecogypsum®, plant development, salinization

Introduction

Industrial and mining processes produce a wide spectrum of reactive or inert residual which may be harm- or stressful for the environment. Especially the Minas Gerais State, one of the center of mining industry of Brazil, produce a big amount of these substances.

The production of contaminated sulfuric acid is one of them together with the big amount of $CaCO_3$, $CaMg(CO_3)_2$ sl or $(CaOH)_2$ in a wide variety of chemical composition and concentration from mining, industry, improvement and recovering processes. At Minas Gerais, these materials are widely produced in metal mining and processing, cellulose production and in the recovering of industrial waste like batteries, etc.

On the other hand, agricultural carbonate and plaster are very important materials for the correction and desalinization of soil and the enhancement of plant growing. Soils from various regions, due to their mineralogical and edaphoclimatic characteristics or due to flaws in irrigation management, have high alkalinity. Considering only salinization as a degradation factor, it is estimated that approximately 7.0% of the entire land surface is salinized. The present work aimed to evaluate the production and the action of Ecogypsum® produced from the chemical reaction of hydrolyzed and recycled sulfuric acid from different industrial sources with mining calcitic limestone or industrial $Ca(OH)_2$, in reducing these damages in the soil and in the development of corn plants. Fig. 1 shows the soil distribution and the principal soured region for the raw materials of plaster production.

Many studies about nocives effects of salts and correction with sulfate were executed. Joel *et al.* (2018) evaluated the effect of sulfur on Cambisol soil irrigated with saline water sorghum cultures. They found that the use of sulfur in doses of 1.39 to 1.99 $t \cdot ha^{-1}$ even in saline rich environment promoted the reduction of the electrical conductivity of the soil, the salinization and in this way a better growth of sorghum plants.

Previous studies

Araújo *et al.* (2017) evaluated the various soil conditions in the tree species grown in saline soils and observed that the use of S and $CaSO_4$ reduced the negative effects of salinization increasing the photosynthetic rate of *Cnidosculus philicanthus, Moringa oleifera* and *Caesalpinia ferrea* and an increase of the dry matter production of *Caesalpinia ferrea* and *Moringa oleifera*.
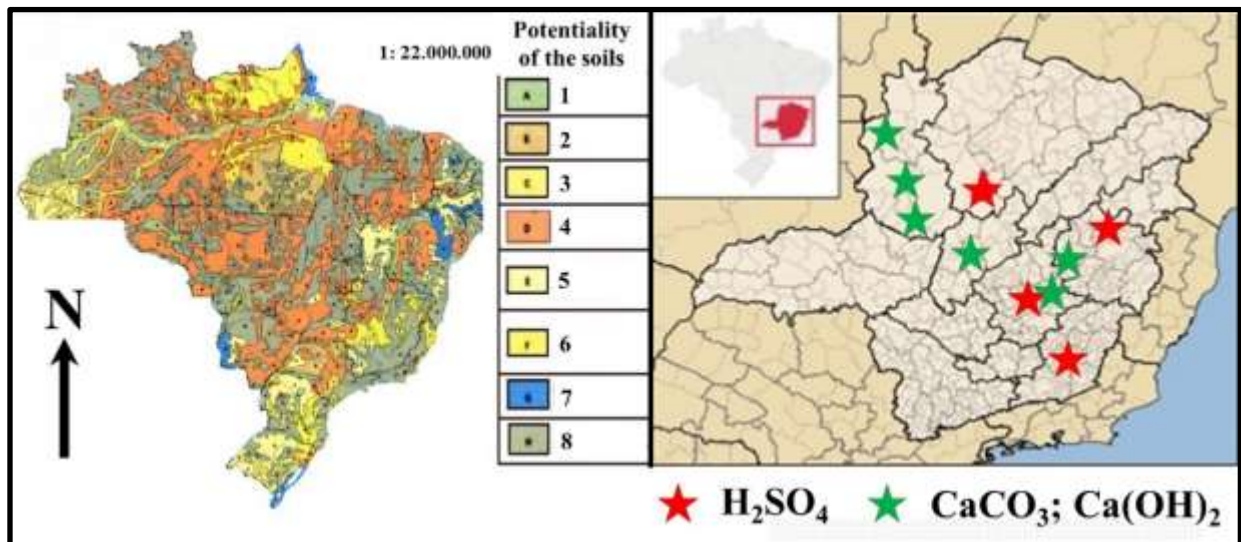
Fig. 1. The map shows the raw material sources and the soil which can be treated in the Minas Gerais State. 1: Good, without restrictions; 2: Good to regular, low nutrients; 3: regular to good, risk of inundations, low nutrients; 4: Regular to restrict, high Al, low depth, lack of nutrient; 5: Restrict, high humidity, luck of nutrients, high Al; 6: Restrict to unfavorable, high Na, high humidity; 7: Not advisable for use, morphological problems; Source: IBGE (1992), modified.

Toledo et al. (2017) have executed studies evaluating the effects of soil salinization on the evapotranspiration of sugarcane cultivars, and have found negative changes of the in soils with high sodium levels. Braga et al. (2009) observed similar results using *Enterolobium schomburgkii* and application of NaCl and $CaCl_2$. In experiments with *Erythrina velutina*, Guimarães et al. (2013), found negative effects of soil salinization over the rate of germination and the initial development of plants. A negative water potential of the soil severely interferes with the absorption of water by the seeds and the physiological events that occur inside them, Mikusinsk (1987) observed reducing the speed and the total number of germinated seeds. Stefanello et al. (2008) observed that seeds of each species have their physiological peculiarities, requiring a minimum amount of soil water potential for water absorption. Germination does not occur below the minimum values. The high concentrations of salts in the soil solution reduce water potential, making water less available to plants similar to water deficit were studied by Nars et al. (2012). Ribeiro et al. (2001) and Esteves and Suzuki, (2008) observed that if the absorption by the seeds occurs, the excess of salts has a toxic effect promoted by the increase of its concentration inside the cell delaying the germination of the seeds

Materials and methods
The raw material, $CaCO_3/Ca(OH)_2$ and H_2SO_4 are obtained from Zn-mining/Cellulose industry and Zn-refining/battery recovering, respectively.
The methodology of plaster production is shown in Fig. 2. The different compounds were cleaned by e.g. micro filtering to retain dangerous particles, mixed together, the product retained by decantation and washing, dried, grinded and then used in agricultural tests.
The work was carried out at the soil laboratory of the Vale do Rio Doce University in Governador Valadares, Minas Gerais. For the tests, common soil samples with regional context (Table 1) were added with NaCl solution and treated with the Ecogypsum® and compared with the salted-not treated and not salted soil samples.
30 cm long PVC tubes, 11 cm wide, were filled with a B-horizon of medium clay texture, dried and grained to < 2.0 cm. The pots were saturated with water and five seeds of hybrid BT corn (*Zea mays* L.) were sown at a depth of 3 cm. A NaCl solution of different concentrations (0 ppm, 100 ppm, and 300 ppm) was applied and then Ecogypsum® in powder form was added on the surface in the dosages of 0, 3, 6 and 9 t·ha^{-1} and then irrigated at every day throughout the test.
During 10 days, the germination was observed, until the plumule broke the surface and ten days after only two plants per pot were kept.
After 30 days the aerial part of the plants was cut, the roots collected, and the green weight determined separately, dried at 75° C to obtain a constant dry weight for the two samples.
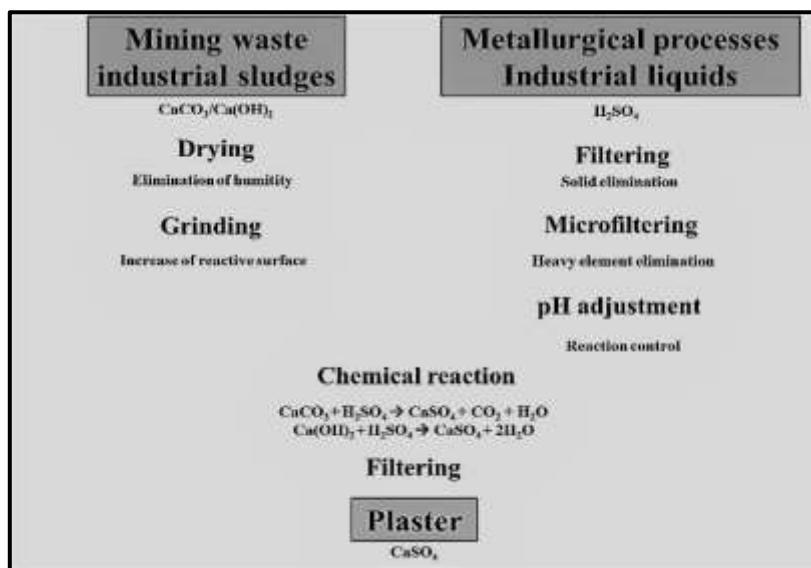
Fig. 2. Flowchart of plaster (Ecogypsum®) production.

Table 1. Physical-chemical parameters of the used soil.

pH	P	K	Ca	Mg	Al	H+Al	S	M.O.	V	t	T	m
	Mg/dm³				cmolc/dm³			dag/kg	%	cmolc/dm³		%
5.6	5.2	119.7	0.67	0.56	0.12	2.3	1.54	0.54	40.1	1.66	3.84	7.23

P=Phosphorus; K=Potasium; Ca=Calcium; Mg= Magnesium; Al=Aluminum; H=Hydrogen; S= total basis; M.O.= Organic Matter; V= base saturation; t= effective cation exchange capacity; T= total cation exchange capacity; m= Aluminum saturation.

The experiment was conducted in a 3x4 factorial scheme with three replications each, the first factor being the NaCl doses and the second factor the Ecogypsum® doses. The data were evaluated using a regression model.

Results and discussion

In Fig. 3 can be observed that the use of Ecogypsum® enhance the germination in substrates with high saline concentrations in comparison of the samples without.

In the absence of salts and the use of plaster, the behavior of the plants is similar with 70% of germination after 6 days evaluating to 90% after 10 days. With increasing doses of NaCl (100 to 300ppm) the germination index reduces significantly down to 60% (Fig. 3.1).

In Fig. 3.2 the effects of adding 3.0 t·ha⁻¹ of Ecogypsum® can be observed. A strong increase of germination with use of this supplement in saline soils in comparison without can be observed. These results indicate that Ecogypsum® acted positively in the germination of the seeds, stimulating the physiological and metabolic process. Another important point occurs due to its characteristic of medium solubility, reducing the risks of osmotic problems in the soil.

Fig. 3.3 shows the effects of the use of 6.0 t·ha⁻¹ of Ecogypsum® also at saline soils. An initial increase with using salt may be the result of a faster Na resorption by SO_4^{2-}, inhibiting the initial osmotic action of this element. Using this higher plaster quantity, the germination in saline soils reaches values around 80% after 6 days and 83% after 10 days, visible higher than without plaster.

At the application of 9.0 t·ha⁻¹ the germination is more uniform in different saline soils.

Analyzing these figures, it is possible to evaluate the positive effect of Ecogypsum® for germination in saline rich soils. The germination rate increases significantly probably due to the potential to neutralize the harmful effects of NaCl in the soil.

Fig. 4 shows the effect on dry weight of Ecogypsum® over germination for the 10th day. There is a significant increase of germination with the use of doses of plaster in saline soils. Soils with higher salt contents reaches with the application germination values of soils without salts.
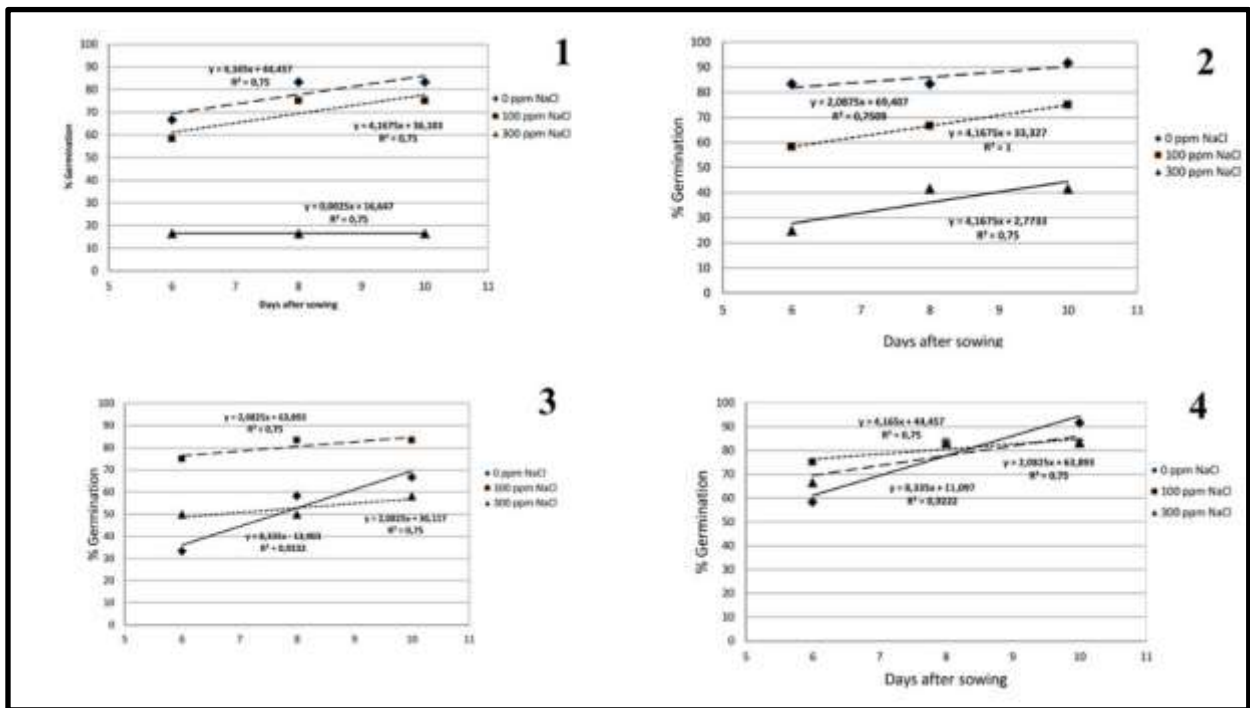
Fig. 3. The figure shows the germination for corn between 6th and 10th day the different environments. **1:** without Ecogypsum® and different NaCl doses; **2:** 3.0 t·ha⁻¹ of Ecogypsum® and different NaCl doses; **3:** 6.0 t·ha⁻¹ of Ecogypsum® and different NaCl doses; **4:** 6.0 t·ha⁻¹ of Ecogypsum® and different NaCl doses.
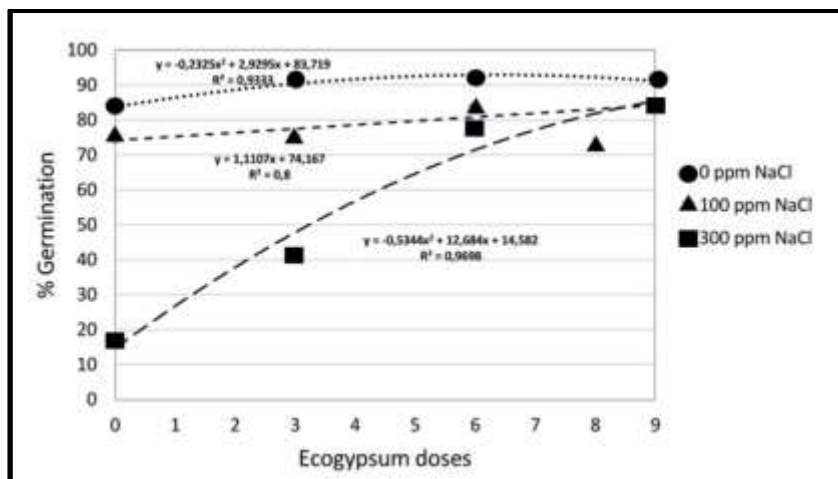
Fig. 4. Here is shown the germination development of the plants with different doses of Ecogypsum® in saline environment during 10 days.

Fig. 5 shows the dry weight evolution of the plants in function of salt concentrations and plaster application. In Fig. 5.1 it can be seen the slight increase of dry weight with the application of higher doses of Ecogypsum®, from 4.7 to over 5.5g.

Fig. 5.2 presents the dry weight evolution in function of salt concentration in the soil. A strong negative correlation is to observe, from about 5.2g to lower than 4.9g.

In Fig. 5.3 is presented the evolution of the dry weight of the aerial parts of corn for three distinct NaCl concentrations increase of Ecogypsum® doses in t·ha⁻¹. The figure gives the impression that the plaster application has to be done in a function of salt concentration in the soils. More salt-higher application, low salt – lower doses.

Fig. 5.4 enhances and give more visibility to the fact that the application of plaster increases the productivity (dry weight) of corn in saline soils.
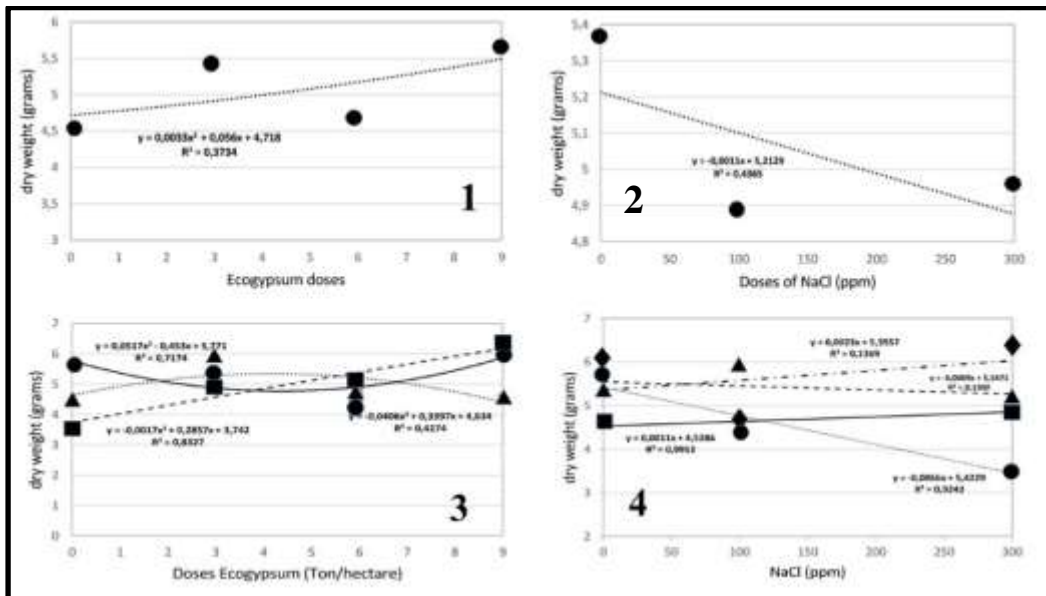
Fig. 5. Dry weight of the collected corn plants in saline environment with **1:** different doses of Ecogypsum®; **2:** different doses of salt solution; **3-4:** different doses of Ecogypsum® and salt solution. **3:** circle: 0mg H_2SO_4; triangle: 100mg H_2SO_4; square: 300mg H_2SO_4. **4:** circle: $0t \cdot ha^{-1}$; triangle: $3t \cdot ha^{-1}$; square: $6t \cdot ha^{-1}$; diamond: $9t \cdot ha^{-1}$.

The green weight of the plants also reacts positively to the application of Ecogypsum®, which is neutralizing the effects of salts in the soil (Fig. 6).
Fig. 6.1. shows the evolution of green weight in function of plaster application for three different salt levels. A very strong increase of green weight, especially, for very saline soils is to observe, once more indicating the relation between application and salt concentration. In Fig. 6.2 three common application rates are shown in function of increasing salt levels. Only for soils without salt, the results are unfavorable.
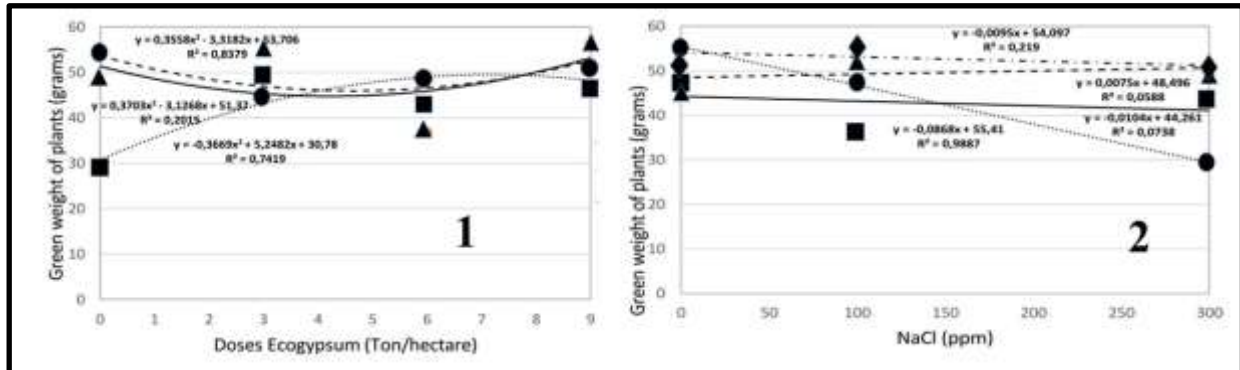
Fig. 6. Green weight behavior of the aerial parts of corn after 30 days. **1:** with different salt levels **2:** with different Ecogypsum® application. **1:** circle: 0mg H_2SO_4; triangle: 100mg H_2SO_4; square: 300mg H_2SO_4; **2:** Circle: $0t \cdot ha^{-1}$; triangle: $3t \cdot ha^{-1}$; square: $6t \cdot ha^{-1}$; diamond: $9t \cdot ha^{-1}$.

Conclusions
The results indicate that Ecogypsum® is able to reduce the negative deleterious effects of the salinization process in soils caused by NaCl by formation sodium sulfate, which is less reactive.
In this way, the possibility of absorption and intoxication of the seeds and roots of plants is reduced, the effects of Na^+ in the water potential of the soil is avoided, the absorption of water and nutrients by the germing seeds and the roots maintained, improving a normal germination and plant development.
Corn plants responded positively to the presence of Ecogypsum® and the neutralization of sodium in the soil with a strong increase of development.

References

Araújo J.L., Oliveira S.R., Sousa F.Q. Silva A.P. (2017) Initial growth of tree species grown on salinized soil with conditioners. Comunicata Scientiae, 2, p. 375-382. https://doi.org/10.14295/cs.v8i2.1590

Braga L.F., Sousa M.P., Almeida T.A. (2009) Germinação de sementes de *Enterolobium schomburgkii* Benth. Submetidas a estresse salino e aplicação de poliamina. Revista Brasileira de Plantas Medicinais, 1, p. 63-70. https://doi.org/10.1590/S1516-05722009000100011

CPRM 2018 Atlas of mineral deposits and selected mineral occurrences of continental Brazil. Brasília, 78 p. ISBN 978-85-7499-354-6 (print); ISBN 978-85-7499-355-3 (pdf)

Esteves B.S., Suzuki M.S. (2008) Efeito da salinidade sobre as plantas. Oecologia Australis, 4, p. 662-679.

Guimarães I.P., Oliveira F.N., Vieira F.E.R., Salvador T.B. (2013) Efeito da salinidade da água de irrigação na emergência e crescimento inicial de plântulas de mulungu. Revista Brasileira de Ciências Agrárias, 1, p. 137-142. https://doi.org/10.5039/agraria.v8i1a2360

IBGE (1992), Atlas Nacional Digital do Brasil. https://www.ibge.gov.br/apps/atlas_nacional/.

Joel J.A., Oliveira F.J.M., Pessoa L.G.M., Nascimento S.A.S., Souza E.S., Barros G., Miranda M.F.A., Oliveira A.C., Freire M.B.G.S. (2018) Effects of elementar súlfur associeted with gypsum on soil salinity attenuation and sweet sorgum growth under saline water irrigation. Australian Journal of Crop Science. 2: p. 221-226.

Mikusinsk O.M. (1987) Testes de embebição e germinação em sementes de Ipomoea aristolochiaefolia. Revista Brasileira de Sementes, 3, p. 103-108.

Nars S.M.H., Parsakhoo A., Naghavi H., Koohi S.K.S. (2012) Effect of salt stress on germination and seedling growth of Prosopis juliflora (Sw.) New Forests, 1:45-55. https://doi.org/10.1007/s11056-011-9265-9

Ribeiro M.C.C., Marques B.M., Amarro Filho J. (2001) Efeito da salinidade na germinação de sementes de quatro cultivares de girassol (*Helianthus annus* L.) Revista Brasileira de Sementes,1p. ,281-284.

Toledo J.V., Zolnier. S., Silva T.G.F., Boehringer D., Neto A.J.S. (2017) Alterations on the evapotranspiration of sugarcane cultivar under distinct salinity levels applied in the fertigation. Journal of the Brazilian Association of Agricultural Engineering, 7, p. 940-952. https://doi.org/10.1590/1809-4430-eng.agric.v37n5p940-952/2017

MELT-MELT-FLUID IMMISCIBILITY EVIDENCE BY MICROTHERMOMETRY AND RAMAN SPECTROSCOPY IN PORPHYRY COPPER GENESIS: BUCIUM TARNIȚA PORPHYRY Cu-Au ± Mo DEPOSIT FROM METALIFERI MOUNTAINS (WESTERN ROMANIA)

Ioan PINTEA[1*], Sorin Silviu UDUBAȘA[2], Eduard GHINESCU[1], Elena Luisa IATAN[3], Ion BERBELEAC[3]

[1]Geological Institute of Romania, 1, Caransebeș Str., 012271 Bucharest, Romania;
[2]University of Bucharest, 1, N. Bălcescu Blv., 010041 Bucharest, Romania;
[3]Institute of Geodynamics *"Sabba S. Stefanescu" of the* Romanian Academy, 19-21, J.-L. Calderon Str., 020032 Bucharest, Romania.
[*]corresponding author: *ipinteaflincs@yahoo.com.*

Abstract: The paper deals with the hydrosilicate-hydrosaline-fluid immiscibility in the potassic and phyllic zones of the internal part of the Bucium Tarnița subvolcanic structure as a porphyry Cu-Au ± Mo deposit which belongs to the Rosia – Bucium – Baia de Aries metallogenic district, in the Miocene volcanic zone of the Metaliferi Mountains (western Romania). The microthermometric experiments (n=70) in hard quartz samples recorded temperatures between 518° and ≥1094°C, salinity between 62-84 wt% NaCl equiv., pressures of 0.4-2.1 kb, the density of 1.2-1.3 g/cm³, and an estimated minimum depth formation of about 1.2 km.

Keywords: hydrosilicate, hydrosaline, immiscibility, microthermometry, Raman spectroscopy.

Introduction

Immiscibility between silicate melt and salt melt, splitting of the magmatic fluid in low salinity vapor "melt" and brine pairs, boiling and condensation are the most important processes during retreating downward crystallization of the shallow porphyritic intrusive plug by decreasing pressure and temperature of the repeated injection of sulfur-rich vapor plume at the bottom of the magma chamber(s) associated with the stratovolcano or caldera formation in the Metaliferi Mountains.

Generally, four stages of alteration–mineralization could be reconstructed by studying the various types of fluid and melt inclusions trapped mainly in quartz veinlets (but also in anhydrite, calcite, barite, sphalerite, enargite, etc.) in the characteristic stockworks. These are correspondent to at least four intermediate magma batches (stages) underlying the successive propylitic, potassic, phyllic, and argillic zones defining a complex porphyry copper and epithermal (high-, and/or low sulfidation) characteristic ore deposit prospects (e.g., Wilkinson, 2013).

Geological setting

Based upon tectono-magmatic features, there are two evolutive models of porphyry copper deposits in the "Golden Quadrangle" of the South Apuseni Mountains, Romania (Borcoș et al., 1998): the Valea Morii model - Diorite type, Cu-Au polyascendent evolution with epithermal veins halo, and the Rosia Poieni model - Diorite type, Cu-Mo polyascendent evolution with pyrite halo.

In this work, it is emphasized based upon fluid and melt inclusions studies, that in the first type of model, endogeneous metasomatic processes prevailed (Pintea, 2010; 2014), while the orthomagmatic process is more representative for the second model, although a mixture of these basic evolutionary features is frequently observable. In any case, the porphyry copper mineralization is centered on the ultimate shallow intrusive(s) associated with the complex stratovolcanoes or caldera volcanic environment (Berbeleac et al., 1995; Popescu and Neacșu, 2012).

Bucium Tarnița porphyry Cu-Au ± Mo deposit is the second porphyry mineralized structure associated with the Rosia Poieni porphyry copper, Rosia Montana and Bucium Rodu-Frasin epithermal Au-Ag deposits, in the Rosia - Bucium Area (Udubasa et al., 2001, Iatan and Berbeleac, 2012).

Bucium-Tarnita is a porphyry Cu-Au system with high-sulfidation style epithermal overprint and with a subvolcanic setting (USGS website).

According to K-Ar data (Rosu et al., 2004) Bucium Tarnita, that occupies the southern part of the Rosia – Bucium – Baia de Aries metallogenic district (Fig. 1) is the oldest volcano-intrusive structure of the mentioned district (14.87-14.60 Ma).
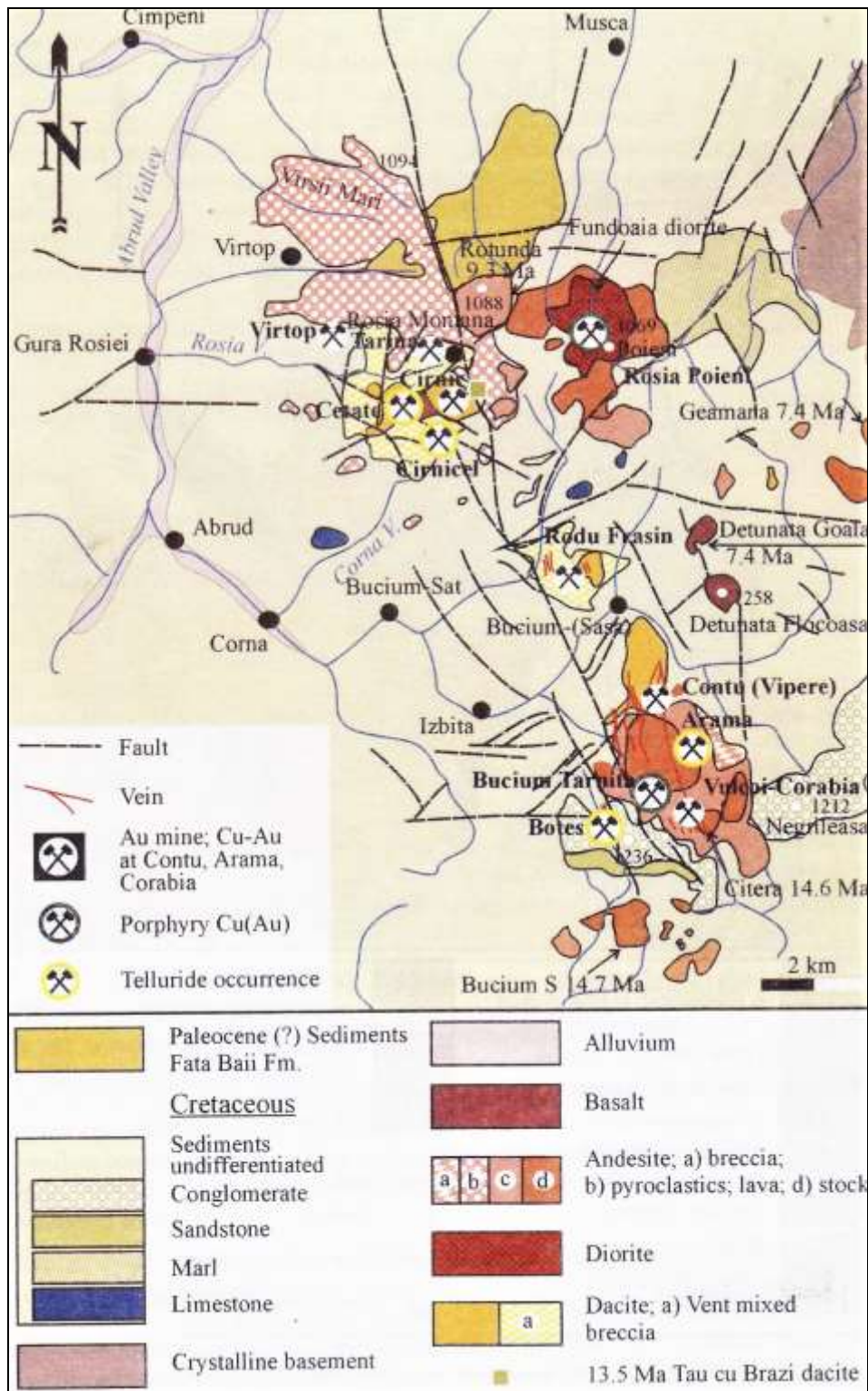
Fig. 1. Sketch map of ore deposits in the Rosia - Bucium area (Ciobanu et al., 2004).

The porphyry copper deposit of Bucium Tarnita occupies an area of about 700 m x 700 m and has the potential to host a significant tonnage deposit, with 2.700.000 t Cu and 120 t Au (Andrei, pers comm., 2011). The Romanian State's historical exploration of the deposit involved underground development (exploration drives and crosscuts), surface and underground diamond drilling, as well as surface pitting and trenching during 1972-1983. Vertical surface diamond drilling holes were drilled to depths of up to 1,200 meters during the survey (Gabriel Resources website).

Bucium-Tarnita is hosted in a cilindric amphibolic andesite body of Calvaria Hill that penetrate Cretacous sediments, placed in the supperior basin of Izbita rivulet (Fig. 2) (Andrei and Calota, 1975;

Vlad, 1983; Popescu, 1986). The drillings show that the subvolcanic body of Bucium-Tarnita has an accentuated dip to the north (Andrei and Calota, 1975).

The sub-volcanic body has endogenous transformations with a zonal arrangement. Thus, in the central-northern part of the structure, we notice the association of neominerals like quartz-biotite-potassium feldspar-chlorite, etc., which towards the eastern, northern and western periphery gradually passes to sericite-clay minerals-quartz paragenesis. The southern part of the subvolcanic body is affected by low temperature propylitization (Andrei and Calota, 1975).

The internal potassic zone contains several coarse quartz veinlets (A and B type) with potassium feldspar – chlorite – actinolite – pyrite – chalcopyrite – magnetite ± anhydrite; potassium feldspar – chlorite – biotite – pyrite – chalcopyrite – magnetite ± anhydrite and potassium feldspar – chlorite – chalcopyrite ± anhydrite within D vein type with pyrite ± chalcopyrite. The outer sericitic zone contains mainly chlorite - clay minerals and quartz - pyrite associations (fig. 2) (e.g., Bostinescu, 1984).
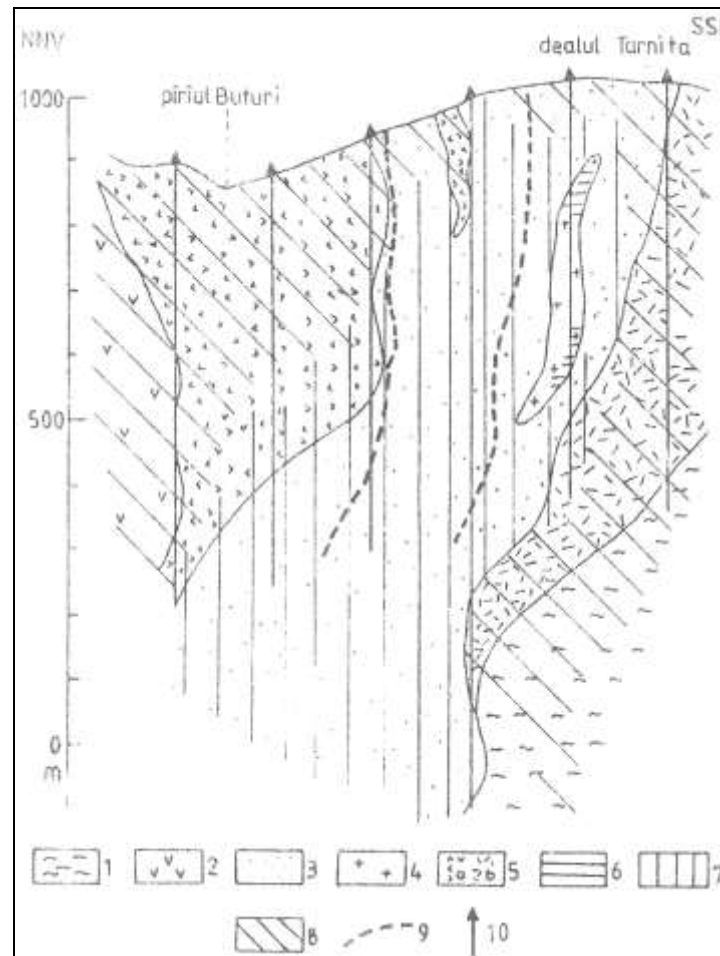
Fig. 2. Geological sketch section of Bucium Tarnita deposit (Popescu, 1986): 1. Cretaceous sedimentary rocks, 2. Arama type andesites, 3. Tarnita type andesite (periphery), 4. Tarnita type andesite (central), 5. Breccias: a. andesitic, b. sedimentary, 6. Alkali feldspar – clorite (biotite) zone, 7. Sericite – argillic minerals zone, 8. Clorite – calcite – epidote zone, 9. Cupriferous impregnation limit, 10. Drills.

A chlorite-dominated propylitization is mentioned in the axial zone of the Bucium-Tarniţa deposit (Boştinescu, 1984). Argillic alteration affects the upper part of the porphyritic body and the volcanic country rocks (Vlad, 1983, in Cioaca et al., 2014).

In the interior of the biotitization and argilization-sericitization zones of the sub-volcanic body, as well as in the cretaceous cornified deposit of its periphery, a dispersed mineralization of the porphyry copper type develops. The establishment of porphyry copper mineralization was favored by the increased permeabilization of the sub-volcanic body both by very pronounced cracking and by the above-mentioned endogenous transformations. As in Rosia Poieni porphyry copper deposit case, the porphyry copper mineralization of Bucium Tarniţa comprises an oxidic phase represented in particular by magnetite, followed by a sulphidic phase characterized by the preponderant deposition of pyrite and chalcopyrite (Andrei and Calota, 1975).

The microfractured andesite contains partings, fractures and veinlets of chalcopyrite associated with intense hydrothermal alteration (Nafinance website).

Late reactivation of NV-SE and NNV SSE fractures results in the appearance of polymetallic mineralizing veins (pyrite, blende, galena, chalcopyrite, tetrahedrite) accompanied by argillizations (Vlad, 1983).
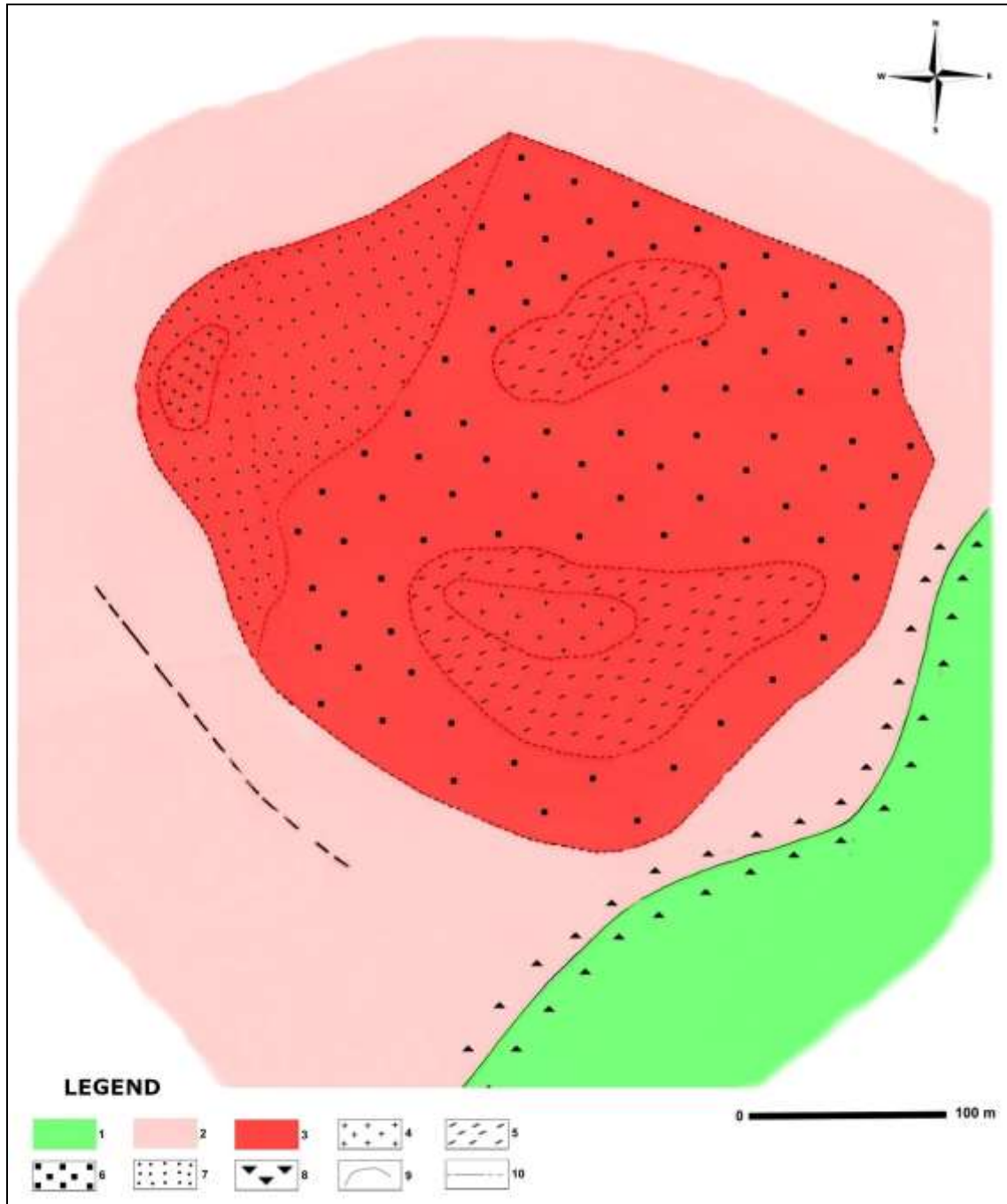
Fig. 3. Schetch map of +880 m level of Bucium Tarnita exploitation showing the main alteration patterns (modified after Bostinescu, 1983). 1. Albian deposits, 2. Tarnita andesites (lava), 3. Tarnita andesites (stock), 4. Tarnita andesites (central unaltered deep facies), 5. Phyllic alteration zone, 6. Potassic alteration zone, 7. Argillic zone, 8. Breccia, 9. Geological boundary, 10. Vein.

Fluid inclusion typology

Fluid and melt inclusions from quartz veinlets were studied in a dozen of double-polished thin sections from samples collected from the 880 m level (Fig. 3) of the old exploration prospect (Bostinescu et al., 1983, unpubl. IGR report) and dump fragments.

10

At room temperature conditions, the main type of solid, melt, and fluid inclusions observed by optical microscopy in the coarse grain quartz veinlets are the following: a. isolate solid remnants or grain formations in trails or bordering the growth zones, represented by anhydrite, apatite, zircon, and opaque grains of ilmenite, magnetite, pyrite, and chalcopyrite; b. glassy "anhydrite" or silicate glass inclusions with vapor bubble(s) and solid daughter salt including opaque phases; c. multiphase (solids + vapor bubble) hydrosaline melt inclusion ± visible liquid phase; d. vapor-rich "melt" inclusions ± solid(s); e. biphasic aqueous fluid inclusions with liquid and vapor bubble; f. aqueous (?) liquid inclusions, frequently with continuous mobile bubble in characteristic "sweat" assemblage.

Microthermometry

The microthermometric experiments from Bucium Tarnița (n=70, Table 1) were done in glassy, hydrosaline melt, and aqueous inclusions in a calibrated microthermometric device up to 1100°C (Pintea, 2014). Immiscibility is assumed from the final fluid phase state observed at the final homogenization temperature and it was evidenced directly in a single complex silicate melt inclusion presented in Fig. 4. Nevertheless, a thin film of silicate liquid could be often seen in the homogenized hydrosaline melt inclusion, suggesting that a pure melt droplet was trapped as primary and pseudosecondary inclusion assemblages.

Table 1. P-T-X data based on measured and/or estimated at the cut-off temperature stage by Sowat (Driesner and Heinrich, 2007). Depth estimation was based upon an average lithostatic load of density of 2.8 g/cm^3 (Mernagh et al., 2020) or 250-270 bar/km (Naumov et al., 2015). It is worth noting that "independent estimates of formation pressure at the deposit would be generally less than or equal to the pressures obtained from Fis" (Lecumberi-Sanchez et al., 2015). So, in this specific data set from Bucium Tarnița deposit, the estimated formation depth of minimum 1.2 km would be close to the relative exploration gallery level of 880m where the samples were collected, considering that minimum 320m above were eroded, which give about 21 m/Ma erosion rate (see for comparison, Dibacto et al., 2020). The maximum values are probably overestimated (e.g., up to 6.0 km) because of heterogeneous trapping and even post entrapment modifications or some of the hydrosaline melt inclusion assemblages (trails) were trapped at different underground depth levels (e.g., Pintea, 2014).

Homogenization type	Temperature, °C	X_{NaCl}	Pressure, kb	Depth, km	Initial fluid state
By vapor bubble	620 - 1079 (**a**) 735 - ≥ 1094 (**b**) 633	0.4 - 0.6 0.37 - 0.62 0.51	0.4 - 2.1 0.4 - 2.1 1.7	1.2 – 6.0 1.2 – 6.0 6.0	Single phase state (n= 29) V+L (n= 28) L+H (n= 1)
By halite dissolution	518 - 583 (**a**) 518 - ≥ 585 (**b**)	0.34 - 0.44 0.34 - 0.44	0.4 - 1.5 0.4 - 1.7	1.2 – 6.0 1.2 – 6.0	Single phase state (n= 8) L+H (n= 4)

The final homogenization took place by vapor bubble disappearance (directly recorded) and that value is considered to be the minimum trapping temperature (formation temperature of the inclusion) of the homogeneous (single-phase state) or heterogeneous (V+L or H+L), i.e., **a, b** in Table 1. When this could not be recorded during heating procedures in the stage because of the vapor bubble persistence at unreasonable high-temperature value (around 1100°C, the maximum stage temperature in this study), the heating was cut-off and this maximum recorded temperature was used in Sowat software (Driesner and Heinrich, 2007) to estimate a minimum homogenization temperature (**b** in Table 1), and also relative salinity converted to mole fractions of NaCl (X_{NaCl}), pressure (bars) and density (i.e., 1.2-1.3 g/cm^3). Frequently, brine inclusion homogenized by halite dissolution after vapor bubble disappearance, and that value computed the P-T-X snapshot of the trapping moment (**a, b** in Table 1). It is worth noting that this kind of hydrosaline melt inclusion usually homogenized at very high temperatures suggesting heterogeneous trapping or an unknown fluid phase equilibria in a more complex system such as Fe-P counterpart to the Si-rich melt (Pintea, 2014, 2015; Tornos et al., 2016; Mernagh and Mavrogenes, 2019).

Raman Spectroscopy

Raman microspectroscopy analyses (n= 20) on doubly polished quartz samples were performed at the Geological Institute of Romania on a Raman Renishaw spectrometer equipped with a Leica DM 2700M and 50x objective lens. The 532 nm green wavelength was used with gratting of 1800 l/mm and 1200 l/mm, variable exposing time between 1 to 120 sec and 1 to 10 accumulations. The resolution ranged between 1-2 cm^{-1}, sometimes more, depending especially on the laser power and distance to the

enclosed fluid inclusion inside the host quartz. Calcite and anhydrite were determined in this study by Raman spectroscopy in the same quartz veinlets mentioned above. In the complex silicate-hydrosaline-, and hydrosaline melt inclusions only CO_3^{2-}, anhydrite, Mg-calcite, amicite, chabazite-Ca, chalcopyrite, fizélyite, and a K-Zn tetrafluoride compound were tentatively identified based upon Frezzotti et al. (2012), Hurai et al. (2015), and Rruff database from the internet (Fig. 5).
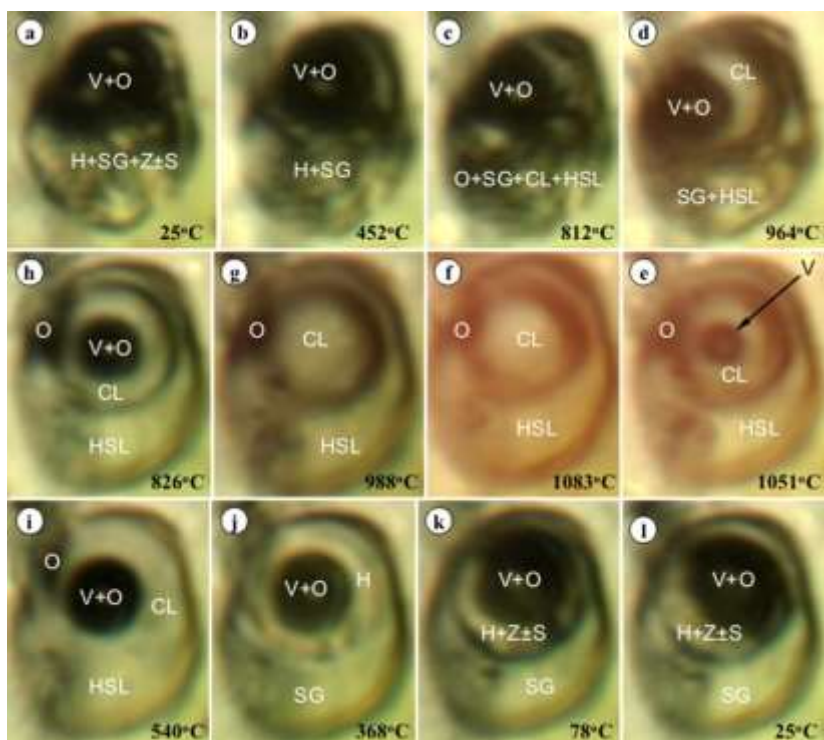
Fig. 4. Melt-melt-fluid immiscibility in remelted silicate glass inclusion from quartz of Bucium Tarnița porphyry Cu-Au ± Mo deposit; (Metaliferi Mountains, Romania). Th(CL)= 1078°C, X_{NaCl}= 0.43, P= 1.6 kb, d= 1.0726 g/ccm, initial fluid state: V+L. Notations: V-vapor, H- halite, SG- glass, S- another salt, O- opaque, CL-chloride liquid, HSL- hydrosilicate liquid, Z- zeolite-like compound.
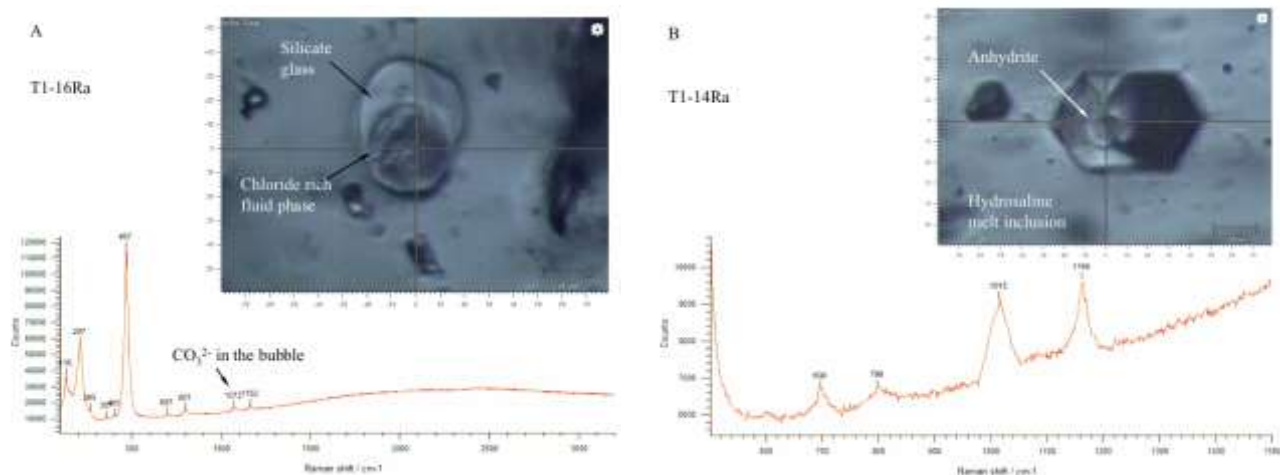
Fig. 5. Raman spectra of the same complex silicate-hydrosaline melt inclusion pictured in Fig.4 showing the presence of carbonate ion in the bubble of the salt melt phase surrounded by silicate glass (**A**) and anhydrite daughter phase (**B**) formed in hydrosaline melt inclusion (without liquid phase at room temperature) from the same quartz sample.

Conclusions

It is emphasized (preliminary) that Bucium Tarnița porphyry Cu-Au ± Mo deposit was formed during shallow magmatic (endogeneous metasomatic) - hydrothermal processes by a secondary hydrosilicate - (chloride-sulfate-carbonate-phosphate) melt (hydrosilicate gel-like liquid or magmatic

emulsion) fractionating chloride, sulfate and (Fe-S-O) immiscible droplets during cooling and decompression from which ore minerals (pyrite, chalcopyrite, and magnetite) precipitated in the potassic and phyllic zones. Several successive episodes of supercritical water metasomatism and/or boiling (and/or condensation) events could be envisaged at lower temperatures by the characteristic microtexture features ("sweat" assemblages), especially around the opaque solid "remnants".

References:

Andrei J., Calota C. (1975) Étude géophysique des corps andésitiques de Rosia Poieni et de Bucium-Tarnita (Monts Métallifères) à l'aide du modelage des sources des champs potentials. Rev. Roum. Geol. Geoph. Geogr., Geophysique, Tome 19, p. 113-135.

Berbeleac I., Popa T., Ioan M., Iliescu D., Costea C. (1995) Main characteristics of Neogene-volcanic-subvolcanic structures and hosted deposits in Metaliferi Mountains. Geol. Macedonica, 9, p. 665-670.

Borcos M., Vlad S., Udubasa G., Gabudeanu B. (1998) Qualitative and quantitative metallogenetic analysis of the ore genetic units in Romania. Rom. J. Min. Dep, 78, 158p.

Bostinescu S. (1984) Porphyry copper systems in the South Apuseni Mountains, Romania. An. IGG., 64, p. 163-174.

Cioaca M.E., Munteanu M., Qi L., Costin, G., (2014) Trace element concentrations in porphyry copper deposits from Metaliferi Mountains, Romania: A reconnaissance study: Ore Geology Reviews, v. 63, p. 22–39.

Ciobanu C., Găbudeanu, B., Cook, N.J. (2004) Neogene ore deposits and metallogeny of the Golden Quadrilateral, South Apuseni Mts., Romania. In: Gold-Silver-Telluride Deposits of the Golden Quadrilateral, South Apuseni Mts., Romania. 31st August – 7th September, Alba Iulia. IAGOD Guidebook Series 12, p. 25-88.

Dibacto S., Lahitte P., Karátson D., Hencz M., Szakács A., Biró T., Kovács I., Vres D. (2020) Growth and erosion rates of the East Carpathians volcanoes constrained by numerical models: Tectonic and climatic implications.Geomorphology 368 (2020) 107352.

Driesner T., Heinrich C. A., 2007. The system H_2O–NaCl. Part I: correlation formulae for phase relations in temperature-pressure-composition space from 0 to 1000ºC, 0 to 5000 bar, and 0 to 1 XNaCl. Geochim. et Cosmochim. Acta, 71, p. 4880–4901.

Frezzotti M.L., Tecce F., Casagli A. (2012) Raman spectroscopy for fluid inclusion analysis. Jour. of Geochem. Exploration, 112, p. 1-20.

Hurai V., Huraiova M., Slobodnik M., Thomas R. (2015). Geofluids-Development in Microthermometry, Spectroscopy, Thermodynamics and Stable Isotopes. Elsevier, 504 p.

Iatan E.L., Berbeleac I. (2012) Preliminary fluid inclusions study in the Bucium Rodu - Frasin neogene volcanic structure, Metaliferi Mountains, Romania. Geophys. Res. Abstr., vol 14, EGU2012-6264, EGU General Assembly 2012.

Lecumber-Sanchez P., Steele-MacInnis M., Weis P., Driesner T., Bodnar R.J. (2015) Salt precipitation in magmatic-hydrothermal systems associated with upper crustal plutons. Geology, 43, 12, p. 1063-1066.

Mernagh T.P., Mavrogenes J. (2018) Significance of high-temperature fluids and melts in the Grasberg porphyry copper-gold deposit. Chem. Geol., 508, p. 210-224.

Mernagh T.P., Leys C., Henley W.R. (2020) Fluid inclusion systematics in porphyry copper deposits: The super-giant Grasberg deposit, Indonesia, as a case study. Ore Geol. Rev., 123, 103570.

Naumov V.B., Dorofeeva V.A., Mironova O.F., Prokof'ev V.Yu. (2015) Sources of high – pressure fluids involved in the formation of hydrothermal deposits. Geochem. Internat., 53, 7, p. 590-606.

Pintea I. (2010) Fluid and melt inclusions evidences for autometasomatism and remelting in the alpine porphyry copper genesis from Romania. Rom J. Min. Dep., 84, Spec. issue, p. 15-18.

Pintea I. (2014) The magmatic immiscibility between silicate-, brine-, and Fe-S-O melts from the porphyry (Cu-Au-Mo) deposits in the Carpathians (Romania): a review. Rom. J. of Earth Sciences vol 87, issue 1, online first, p. 1-32.

Pintea I. (2015) Fluid in the earth crust and upper mantle: an atlas of the fluid and melt inclusions from Romania. Romanian Journal of Earth Sciences (in review).

Popescu Gh. (1986) Metalogenie aplicata si prognoza geologica. Partea a II-a. Bucuresti, p. 316.

Popescu G.C., Neacsu A. (2012) Modeling of epithermal gold and porphyry copper deposits from Metaliferi Mountains (Romania). R. J. Min. Dep., 85, 1, p. 7-14.

Rosu E., Seghedi I., Downes H., Alderton D., Szakacs A., Pecskay Z., Panaiotu C., Nedelcu L. (2004) Extension-related Miocene calc-alkaline magmatism in the Apuseni Mountains, Romania: Origin of magmas. Schweiz. Mineral. Petrograph. Mitt., 84, p. 153-172.

Tornos F., Velasco F., Hauchar J.M. (2016) Iron-rich melts, magmatic magnetite, and superheated hydrothermal systems: The El Laco deposit, Chile. Geology, 44, 6, p. 427-430.

Udubasa G., Rosu E., Seghedi I., Ivascanu P. M. (2001) The "Golden Quadrangle" in the Metaliferi Mountains, Romania: what this really mean? Rom. J. Min. Dep., 79, suppl 2, p. 24-34.

Vlad S. N. (1983) Geology of the porphyry copper deposits. Editura Academiei București, Bucarest (in Romanian).

Wilkinson J. (2013) Triggers for the formation of porphyry ore deposits in magmatic arcs. Nature Geosci. 6, p. 917–925, https://doi.org/10.1038/ngeo1940.

***Andrei J., 2011: *https://www.cotidianul.ro/apelul-unui-mare-patriot-si-inginer-geolog*

***Gabriel Resources: *http://www.gabrielresources.com/site/bucium.aspx*

***Rruff database: *https://rruff.info/*

***Nafinance: *http://www.nafinance.com/listed_co/English/gabriel_e.htm*

***USGS: *https://mrdata.usgs.gov/sir20105090z/show-sir20105090z.php?id=356*

GEOLOGY, MINERALOGY, GEOCHEMISTRY, AND FLUID INCLUSION CHARACTERISTICS OF CAPOEIRANA – NOVO EMERALD DEPOSITS, BRAZIL.

Adolf Heinrich HORN[1*], Ioan PINTEA[2], Yves FUCHS[3], Eduard GHINESCU[2], José Maria LEAL[4], Sorin Silviu UDUBAŞA[5]

[1] Institute of Geosciences, Research Center Prof. Manoel Teixeira da Costa. Avenida Antônio Carlos, 6627. Pampulha. Cep 31270901 - Belo Horizonte, MG, Brazil; *hahorn@ufmg.br*
[2] Geological Institute of Romania, 1Caransebes Str., 012271, Bucharest, Romania; *ipinteaflincs@yahoo.com*
[3] Laboratoire Géomatériaux et Environnement, Université Gustave Eiffel, Paris, France
[4] Federal University of Jequitinhonha e Mucuri Valley- Diamantina, MG, Brazil; *jose.leal@ict.ufvjm.edu.br*
[5] University of Bucharest, 1, N. Bălcescu Blv., 010041 Bucharest, Romania.

Abstract: The Capoeirana emerald deposit is located near Nova Era, in the southeastern part of Minas Gerais, Brazil. Two distinct lithologies compose the geology of the zone. One consists of undifferentiated granitoid rocks and the other is formed by volcano-sedimentary rocks, both of them being strongly altered. Emeralds occur in three types of associations. The main one is a meta-ultramafic rock, and the others are quartz- and pegmatitic veins. The mineralization is located at the tectonic contact of the volcano-sedimentary sequence with the gneissic rocks. The best specimen crystallized around quartz fishes in their pressure shadows. Pegmatite veins are the Be source and granitic bodies caused the hydrothermal processes. Chemical investigations on the zoned emeralds show there was an evolution starting with low Cr and very low V concentrations. Micas, picotite, and amphibole microprobe analyses indicate at least two mafic components and a multistage process of formation. The CO_2 ($\pm CH_4$) - H_2O - NaCl fluid inclusion type showed the CO_2 density between 0.55 - 0.78 g/cm^3, the aqueous phase indicated the salinity between 2 - 17 wt.% NaCl eq., the pressure between 0.8 - 2 kb, and the formation temperature between 420° and 690°C. Informally, the CO_2 diad based calculation gives 0.479898 g/cm^3 density. Sometimes, CO_2-rich inclusions show critical homogenization. Complex carbonate/silicate primary and pseudo-secondary inclusions suggest an immiscible process at high temperature trapping conditions.

Keywords: emerald, genesis, geology, mineralogy, geochemistry, fluid and melt inclusions, Capoeirana, Brazil

1. Introduction

1.1. Location

The Capoeirana emerald deposit is located between the Nova Era and Itabira municipalities, in the central-southeast part of the Minas Gerais State, Brazil. At a distance of 140 km from Belo Horizonte, the access is by the highways BR-262 and BR-381 to Nova Era. From there the Capoeirana deposit is reached after 10 km by the state highway MG-120.

This deposit is exploited in a rudimentary way by small-scale miners (*garimpeiros*), aggregated in a cooperative, exploiting the emeralds independently, each one developing their mine without any engineering technique and geological knowledge (Figure 1). The emeralds found and explored are of good quality and great gemological use (Leal, 1998).

1.2. Geological setting

The local geology of the region consists essentially of two lithological groups. The first group is formed principally by granitic rocks (granites/gneiss), while volcano-sedimentary rocks (amphibolites, phlogopite and biotite schists) compose the other. Both are deformed, and suffered changes during greenschist to upper amphibolite facies metamorphism, and are strongly affected by weathering and hydrothermal processes (Souza, 1988). Figure 1 shows the local geology, tectonic situation, and the most important emerald deposits at Belmont and de Capoeirana mines (Souza, 1988; Schorscher, 1992; Machado, 1994).

The main tectonic structures and events are shown in Table 1 and Figure 2. There are different possibilities for emerald formation and recrystallization during evolutional history. In Table 1, the geological events occurred and the structures identified in the emerald deposit are shown, as well as a sequence of crystallization of the emeralds in the deposit of Capoeirana.

1.3 Emerald deposits

- The emerald deposit of Capoeirana is located in the northeast of the Iron Quadrangle of Minas Gerais State, Brazil. Phlogopite-amphibole-emerald-quartz schists, inserted in highly deformed granitic rocks of Archean Age, compose the rock sequence. The deposit is characterized by some authors (Schwarz, 1987; Guliani et al., 2019) as type I/A_2 or I/A respectively, with fewer mica inclusions, more fluid inclusions, and low Cr- and very low V-content in the emeralds.
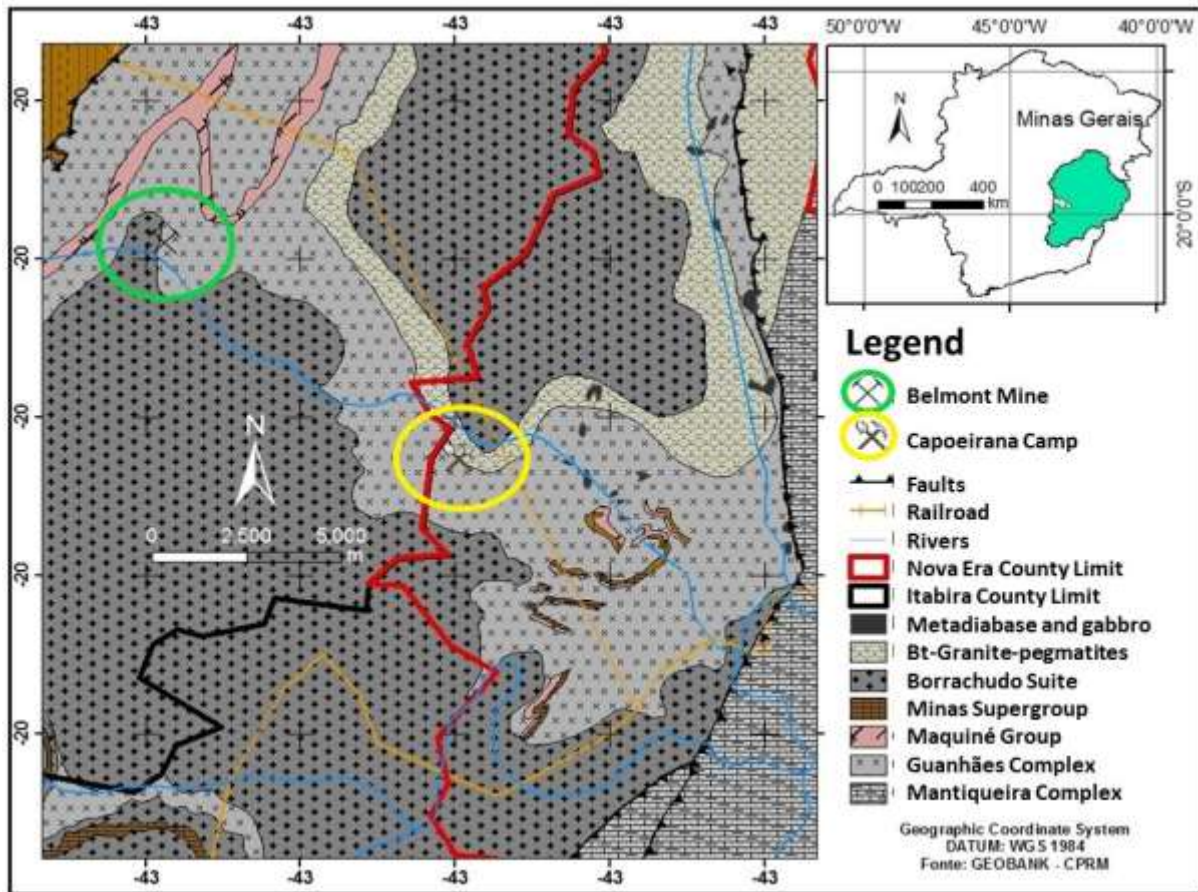
Fig. 1. Geology of the Nova Era-Itabira emerald field showing the location of the investigated deposit (after Horn and Pintea, 2019, modified).

Table 1. The main structures identified in the rock samples from the Capoeirana digging places (after Ribeiro, 2006; modified). The formation events of emerald crystallization are pointed out.

Structures	Main observations	Emerald formation	Deformation event
Mylonitic foliation	Anastomosed mylonitization foliation, in axial plane position of tight and ruptured folds, intensely transposed	Tiny emerald formation	
Strain lineation - L1	Lineation conformed by the preferential orientation of mica minerals and lenses of quartz, amphibolite, chromite and/or stretched pegmatoids, foliation S1		
Folding system - B1	Tight intrafolial folds of mylonitic foliation S1, with axial plane foliation, usually ruptured and transposed.		
Shear zones	Responsible for the generation of F1 Clearance Failures, structural elements nucleated in E1 and mineralized tectonic contacts in emeralds between the Phlogopite gneisses	1st emerald formation	E1
Folding system - B2	Open or closed folds of nucleated structures formed in E1. They present not harmonic style without development of axial plane foliation.		
Gravity faults; distension fractures	Normal failures and nucleated distension fractures in late phases of the deformation event E2. Oriented approx. subparallel to the directions of the folded mylonitic foliation S1.		
Lineation - L2	Stretch marks and grooves printed on rocks during the development of F2 faults. They are oriented according to the main directions of the movement and printed as slickensides.		E2
Strain slip cleavage - S3	Axial flat cleavage of corrugated-looking asymmetric mini-folds.		
Lineation of crenulation; axes of kink folds - B3	Axes and hinges of asymmetric mini-folds and/or kink-folds. They double the foliation already folded S1, affecting all rocks and structures generated in E1 and E2.		E3
Diverse fractures and other structures	Joints and fractures generated, probably, in the late extension phases of E3 or even E2 deformation event.	2nd emerald crystallization	E2 and E3

16
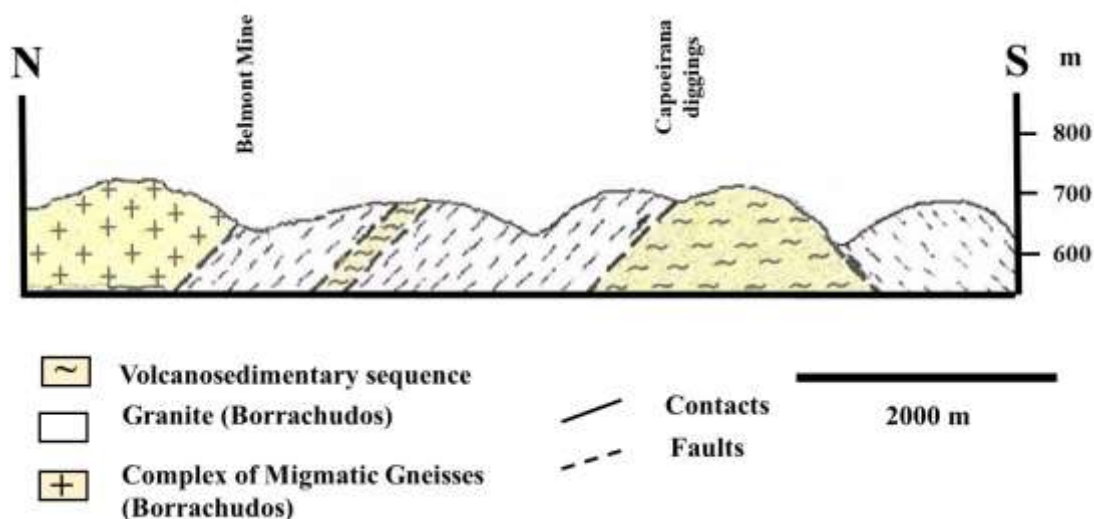
Fig. 2. Geological cross section showing the emerald deposits in the geologic and tectonic environment of the investigated area.

The age of the formation is still in discussion. The dating of pegmatites and minerals (Ribeiro-Althoff et al., 1997; Morteani, verb. comm.) indicate two periods of emerald formation connected to two possible pegmatite generations.

The deposits are located at the contact between Archean paragneisses and the often highly deformed Borrachudo granite of metaluminous character (~1,73 Ga crystallization age of Pb/Pb in zircons; Dossin et al., 1993). The metamorphic sequence is composed of meta-arenites and metagraywackes with intercalated mafic and ultramafic formations, which are dated as lower Proterozoic. These formations with NE striking and steep W dip are widely transformed into biotite-quartz-schists, phlogopite-quartz-schists, and talc-chlorite schists, often with Cr-spinels, chromite crystals or tiny emeralds (Schorscher et al., 1982; Guliani et al., 1990).

A significant number of pegmatites, probably of principally Brasiliano but also Transamazonian age, intrude the rocks of the region. These veins, dikes, and irregular bodies cut the rocks normally along existent fractures and deformed rock contacts. The pegmatites are altered by metasomatism showing loss of quartz transported to fractures or foliation planes in the para-sediments, and feldspatization and kaolinization. The pegmatites in contact with the Cr-source rocks show weakly colored emeralds, aquamarines, beryl *sl*, and black tourmalines. The darker green emeralds were formed at the schists-pegmatites contact, in the pressure shadows of quartz fishes, amphibolite restites, and of crystal agglomerates, in fractures and fold axis (Figure 3). Emerald occurs sometimes closely associated with chrysoberyl and alexandrite.

2. Materials and methods

Three field campaigns were realized in the area of Belmont, Piteiras, and Capoeirana. Rock samples and mineral specimens were collected from different outcrops, digging places, and mines.

The samples were cut, a part crushed, and thin and double polished sections prepared at the CPMTC (Centro de Pesquisa Prof. Manoel Teixeira da Costa). Microthermometry was done preliminary in the double calibrated stage (homemade) between 20° and 398°C and between 398° and 1100°C with a precision of ±1° to ±15°C. Raman analyses were done in an InVia Raman Renishaw microprobe equipped with Leica DM 2700M Microscope with 50x objective lens, 532nm excitation line, 1800 l/m grating, up to 90 sec. time exposure and 3 accumulations, at the Geological Institute of Romania, Bucharest.

The chemical analyses were performed at the Camparis Unit (University Pierre et Marie Curie, Paris) using a Camebax SX 50 microprobe.

3. Results and discussion

3.1. Chemical analyses

The chemical data of emeralds from the Capoeirana deposit show that the predominant chromophore element is chromium, the presence of vanadium is very low or below the detection level. Table 2 shows the results for emeralds calculated in structural units (CPFU).
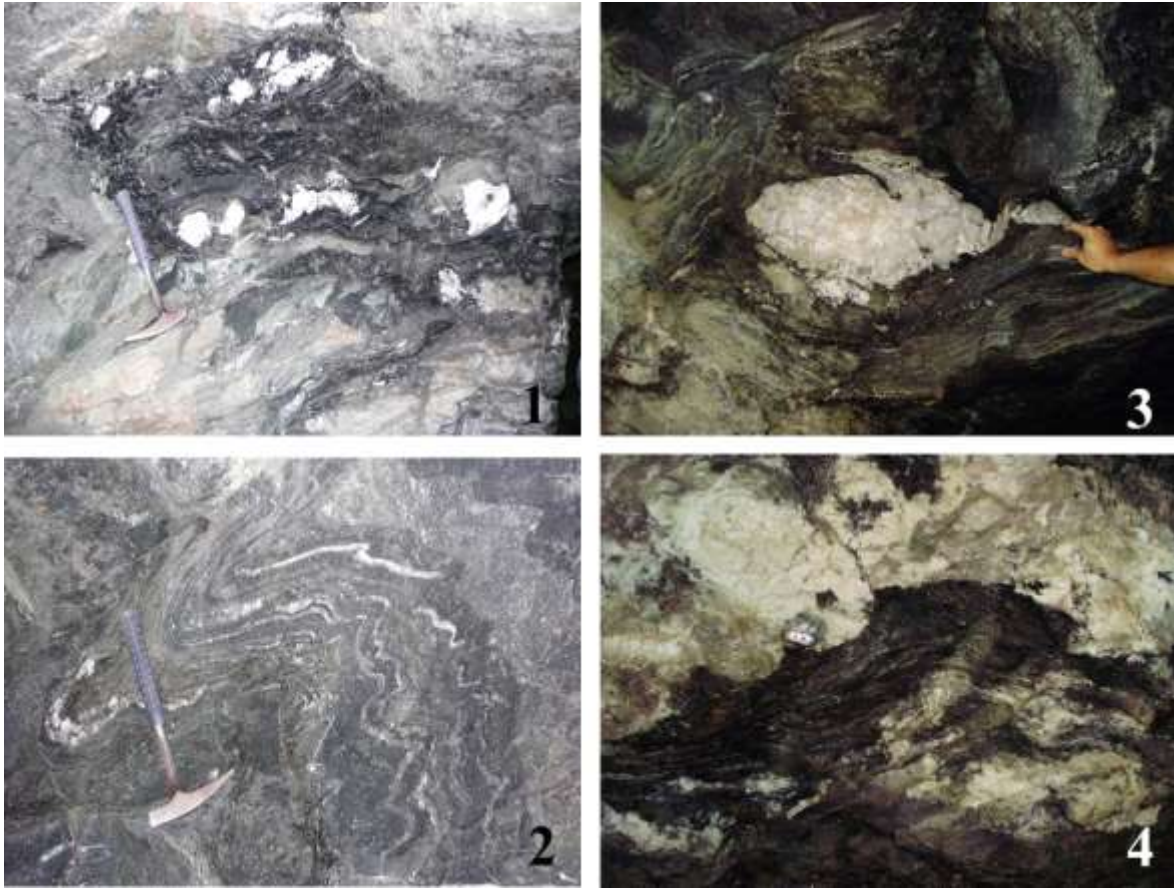
Fig. 3. 1. A concentration of sheared pegmatoid veins cutting the phlogopitite 2. A package of folded rocks. The emeralds are concentrated in the joints of folds; 3. Quartz fish with emeralds in the pressure shadow; 4. Pegmatite vein intercalated with the biotite-phlogopite-quartz schist (Photos: Leal- 1, 2; Horn- 3, 4).

Table 2. Structural composition of analyzed emeralds from Capoeirana mining place in CPFU. Al varies from 1.5 to 1.67, Fe from 0.046 to 0.03. The Cr content ranges from 0.02 to 0.033, and V is always <0.006.

	14	15	16	17	18	19	20	21	24	25	28	29	31	32
Si	5.905	5.928	5.849	5.912	5.838	5.842	5.757	5.857	5.636	5.904	5.898	5.856	5.871	5.868
Al	1.553	1.587	1.552	1.567	1.552	1.578	1.578	1.620	1.489	1.760	1.587	1.540	1.672	1.645
Ti	0.000	0.002	0.000	0.000	0.002	0.000	0.000	0.001	0.004	0.000	0.000	0.000	0.000	0.000
Cr	0.030	0.033	0.032	0.021	0.028	0.023	0.023	0.017	0.087	0.020	0.027	0.026	0.023	0.023
V	0.000	0.000	0.002	0.000	0.006	0.000	0.000	0.004	0.003	0.000	0.000	0.000	0.001	0.000
Fe	0.041	0.039	0.041	0.038	0.035	0.035	0.036	0.046	0.098	0.030	0.039	0.043	0.039	0.030
Mn	0.001	0.000	0.000	0.000	0.000	0.000	0.003	0.004	0.000	0.002	0.008	0.002	0.000	0.000
Mg	0.304	0.303	0.300	0.269	0.278	0.274	0.260	0.254	0.516	0.154	0.273	0.301	0.224	0.238
Ca	0.008	0.004	0.003	0.002	0.004	0.002	0.004	0.004	0.011	0.003	0.004	0.006	0.001	0.003
Na	0.159	0.100	0.217	0.214	0.254	0.242	0.338	0.193	0.156	0.128	0.163	0.229	0.165	0.192
K	0.002	0.004	0.005	0.000	0.003	0.004	0.002	0.006	0.001	0.000	0.001	0.003	0.003	0.001

Microprobe analyses were done on several minerals from the host rocks of the mineralization. The results are presented in Table 3, in which the composition, calculated in oxides, of phlogopite, picotite, and amphibole is shown.

The presence of picotite, a Cr-spinel, indicates the high Cr-content of the original mafic rocks. The presence of picotite is evident in the absence of emeralds and vice versa.

	Phlogopite								
SiO$_2$	37.98	38.57	40.43	39.11	37.57	38.67	40.69	35.55	36.30
Al$_2$O$_3$	14.46	14.94	14.04	15.29	14.71	14.93	15.39	16.27	15.40
TiO$_2$	0.57	0.58	0.75	0.51	0.55	0.66	0.61	1.85	1.75
FeO	10.62	11.44	8.88	9.61	9.46	8.05	8.29	14.45	13.51
MgO	17.96	18.91	19.57	19.14	18.22	19.71	19.36	15.55	16.08
V$_2$O$_5$	0.13	0.003	0.11	BDL	BDL	BDL	0.03	0.08	0.10
Cr$_2$O$_3$	0.53	0.74	1.20	0.20	0.21	0.54	0.71	0.05	0.16
MnO	0.06	0.12	BDL	0.15	BDL	0.01	0.00	0.00	0.01
K$_2$O	7.58	8.02	8.19	8.36	8.00	7.77	8.30	7.76	7.72
Na$_2$O	0.28	0.41	0.54	0.46	0.41	0.47	0.51	0.45	0.44
CaO	0.13	0.01	0.00	0.00	0.07	0.07	0.00	0.00	0.02
F	0.35	0.35	0.79	1.20	0.99	0.22	0.00	0.69	1.18
Sum	90.64	94.10	94.49	94.04	90.20	91.10	93.88	94.67	92.66

Table 3. Element concentration of the investigated minerals from the host rocks: phlogopite, picotite (Fe,Mg)(Al,Cr)$_2$O$_4$, and amphibole. BDL = below detection limit.

	Picotite								Amphibole								
SiO$_2$	0.02	0.16	0.07	0.07	0.10	0.05	0.15	0.01	55.23	56.36	49.48	54.57	52.94	52.61	52.61	52.94	56.15
Al$_2$O$_3$	5.12	5.23	5.58	5.58	12.90	14.22	12.26	11.75	3.16	1.63	9.92	2.62	4.64	3.45	4.43	4.64	1.18
TiO$_2$	0.06	0.72	0.12	0.12	0.11	1.79	0.12	0.08	0.06	0.07	0.39	0.05	0.08	0.00	0.07	0.08	0.01
FeO	31.83	31.83	31.90	31.90	34.63	33.42	33.90	34.89	12.89	14.81	15.01	9.33	8.86	7.79	7.97	8.86	6.25
MgO	0.36	0.38	0.44	0.44	0.81	1.09	0.81	0.76	21.67	22.79	16.33	19.94	18.05	19.26	18.22	18.04	20.31
V$_2$O$_5$	0.18	0.46	0.14	0.14	0.16	0.28	0.21	0.28	BDL	0.05	0.13	BDL	0.13	BDL	BDL	0.13	0.13
Cr$_2$O$_3$	60.66	59.80	59.86	59.86	49.50	47.86	51.46	51.85	0.20	0.09	0.49	0.15	0.59	0.37	0.27	0.59	0.46
MnO	0.36	0.29	0.20	0.20	BDL	BDL	BDL	0.00	0.16	0.34	0.11	0.24	0.20	0.09	0.14	0.20	0.08
K$_2$O	BDL	0.01	0.12	0.12	0.03	BDL	0.05	0.01	0.03	0.00	0.09	0.11	0.11	0.07	0.03	0.11	BDL
Na$_2$O	BDL	0.14	0.09	0.09	0.038	0.10	0.04	0.10	0.26	0.17	1.26	0.34	0.60	0.65	0.75	0.60	0.30
CaO	BDL	BDL	BDL	BDL	BDL	BDL	0.01	0.09	3.28	0.60	10.55	8.13	10.86	10.33	11.12	10.86	11.25
F	1.50	1.75	1.23	1.23	1.22	1.23	0.99	1.64	BDL	BDL	0.08	0.00	0.27	BDL	BDL	0.27	0.70
Sum	100.08	100.12	99.76	99.76	99.49	100.04	100.00	101.45	96.93	96.90	96.27	95.47	96.65	94.62	95.58	96.65	96.81

3.2. Fluid and melt inclusions

There are two main kinds of fluid inclusions in the Capoeirana emeralds. The first type is generally primary and pseudo-secondary containing a carbonate phase (solid + fluid) trapped together with a silicate glassy phase and/or quartz. The second type contains carbonic fluid phases (CO_2 liquid + CO_2 vapor) together with an aqueous phase and/or silicate glass trapped in pseudo-secondary and secondary trails. In between, there are various trail assemblages with variable composition containing frequently solid daughter salty minerals with aqueous fluid, carbonic and silicate glassy content. At room temperature conditions a CO_2 phase (liquid + gas), between 40-60 vol.%, appears associated frequently with several mineral grains (some of them with birefringence), sometimes a liquid visible phase being also present. They are mainly primary and pseudo-secondary and are associated with silica-rich solid inclusions (now quartz) containing the same carbonic assemblage suggesting heterogeneous trapping. Frequently rounded and transparent solid bodies (often with slight birefringence) are also present as primary and pseudo-secondary inclusions, reminding the silicate glass inclusions described in topazite (e.g. Williamson et al., 1997). More often, the same assemblage is founded in narrow glassy capillary tubes arranged in parallel alignment of primary origin. They have 1-20 µm in width and up to 800 µm in length, sometimes more. The carbonate rich inclusions have various shapes, from small barrels, quadrangle or irregular forms, because of partial decrepitation. Their size ranges between 10 µm and more than 150 µm being distributed parallel to the capillary glassy tubes or decorating cicatrized fissures frequently perpendicular to the parallel tube assemblage. The small quartz microcrystal formed after trapping have generally short knife shape (or wedges) of 40 to 100 µm in length. It always contains a solid carbonate assemblage attached to the base of the little prism. Generally, the sharp part of the prism is clean, without any solid around. Frequently the wedges and the rounded silicate glass inclusions display one ore more black zones (dots) which represent probably shrinkage bubbles.

During heating the gas CO_2 bubble homogenized onto the liquid CO_2 phase around 29-30°C, sometimes showing critical homogenization by fading disappearance of the constant vapor volume around the critical point of CO_2 (i.e. 31.1°C). On further heating, generally the inclusions of both types (i.e. carbonic and glassy silicatic) decrepitated around 300°C, so the final homogenization temperature cannot be recorded (see also Lynch et al., 2014). Schwarz (1987) observed in samples from the Belmont mine primary and secondary fluid inclusions of "solid-liquid-gas" type, especially some with two liquids (liquid-liquid), others with two liquids and gas (liquid-liquid-gas), and with two liquids, a gas, and a solid (solid-liquid-liquid-gas). He also identified a few solid inclusions formed by phlogopite, biotite, hematite, andradite, apatite, dolomite, tourmaline, beryl, and quartz.

19

Leal (1998) estimated the CO_2 density between 0.55 and 0.78 g/cm^3, sometimes with traces of CH_4. The salinity of the aqueous phase was estimated between 2 and 17 wt.% NaCl eq. The formation temperature of this fluid inclusion type is calculated between 420° and 690° C with a local pressure of 800-2000 bar. Raman spectroscopy determined the presence of CO_2, CO_3^{2-}, emerald, and quartz by characteristic peaks (Fig. 4 and Fig. 5) (Frezzotti et al., 2012, Hurai et al., 2015, and Ruff database on the web).
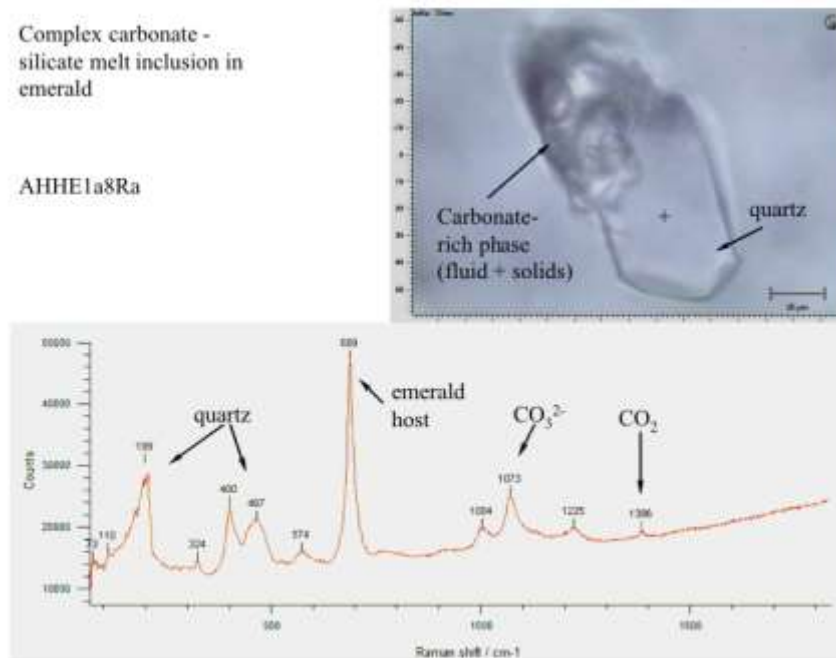
Fig. 4. Multiphase inclusion suggesting fluid-fluid-melt immiscibility at trapping conditions in emerald from Capoeirana.
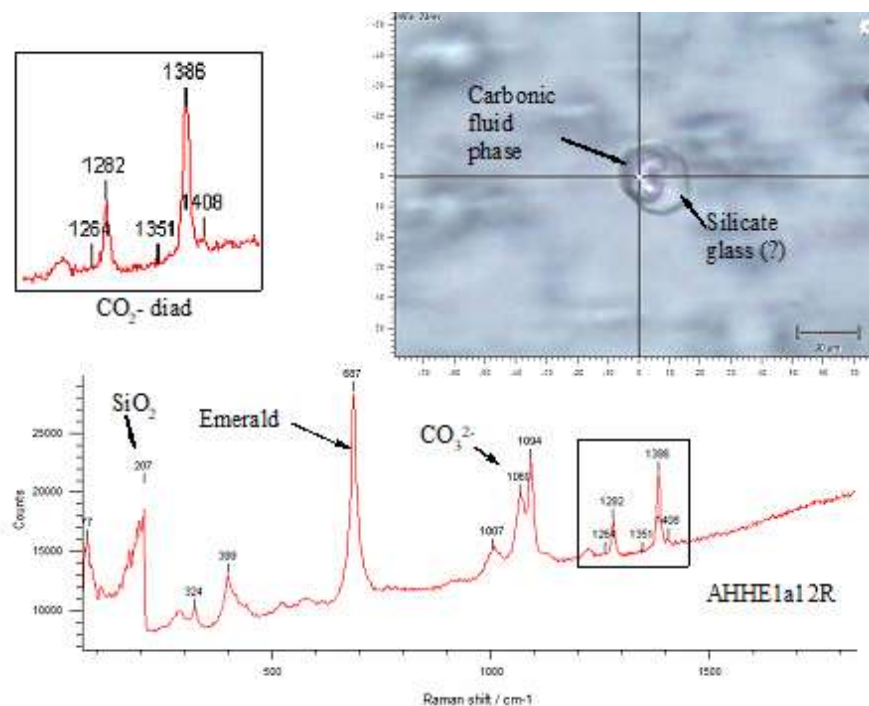
Fig. 5. Raman spectra of the fluid carbonic (liquid CO_2 + gas CO_2), and glassy silicate solid phase in emerald from Capoeirana. Informally, the calculated pressure of this inclusion based upon CO_2 diad (in medallion) with $\Delta = + 104$ cm^{-1} gives a calculated density of 0.479898 g/cm^3 (Lamadrid et al., 2017).

At higher temperatures (Pintea and Horn, 2019) it was shown that in the complex carbonate-silicate inclusions some of the solid phases start to melt and turned in a dark liquid phase supposed to be a carbonate liquid (somehow similar to carbonate melt from Oldoinyo Lengai volcanic lava). Accidentally, one carbonate inclusion containing (CO_2 liquid + CO_2 gas) did not decrepitate and after quenching from about 800ºC showed the same fluid carbonic assemblage as before heating. This could be interpreted that the CO_2 fluid phase was generated from the carbonate liquid phase "in situ" when the temperature reached the critical temperature, back to quenching.

Perhaps the same process was involved after the initial trapping of the carbonate melt when the CO_2 separates as CO_2-liquid+CO_2-gas function of temperature decrease. Because there are complex inclusions at room temperature containing both carbonate and silica rich phases as quartz and/or silicate glass, we can presume that at the initial trapping condition two immiscible melts were trapped, one reactive carbonate phase and a viscous silicate melt. This could be the most important petrographic evidence of the presence of such a complex melt/fluid phase during the emerald crystallization. The presence of carbonate silicate fluid–melt immiscibility is a common process in pegmatite genesis, supposing that the involved melt is a silicate gel or a silicothermal fluid (e.g. Thomas and Davidson, 2016).

4. Conclusions

Using the geochemical and fluid inclusion data, it is possible to confirm the following about the emerald formation process:

1. Fluid inclusions and chemical zoning in minerals suggest that Cr-bearing minerals formed probably during a multistage process or by two distinct processes (Transamazonian and Brasiliano events) in one sequence.
2. Cr-sources are the mafic to ultramafic regional rocks (e.g. picotite rich rocks*?*; amphibolites) and the liberation of Cr formed first Cr-poor and later Cr-rich emeralds (the reverse for micas and amphiboles). Probably the picotite presence or crystallization inhibited the formation of emerald in the picotite rich rocks(?).
3. Be-sources are probably the consolidated Transamazonian and new forming Brasiliano pegmatites;
4. First crystallized micro-emeralds transformed afterward by solid stage transport (Brasiliano Event) in bigger specimens localized within the quartz- and amphibolite boudins and in their pressure shadows;
5. During later tectono-metamorphic stages, rotation and fracturing created irregular internal structures;
6. These tectonic events (phases?) created a complicated fold-fault system with an alternate sequence of emerald-bearing and emerald-free units dipping SE with an ~E-W orientation.

5. Acknowledgements

6. References

Dossin I.A., Dossin T.A., Charvet J., Cocherie A., Rossi P. (1993) Single-Zircon dating by step wise Pb-evaporation of Middle Proterozoic magmatism in the Espinhaço Range, southeastern São Francisco craton (Minas Gerais-Brazil). An. II Simp. Craton São Francisco, Salvador, p.39-42.

Giuliani G., Groat L.A., Marshall D., Fallick A.E., Branquet, Y. (2019) Emerald Deposits: A Review and Enhanced Classification. Minerals, 9, 105, p.2-63. doi:10.3390/min9020105www.

Frezzotti M.L., Tecce F., Casagli A. (2012) Raman spectroscopy for fluid inclusion analysis. Jour. of Geochem. Exploration, 112, p.1-20.

Horn A. H., Leal, J.M., Fuchs Y. (2011) Geochemistry of chromium-rich minerals in the host rocks of the Capoeirana emerald deposits (Nova Era district, Minas Gerais, Brazil). In *Memorias* 14th Colombian Geological Congress, Medellin, 1, p.271-272.

Hurai V., Huraiova M., Slobodnik M., Thomas R. (2015) Geofluids-Development in Microthermometry, Spectroscopy, Thermodynamics and Stable Isotopes. Elsevier, 504p.

Lamadrid H.M., Moore L.R., Moncada D., Rimstidt J.D., Burruss R.C., Bodnar R.J. (2017) Reassessment of the Raman CO_2 densimeter. Chemical Geology, 450, p.210-222.

Leal, J.M. (1998) Estudo das inclusões fluidas em esmeraldas e quartzos associados do garimpo de Capoeirana, Nova Era, MG. UFMG, Belo Horizonte, Msc. Thesis, 154p.

Lynch E.P., Constanzo A., Feely M., Blamey N.G.F., Pironon J., Lavin P. (2014) The Piteiras emerald mine, Minas Gerais, Brazil: fluid – inclusion and gemological perspectives. Min. Mag. 78, 7, p.1571-1587

Machado G.A.A. (1994) Geologia da região e aspectos Genéticos da jazida de esmeraldas de Capoeirana e Belmonte, Nova Era – Itabira, MG. IGC/USP, São Paulo, Msc Thesis, 134p.

Morteani G., Silva L.J.H.D., Couto P. (1990) Origen of emerald deposits of Brazil. Mineral. Deposita, 25, p.7-64.

Ollier N., Fuchs Y., Leal J.M., Horn A.H., Rossano S., Noirfontaine M.N.de. (2011) Cr^{3+} optical properties of Brazilian beryl and chrysoberyl (alexandrite and emerald). In *Anais:* 7th European Conference on Mineralogy and Spectroscopy (ECMS 2011) - Potsdam, 1, p.55.

Pintea I., Horn A.H. (2019) First qualitative observations and interpretation of fluid and melt inclusions from Capoeirana and Nova Era emerald deposits, Minas Gerais, Brazil. In *Terra Nostra:* 25th Latin-American Colloquium of Geosciences - Hamburg, 1, p.72.

Ribeiro P.A. (2006) Geologia e controle estrutural dos corpos mineralizados em esmeraldas do Garimpo de Capoeirana, Nova Era/MG. Msc. Thesis, Federal University of Ouro Preto, Ouro Preto, 128p.

Ribeiro-Althoff A.M., Cheilletz A., Giuliani G., Féraud G., Barbosa Camacho G., Zimmermann J.L. (1997). Evidences of two periods (2 Ga and 650-500 Ma) of emerald formation in Brazil by K-Ar and Ar dating. Int. Geol. Rev., 39, p.924–937.

Schorscher H.D. (1992) Arcabouço petrográfico e evolução crustal de terrenos pré-cambrianos do sudeste de Minas Gerais: Quadrilátero Ferrífero, Espinhaço Meridional e domínios granito-gnáissicos adjacentes. IGC/USP, São Paulo, Habil. Thesis, 274p.

Schwarz D. (1987) Emerald – Inclusões em gemas. UFOP, Imprensa Universitária: 439p. CDU-553.832.

Souza J.L. (1988) Mineralogia e Geologia da Esmeralda da Jazida de Itabira – Minas Gerais. IGC/USP, São Paulo, Msc. Thesis, 192p.

Thomas R., Davidson P. (2016) Revisiting complete miscibility between silicate melts and hydrous fluids, and the extreme enrichment of some elements in the supercritical state - Consequences for the formation of pegmatite and ore deposits. Ore Geol., Rev., 72, p.1088-1101.

Williamson B.J., Stanley C.J., Wilkinson J.J. (1997) Implications from inclusions in topaz for greisenisation and mineralisation in the Hensbarrow topaz granite, Cornwall, England. Contrib. Mineral. Petrol., 127, 1/2, p.119-128.

*** Ruff database: https://rruff.info/

POTENTIAL OF GAMMA-RAY SPECTROMETRY AND SENTINEL-2A DATA TO MAP P-Li-Be CONTENTS FROM EASTERN BRAZILIAN PEGMATITIC PROVINCE.

**Helena Saraiva Koenow PINHEIRO[1], Fernando Machado de MELLO[1], Essaid BILAL [2*],
Júlio César Lopes da SILVA[3], Teresa Rocco Pereira BARBOSA[1]**

[1] Universidade Federal Rural do Rio de Janeiro (UFRRJ);
[2] Ecole Nationale Supérieure des Mines de Saint-Etienne (ENSM-SE);
[3] Universidade Federal do Rio de Janeiro (UFRJ);
[*] corresponding author: bilalessaid@gmail.com

Abstract: The goal of this study was to the characterization of spectral patterns of pegmatites LCT-Type occurrences to support the application of machine learning models at their prospection. To attend the goals the study was based on airborne gamma-ray spectrometric data, Sentinel-2 MSI data, and numerical terrain models to represent landscape morphometric patterns, gather with true field data. Airborne gamma-ray data were processed at Oasis Montaj[TM] (Geosoft) v. 9.4 by using Minimum Curvature interpolation method to create maps with a spatial resolution of 100 m to represent K (%), eTh (ppm), and eU (ppm), ratios between the elements, additionally, the ternary composition map (Red-Green-Blue) and total content of the three elements (K, eTh and eU). Sentinel-2 MSI data were processed at QGIS to create a band radius, with 20 m of spatial resolution. Numerical terrain models were created from a digital elevation model generated in ArcGIS Desktop by *Topotoraster* tool, and the derivate attributes in the SAGA-GIS open-source software. Numerical and spectral data were integrated with field data and posteriorly processed in R and RStudio free open source software (FOSS) the Pearson's correlation. At the same FOSS software multiple linear regression (MLR), boosted regression trees (BRT) and random forest (RF) models were applied to predict Li, Be, P contents at the area. Better performance based on statistical indexes and model generalization was observed to RF models. Regarding Sentinel 2A data for P_2O_5 and Li, several bands and indexes showed significant correlations. At the present study only Be presented correlation with gamma-ray data.

Keywords: pegmatites LCT-Type, airborne gamma-ray spectrometric data, Sentinel-2 MSI data, ArcGIS, randomForest.

1. Introduction

The mineralized pegmatite bodies present restricted occurrence in terms of area and general difficulties to access belt-like deposits embedded at different kinds of rocks, being a challenge for geologists and prospectors (Vikström et al., 2013). Most of the pegmatite bodies present a strong structural control and occurrence as tabular geometry, but they vary widely regarding sizes (centimeters to meters) and shapes (lenticular, ellipsoid, or even irregular).

It is well-known that gamma-ray spectrometric data are useful to relate field data and air-bone spectrometric data that aid in mapping structural and geological domains (Araújo Neto et al., 2018; Silva et al., 2010). Uranium (U), Thorium (Th), and Potassium (K) channels are combined in-band ratios and ternary maps highlighting anomalies that can be related to pegmatite bodies (Silva et al., 2010; Eberle et al., 2010). The integration of geophysical data and automatized unsupervised classification were successfully applied to map pegmatites fields (Eberle et al., 2010; Teixeira et al., 2006; Cardoso-Fernandes et al., 2018; Cardoso-Fernandes et al., 2019). In general, these studies are developed by using multispectral sensors with spectral bands, and indexes, which are related to Li minerals' spectral signatures (Perrotta et al., 2005; Mendes et al., 2017). Other techniques of supervised classification having pegmatites bodies as a target, were presented by Perrotta et al. (2005), based on spectral image data and reference spectral data from mapped pegmatites, using algorithms as Spectral Angle Mapper (SAM), Mixture-Tuned Matched Filtering (MTMF), Spectral Feature Fitting (SFF), originally proposed by Kruse et al. (1993), Boardman et al. (1995), Clark et al. (1990), respectively.

Considering all challenges in map pegmatites, and the importance of study area to mineral prospection, the study goal is to map chemical elements related to the geochemical signatures of LCT pegmatite types and combine them through cluster classification to identify potential areas with the occurrence of pegmatitic fields. The approach here purposed gather remote sensing and geophysical, morphometrical data allied with field data to build numerical models to explain element contents variability that can aid mineral prospection of LCT pegmatite bodies at the Eastern Brazilian Pegmatitic Province (Bilal et al., 2000a; Bilal et al., 2000b, 2012; Nalini 1997; Nalini et al., 2018).

3. Material and methods

3.1. Local Geology (the northwest portion of the Conselheiro Pena - Minas Gerais chart)

The main geological units in the study area are described as follows (Fig. 1):
- Alluvial and Colluvial Deposits, alluvial and colluvial Cenozoic Deposits (QHa).
- Sandy and Clayic Deposits, eluvial Cenozoic deposits (TQ).
- Granitic Dikes (εOpm), post-tectonic fine granites with biotite and muscovite.
- Urucum Granites (Nu), tardi- to post-tectonic porphyritic granites, whitish, coarse grains. It hosts
  pegmatite bodies small to large size.
- Palmital Granites (Np), tardi to post-tectonic white to grayish granites, fine to medium grains, locally
  porphyritic, it hosts pegmatite bodies.
- Córrego da Onça Granites (Non), tardi- to post-tectonic grayish to white granites, medium to coarse grains,
  with biotite, muscovite, and tourmaline. Incipient to well-marked orientation.
- Galiléia Tonalites (Ng), syn to tardi-tectonic.
- São Tomé Formation (Nst), plagioclase-quartz-muscovite schists, it hosts pegmatite bodies.
- João Pinto Formation (Njp), quartzites with fine to coarse grains.
- Pocrane Complex (APpc), finely banded gneiss.
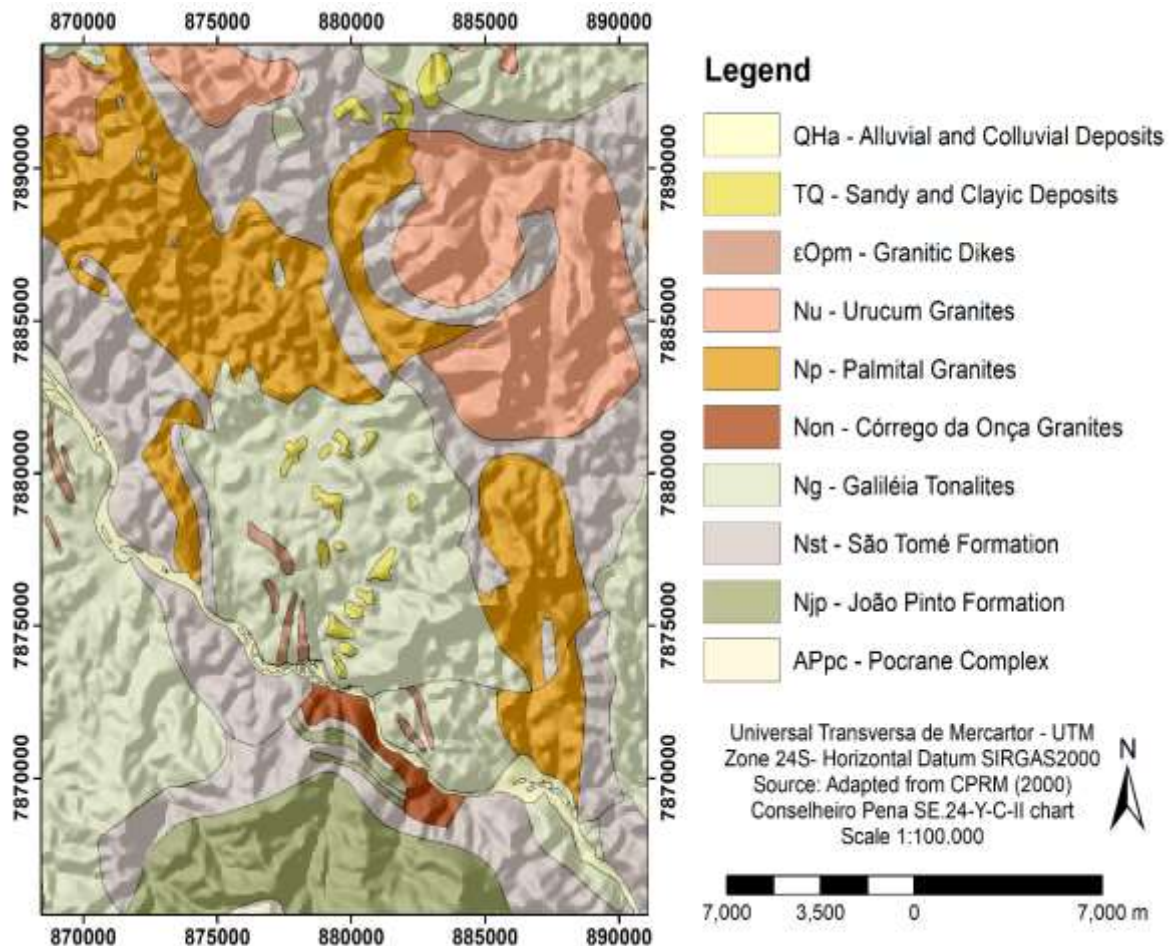
Fig.1. Local geology from the study area. Adapted from CPRM (2000)

3.2. Database acquisition and processing

3.2.1. Sentinel 2-MSI data
The images used were captured by the Sentinel-2A MSI (MultiSpectral Instrument) sensor on November 05-2019 acquired in the ESA Sentinels Scientific Data Hub through the Earth Explorer platform (available at: https://earthexplorer.usgs.gov/). Bands are available with which radiometric and geometric corrections (including orthorectification and recording) and are available in TOA Reflectance (reflectance at the top of

the atmosphere, or apparent reflectance). The data were extracted to the boundaries of the study area, processed at the QGIS Desktop v.2.12.3-Lyon, which is an open-source software (available at: www.gnu.org).

Next, spectral indices to highlight peculiar mineral reflectance were computed, as purposed by Sabins (1999), Ali and Pour (2014), and Cardoso-Fernandes et al. (2019).

Once all bands and indexes were processed the Point sampling tool was used to extract the values to the respective sample points, assigning indexes and band values to each sample point used at the machine-learning procedures described further.

3.2.2. Air-bone geophysical data

Air-bone radiometric and magnetometric data were from Projeto Leste (Area 12) executed by *Companhia de Desenvolvimento Econômico de Minas Gerais* (CODEMIG) and *Companhia de Pesquisa de Recursos Minerais* (CPRM) along the years 2007 and 2008. The data were collected with an interval of 500 m between flight line, flight direction N30W, 100 m flight height, and 0.1 second interval between measurements. The geophysical data (xyz format) were processed in Oasis Montaj 9.8, where a geodatabase (gdb format) was created respecting the boundaries of the study area and the projection system used to all georeferenced data (Universal Transversa Mercator – UTM, Zone 24S, horizontal datum SIRGAS2000).

The gamma-ray spectral data was interpolated by using the minimum curvature method (Briggs, 1974) where regular grids with 100 m spatial resolution were created for the channels eU (ppm), eTh (ppm), eK (%). Beyond the elements channels and the total content (CT), the ratios between then (Th/K; U/Th; U/K) were also calculated. The minimum curvature method provides smoothing surface values closest to the original value.

Regarding the magnetometric data, the interpolation was executed adopting the bidirectional interpolation method (BIGRID) that resulted in the anomalous magnetic field (CMA) map (nT). The BIGRID is widely used to interpolate data originally collected in lines and highlights perpendicular trend among the line direction. From the CMA map, the analytical signal amplitude filter (ASA) was applied (nT/m). The total horizontal gradient (GHT) and the vertical gradient (Gz) were also created after reduction to the pole (RTP) procedure (nT/m, both). The inclination of analytical signal (ISA) was also calculated (rad) from the gradient maps.

Similar to the procedure performed to assign the values from Sentinel 2A bands and indexes to the sample points, all the geophysical data were imported in ArcGIS Desktop v.10.3. software and the Extract Multivalues to Point tool was applied to refer the correspondent values from the radiometric and magnetometric data to the sampled points.

3.2.3. Topographic data

The primary and secondary covariates derived from a Digital Elevation Model (DEM) were used to represent terrain characteristics, which is well-known to be helpful for mapping purposes once they can highlight features as faults surfaces, different textures, and rugosity, as an example.

DEM was created from primary elevation data obtained from the *Conselheiro Pena* Topographic chart (SE-24-Y-C-II), at scale 1:100.000, obtained from the Brazilian army database (*Banco de Dados Geográficos do Exército Brasileiro* – BDGEx; available at: https://bdgex.eb.mil.br/). To create the numerical continuous surface model, with 100 m spatial resolution, the interpolation procedure was performed using ArcGIS Desktop v.10.3 program (*TopotoRaster*). Spurious depressions resulting from the interpolation procedure were corrected in order to obtain a hydrologically consistent model by using the Fill sinks tool, available at the Hydrology toolbox. Several covariates were derived having the DEM as input by using the Terrain Analysis modules of SAGA-GIS software.

3.3. Modelling spatial variability of elements contents

To model the spatial variability of chemical elements (Li, Be, P) a sequence of procedures was adopted. After the selection of the pathfinder elements and removing outlier samples the remaining samples (47) were used to train the algorithms.

In sequence, the potential covariates (independent variables) that present correlation with each one of the predicted elements (Li, Be, P), were selected through a Pearson's correlation analysis, at 95% significance level, executed by using "corrplot" package in R environment (R Development Core Team, 2013). The final covariates dataset was obtained from these procedures and used in the machine-learning steps. The models

applied to map the selected elements were multiple linear regression (MLR), gradient boosted machine (GBM), and random forest (RF).

Multiple linear regressions (MLR) have been widely used to predict the response of a dependent variable from a set of independent variables, as a function of the correlations between them.

RF is a non-parametric technique developed as an extension of CART (Classification and Regression Trees) systems (Breiman, 2001), to improve the performance of the predictors. The Random Forest models (RF) were executed in the R environment through the "randomForest" package (Liaw and Wiener, 2002). To implement the RF model, three parameters are necessary: the number of trees in the forest (ntree); the minimum amount of data in each terminal node (nodesize); and the number of covariates used in each tree (mtry) (Liaw and Wiener, 2002). The ntree value was set to the system default (500) (Grimm et al., 2008). The nodesize value was set to five for each terminal node, and the mtry value chosen in this study was according to Liaw and Wiener (2002), which propose an amount corresponding to the root square of the total number of predictor variables.

Both RF and BRT were considered tree-based models with great performance once they repeatedly fit many decision trees to improve the accuracy of the model. The main difference between them relies on the way that the data to build each tree is selected. They both take a random subset of all data for each new tree that is built, but while RF uses the bagging method, which means that each occurrence has an equal probability of being selected in subsequent samples, BRTs use the boosting method in which the input data are weighted in subsequent trees.

The model's assessment to choose the best map to represent the selected elements comprised the comparison of the three methods (MLR, RF, BRT) regarding statistical indexes as the Root Mean Square Error (RMSE) and coefficient of determination (R2), as well the coherence of the models' generalization to the entire area.

4. Results and discussion

Gamma spectrometry records the lithological diversity caused by the variation in the concentration of radioelements K, U, and Th, and their relationship with hydrothermal events, as observed by Araújo Neto et al. (2018). At the present study only Be presented correlation with gamma-ray data (Fig. 2).

A similar procedure, as presented in Figure 2, allowed to identify the relations among Li, Be, and P, and the remote sensing variables from Sentinel 2A data. Relations between pegmatite occurrences and Sentinel 2A have been previously related by Sabins (1999), Ali and Pour (2014), and Cardoso-Fernandes et al. (2019), where those authors propose a particular combination of band ratios to highlight Li-bearing minerals, as well, different kind of oxides and clay minerals. Among the covariates from Sentinel 2A data, both index Ferric Iron and Iron oxides, purposed by Cardoso-Fernandes et al. (2019) and Sabins (1999), respectively, did not present any significative correlation, as well bands 11 and 12.
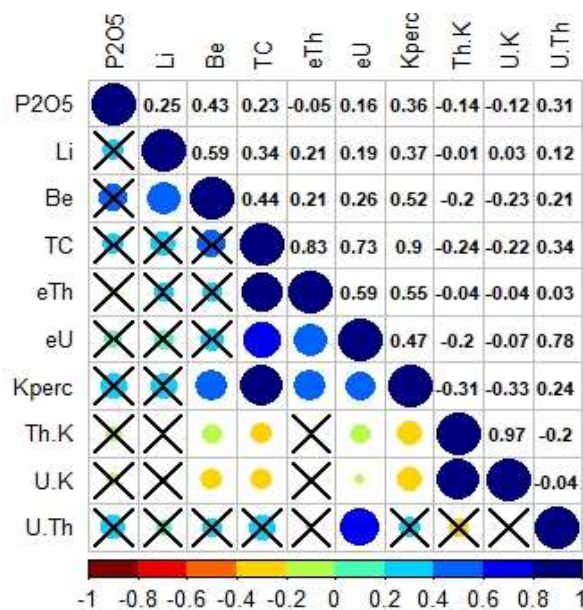
Fig. 2. Pearson's correlation matrix between Li, Be, P with gamma-ray spectrometric data.

Although, the index derived from band 11, purposed by Ali and Pour (2014), presented a correlation with all elements focused on this study, except for P_2O_5. For P_2O_5 and Li, several bands and indexes showed significative correlations, varying between 0.1 to 0.5 (positive or negative). Differently from Cardoso-Fernandes et al. (2019), indexes purposed to identify Li-bearing minerals (spodumene and lepidolite) did not show significative correlation with the Li values from the samples.

From the initial dataset with 52 covariates, some of them did not approach as a goal of this study (magnetometric and topographic), after correlation analysis with geochemical data was possible to remove nine covariates, and the remaining ones were combined at different sets to build the models respecting the correlations pointed out by geochemical data analysis, for each predicted element.

To model the spatial variability of all elements considered the respective set of correlated covariates were used to build the models tested (MLR, BRT, RF) and the statistical indexes (Table 1).

Among the three models tested, the BRT presented a better performance for the training procedure to all elements tested. However, at the validation procedure for most of the elements, the RF models presented a better performance, based on the statistical indexes.

Table 1. Models tested (MLR, BRT, RF) and the statistical indexes.

Models	Indexes	Li	Be	P_2O_5
BRT	R^2	0.81	0.93	0.75
	RMSE	18.902	0.245	0.042
	R^2(CV)	0.16	0.38	0.25
	RMSE(CV)	42.616	0.770	0.079
MLR	R^2	0.72	0.88	0.73
	RMSE	22.718	0.323	0.044
	R^2(CV)	0.12	0.11	0.01
	RMSE(CV)	58.592	3.670	3.443
RF	R^2	0.19	0.41	0.29
	RMSE	39.280	0.728	0.072
	R^2(CV)	0.18	0.41	0.30
	RMSE(CV)	39.540	0.729	0.071

BRT= Boosted Regression Trees; MLR= Multiple Linear regression; RF= Random Forest; RMSE= root-mean-square error; CV= cross validation

In this sense, MLR models showed the worse fit to the models created based on the sample dataset. Models based on linear regression probably will require a larger dataset to better fit the models, when compared with tree-based models (Pinheiro et al., 2018). In addition, is common to observe in the model generalization that the digital map created from MLR models shows values that go beyond the breadth of the input data, which sometimes are unreal and impossible to observe in nature. According to the resulting maps from all models tested (Fig. 3), the models tested to represent Li and Be derived from RF models were chosen once they presented better generalization for the entire area, in addition, they also have better performance regarding the statistical accuracy indexes, and for these reasons were selected to represent those elements (Fig. 3).

A general trend for the higher contents of Li and Be can be observed closer to granites from Urucum suite at the upper high portion of the area. The model generalization for P_2O_5 showed irregular patterns controlled by topographic features and remote sensing data derived from Sentinel 2A. Based on the map generalization assessment is possible to conclude that the maps created from the RF and BRT models showed better coherence with natural landscape patterns and geological features.
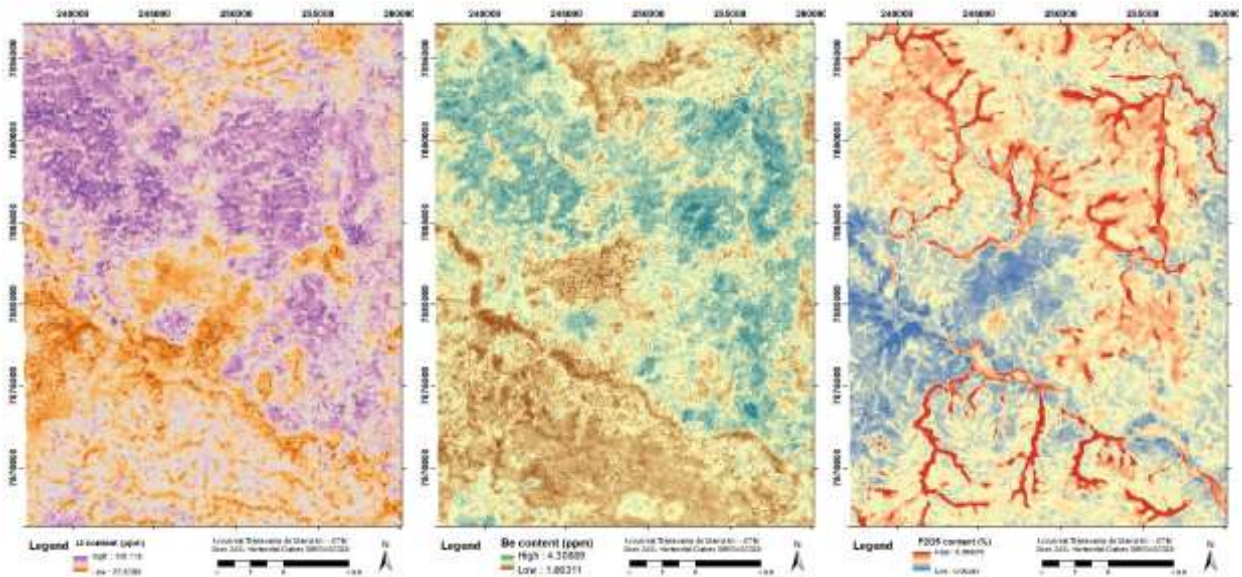
Fig. 3. Best map obtained to represent the spatial variability of Lithium, Beryllium, and Phosphorous from the tree models tested.

5. Conclusion

The approach proposed could satisfactorily address the main goal of the study that was to spatialize Li, Be, and P contents through data mining procedures, that can point out the propitious areas for pegmatite prospection. The strategy to reduce the covariates used to map each selected element by using geochemical data correlation analysis was important to reduce the model's complexity, in this sense providing more efficiency at the machine-learning procedures. In general, the Sentinel and radiometric data were related to all elements tested.

The maps created to represent all elements showed better performance when derived from tree-based models (Boosted Regression Trees and Random Forest models) when compared with linear regression models according to the statistical accuracy indexes and visual assessment, once showed for the last one, values varying beyond that one's found in nature. In general, the models presented a low performance for Li, (R^2 values lower than 0.3). To P_2O_5, those models showed medium performance (R^2 between 0.3-0.5).

Despite the limitations of the input data, regarding the scale of covariates and the reduced number of geochemical data, further work should address fuzzy and neural network analysis to improve the elements models accuracy, as well address the elements clustering to identify mineralized pegmatites bodies.

Additionally, efforts to gather hyperspectral satellite data with spectrometric and radiometric field data should also be addressed to improve the machine-learning approach to select areas for mineral prospection.

References
Ali A., Pour A. (2014) Lithological mapping and hydrothermal alteration using Landsat 8 data: a case study in Ariab mining district, red sea hills, Sudan. Int. J. Basic Appl. Sci. 3 (3) p. 199-208.

Araújo P. J., Lisboa V. A. C., Oliveira J. R. S. (2017) Mapeamento geológico do Pegmatito Alto do Tibiri; aspectos estruturais e mineralógicos. Revista Principia, v. 1, n. 33, p. 29-36.

Araújo Neto J. F. de, Santos G. L., Albuquerque e Souza, I. M. B. de, Barreto S. de B., Santos L. C. M. de L., Bezerra J. P. S., Carrino, T. A. (2018) Integration of remote sensing, airborne geophysics and structural analysis to geological mapping: a case study of the Vieirópolis region, Borborema Province, NE Brazil. Geol. USP, Sér. cient., São Paulo, v. 18, n. 3, p. 88-103.

Bilal E., Horn A. H., Moutte J. (2000a) Zur Mineralogie und chemischen Zusammensetzung der Pegmatite in Ostbrasilien. Münchener Geologische Hefte, Vol. A28, p. 91-97.

Bilal E., Horn H. Nalini Jr. H., de Mello F. M., Correia-Neves J. M., Giret A., Moutte J., Fuzikawa K., Fernandes M. L. (2000b) The Neoproterozoic Granitoid Suites in Southeastern Brazil. Revista Brasileira de Geocience, Vol. 30, No. 1, p. 51-54.

Bilal E., Horn A. H., de Mello F. M. (2012) P-Li-Be Bearing Pegmatites of the South East Brazil. International Journal of Geosciences, 3, p. 281-288. doi:10.4236/ijg.2012.32029.

Boardman J. W., Kruse F. A., Green R. O. (1995) Mapping target signatures via partial unmixing of AVIRIS data. In: Summaries, Fifth JPL Airborne Earth Science Workshop. JPL Publication 95-1, v. 1, p. 23-26.

Breiman L. (2001) Random Forests. Technical report for Version 3. (Available in: http//oz.berkeley.edu/users/breiman/randomforest2001.pdf, Accessed at: 12/28/14).

Briggs I. C. (1974) Machine contouring using minimum curvature. Geophysics, 39(1), p. 39-48. https://doi.org/10.1190/1.1440410

Cardoso-Fernandes J., Lima A., Teodoro A.C. (2018) Potential of Sentinel-2 Data in the Detection of Lithium (Li)-bearing Pegmatites: a Study Case. SPIE Remote Sensing, SPIE, pp. 15.

Cardoso-Fernandes J., Teodoro A. C., Lima A. (2019) Remote sensing data in lithium (Li) exploration: A new approach for the detection of Li-bearing pegmatites. Int J Appl Earth Obs Geoinformation 76. p.10–25. https://doi.org/10.1016/j.jag.2018.11.001

Clark R. N., Gallagher A. J., Swayze G. A. (1990) Material absorption band depth mapping of imaging spectrometer data using the complete band shape least-squares algorithm simultaneously fit to multiple spectral features from multiple materials. In: Proceedings of the Third Airborne Visible/Infrared Imaging Spectrometer (AVIRIS) Workshop. JPL Publication 90-54, p. 176–186.

Companhia de Pesquisa de Recursos Minerais – CPRM (2000) Projeto Leste: Folhas Conselheiro Pena/São Gabriel da Palha - SE.24-Y-C-II and SE.24-Y-C-III (parte), escala 1:100.000. Maria Jose Resende Oliveira – Belo Horizonte: SEME/COMIG/CPRM. 83p, v.23; mapa e anexos (Serie Programa de Levantamentos Geológicos Básicos do Brasil – PLGB).

Eberle D. G., Daudi E. X. F., Muiuane E. A., Pontavida A. M. (2010) Mapeamento aero-geofísico de pegmatitos mineralizados na Província Pegmatítica de Alto Ligonha, no norte de Moçambique. Revista Brasileira de Geociências. 40(4), p.527-536.

Grimm R., Behrens T., Märker M., Elsenbeer H. (2008) Soil organic carbon concentrations and stocks on Barro Colorado Island - digital soil mapping using Random Forests analysis. Geoderma. v.146. p.102-113.

Kruse F. A., Lefkoff A. B., Boardman J. B., Heidebrecht K. B., Shapiro A. T., Barloon P. J., Goetz A. F. H. (1993) The Spectral Image Processing System (SIPS) - Interactive Visualization and Analysis of Imaging spectrometer Data. Remote Sensing of Environment, v. 44, p. 145–163.

Liaw A., Wiener M. (2002) Classification and regression by random Forest. R News. v.2, n.3, p.18-22.

Mendes D., Perrotta M. M., Costa M. A. C., Paes V. J. C. (2017) Mapeamento espectral para identificação de assinaturas espectrais de minerais de lítio em imagens ASTER (NE/ MG). Anais Do XVIII Simpósio Brasileiro De Sensoriamento Remoto p. 5273–5280.

Nalini Jr. H.A. (1997) Caractérisation des suites magmatiques néoprotérozoïques de la region de Conselheiro Pena et Galiléia (Minas Gerais, Brésil). Etude géochemique et structurale des suites Galiléia et Urucum et relations avec les pegmatites à éléments rares associées. Tese de Doutoramento, Saint Etienne, Ecole des Mines de Saint Etienne et Ecole des Mines de Paris.

Nalini Jr. H. A., Machado R., Endo I., Bilal. E. (2008) A importância da tectônica transcorrente no alojamento de granitos pré a sincolisionais na região do vale do médio Rio Doce: o exemplo das suítes graníticas Galiléia e Urucum. Revista Brasileira de Geociências. 38(4), p. 741-752.

Perrotta M. M., Souza Filho C. R., Leite C. A. S. (2005) Mapeamento Espectral De Intrusões Pegmatíticas Relacionadas a Mineralizações De Lítio, Gemas E Minerais Industriais Na Região Do Vale Do Jequitinhonha (MG) a Partir De Imagens ASTER. Anais Do XII Simpósio Brasileiro De Sensoriamento Remoto p. 1855–1862.

R Development Core Team. (2013) R: A Language and Environment for Statistical Computing. R Foundation for Statistical Computing, Vienna, Austria. (Available in: http://www.R-project.org/isbn 3-900051-07-0, Accessed at: 05/08/2015).

Sabins F.F. (1999) Remote sensing for mineral exploration. Ore Geol. Rev. 14 (3), p. 157–183.

Silva S. M. P. da, Crósta A. P., Ferreira F. J. F., Beurlen H., Silva A. M., Santos L. F. dos. (2010) Espectrometria de raios gama de granitos pegmatíticos da Província Pegmatítica da Borborema (PPB), Nordeste do Brasil. Revista Brasileira de Geofísica 28(4), p.673-690.

Teixeira A. de A., Silva A. M., Pires A. C. B., Moraes R. A. V. de, Souza Filho C. R. de (2006) Integração e análise de dados aerogeofísicos por meio da aplicação de técnicas de processamento digital de imagens e classificação não supervisionada: o exemplo do Greenstone Belt Rio das Velhas, quadrilátero ferrífero, MG. Rev. Bras. Geof. [online]. vol.24, n.4, p. 559-572.

Vikström H., Davidsson S., Höök M. (2013) Lithium availability and future production outlooks. Applied Energy, 110, p. 252–266. doi:10.1016/j.apenergy.2013.04.005

NEW SEM-EDS AND EPMA DATA ON TE-BEARING MINERALS FROM SĂCĂRÂMB, APUSENI MOUNTAINS, ROMANIA

Sergiu DRĂGUŞANU[1], Mădălina-Paula ANDRII[1], Călin Gabriel TĂMAŞ[1*]

[1]Babeş-Bolyai University, 1 Kogălniceanu street, 400804 Cluj Napoca, România
[*]corresponding author: *calin.tamas@ubbcluj.ro*

Abstract: Nagyagite, native tellurium and altaite were identified by the means of SEM-EDS analyes and electron probe microanalyses in an ore samples from Săcărâmb ore deposit, South Apuseni Mountains. The new analytical data confirmed the chemical heterogeneity of the nagyagite at the level of individual lamellae and allowed the identification of native tellurium and altaite inclusions hosted by nagyagite. The studied nagyagite belongs in the same time to the As-poor nagyagite and the Au-poor nagyagite types defined previously within Săcărâmb ore deposit.

Keywords: nagyagite, native tellurium, altaite, SEM-EDS, EPMA, Săcărâmb, Apuseni Mountains

1. INTRODUCTION

The mining of Săcărâmb ore deposit started during the late XVIIIth century and several decades perplexed the mineralogists and the miners of the period due to the significant quantity of gold metal obtained from an ore without native gold. This was the first step towards the discovery of the tellurium, of the tellurides and of the economic potential of the Au- and Ag-tellurides ore deposits. Săcărâmb is the type locality of krennerite, petzite, stützite, nagyagite, muthmanite, and museumite (Udubaşa et al., 1992; Şimon et al., 1994; Ciobanu et al., 2004; Bindi and Cipriani, 2004; etc.). Apart tellurides, the ore from Săcărâmb invariably contains sulfosalts. The mineralogy study conducted by Ciobanu et al. (2004) revealed the presence of sulfosalts from tetrahedrite-tennantite, bournonite-seligmanite, and Pb-As/Sb groups. Recently, Dincă and Popescu (2016) and Dincă (2019) identified several other sulfosalt groups at Săcărâmb, *e.g.*, stannite, lillianite, sartorite, as well as Ag-, Tl-, and Te-Bi bearing sulfosalts in close association with tellurides and sulfotellurides.

Nagyagite is a sulfotelluride (Şimon et al., 1994), and apparently is the most common Te-bearing mineral from Săcărâmb (Ciobanu et al., 2004; Dincă, 2019). The name of the mineral was given after the Hungarian name of the village of Săcărâmb, known as Nagyag. According to Ciobanu et al. (2008), the first mention of nagyagite was by Scopoli in 1769 who described it as "*minera aurifera nagyagensis*", while the real name of the mineral was given in 1845 by Haidinger (Ciobanu et al., 2008).

The nagyagite from Săcărâmb was studied by several authors throughout the time. The most recent studies with contributions on the chemical composition of nagyagite were made by Şimon et al. (1994), Ciobanu et al. (2004 and 2008), and Dincă (2019). The present contribution brings new SEM-EDS and EPMA data on nagyagite, native tellurium and altaite from Săcărâmb.

2. REGIONAL SETTING

Săcărâmb ore deposit is located on the southern border of the South Apuseni Mountains, which are part of a regional tectonic puzzle comprising Tisia (Csontos et al., 1992) and ALCAPA tectonic blocs, which are separated by the so-called *mid-Hungarian Line* that is located in the northern sector of the Carpathian - Pannonian region (Csontos, 1995; Fodor et al., 1999). Opposite sense rotations took place between ALCAPA and Tisia lithospheric blocks during Early to Middle Miocene, *e.g.*, Tisia block underwent a clockwise rotation and ALCAPA a counterclockwise rotation (Panaiotu, 1998; Márton et al., 2000). The Apuseni Mountains, as part of the Tisia block, took part in the clockwise rotation while the south-western area of the same tectonic block, *i.e.*, Mecsek and Villany Mountains did not rotate (Csontos et al., 2002). Accordingly, graben-like basins were generated within the Apuseni Mountains and calc-alkaline magmatism developed (Royden, 1988; Săndulescu, 1988; Balintoni and Vlad, 1998; Seghedi. 2004, etc.).

The Neogene volcanic activity from the South Apuseni Mountains took place between 14.7 Ma and 7.4 Ma and after an inactivity period of almost 6 Ma a final volcanic pulse occurred 1.6 Ma ago (Roşu et al., 2004a). The genesis of the magma bodies that controlled the Neogene volcanic activity was considered to be the decompressional melting of a source located at the limit between the lower crust and the upper lithospheric mantle during the clockwise rotation of the Tisia block in Miocene times, and was

triggered by the local extensional setting (Seghedi et al., 2004). During the above mentioned time span calc-alkaline and adakitic-like magmas were the most common ones while alkaline magmas were minor (Seghedi et. al., 2007). The Neogene volcanic rocks are located along two main alignments, *e.g.*, the first one striking WNW-ESE is about 100 km in length between Buteni and Zlatna, and the second one, striking NNE-SSW is about 60 km in length between Baia de Arieş and Deva (Roşu et al., 2001). According to Roşu et al. (2004a) there are four main volcanic areas, (*i*) Baia de Arieş - Roşia Montană - Bucium; (*ii*) Zarand - Brad - Zlatna; (*iii*) Băiţa - Săcărâmb; and (*iv*) Deva. As concerns the lithology of the Neogene volcanic rocks from the Apuseni Mountains, the andesites are the most common while the basaltic-andesites, dacites, and trachyandesites are subordinate (Ghiţulescu and Socolescu, 1941; Borcoş et al., 1972; Berbeleac, 1975; Savu et al., 1993; Roşu et al., 2004a, etc.).

Two main ore deposit types, *i.e.*, porphyry (Cu ± Au, Mo; Au-Cu), and epithermal (Au-Ag ± Te) are associated to Neogene volcanic activity. The porphyry copper deposits were interpreted during the 1980ies according to the Lowell and Guilbert's and the diorite models (Vlad, 1983; Boştinescu, 1984). However, more recent studies indicate the presence of gold rich porphyry deposits, *e.g.*, Colnic, Cireşata-Valea Garzii (Halga et al., 2010) and Bolcana (Ivăşcanu et al., 2018, 2019; Kulcsar et al., 2019). Low sulfidation, intermediate sulfidation, and high sulfidation epithermal ore deposits were recognized in South Apuseni Mountains during the last two decades (Berbeleac et al., 1995; Leary et al., 2004; Tămaş et al., 2006, etc.). According to Manske et al. (2004) and Wallier et al. (2006) the age of Au-Ag mineralization from Roşia Montană epithermal deposit ranges between 13.24±0.1 Ma and 12.71±0.13 Ma, being the oldest metallogenic event associated to the Neogene volcanic activity from South Apuseni Mountains. The most important metalogenic event as number of ore deposits and ore tonnage occurred in Barza area and ranges in age from 12.6 Ma to 10.5 Ma, while the last metallogenic event was between 9.5 Ma and 8.5 Ma and took place in Baia de Arieş (Roşu et al., 2004b).

3. GEOLOGY OF SĂCĂRÂMB ORE DEPOSIT

Săcărâmb was interpreted as epithermal low sulfidation Au-Te ore deposit by Ciobanu et al. (2004) and Cook et al. (2004) being unique among the other ore deposits from the Golden Quadrilateral due to the abundance of tellurides.

The ore deposit is located mainly within the central neck of a stratovolcano and consists of more than 230 veins concentrated on an area of about 1000 m²; the ore bodies developed to a depth of 600 m (Ciobanu et al., 2004). The stratovolcano formed during the Neogene volcanic activity and apart of the central neck it consists of four main andesite stocks, *i.e.*, Sarcău, Haitău, Frăsinata, and Săcărîmb, and several secondary smaller intrusives (Ianovici et al., 1976) (Fig. 1). The andesite stocks (necks) outcrop at the surface and are surrounded by volcanic lava flows. The intrusives pierced out the Faţa Băii sedimentary formation, which is partly covered by the lava flows (Fig. 1). The metamorphic basement outcrops on the southern border of the area (Fig. 1) and consists of sericite schists, chlorite schists, metarhyollites, and marbles.

The vein structures are concentrated within four main groups and are striking along two main directions, *i.e.*, Nepomuc and Magdalena are striking NE-SW and Longhin-Antilonghin and Erzbau are striking NW-SE (Ianovici et al., 1976). The ore deposit has an outstanding Au-Ag-Te character. However, at the ore deposit scale there is a vertical zonation with base metals-sulfosalts ± tellurides near the surface, abundant tellurides at the middle level, and base metals in the deep levels (Ciobanu et al., 2004). According to Căpraru (2004) the mineralogy of the ore in a simplified sequence is pyrite - alabandite - base metal sulfides - sulfosalts - gold/silver/and lead tellurides - quartz - rhodochrosite - carbonates ± clay minerals (glauch).

According to Udubaşa et al. (1992) the metal production from Săcărîmb ore deposit reached about 32 tones of gold and 50 tones of silver.

4. MATERIALS AND METHODS

The present study was carried out on an ore fragment from Săcărâmb composed of several metallic mineral lamellas hosted by rhodochrosite gangue. The ore sample is hosted by the Collection of Metallogeny, Department of Geology, University Babeş-Bolyai from Cluj-Napoca, Romania.
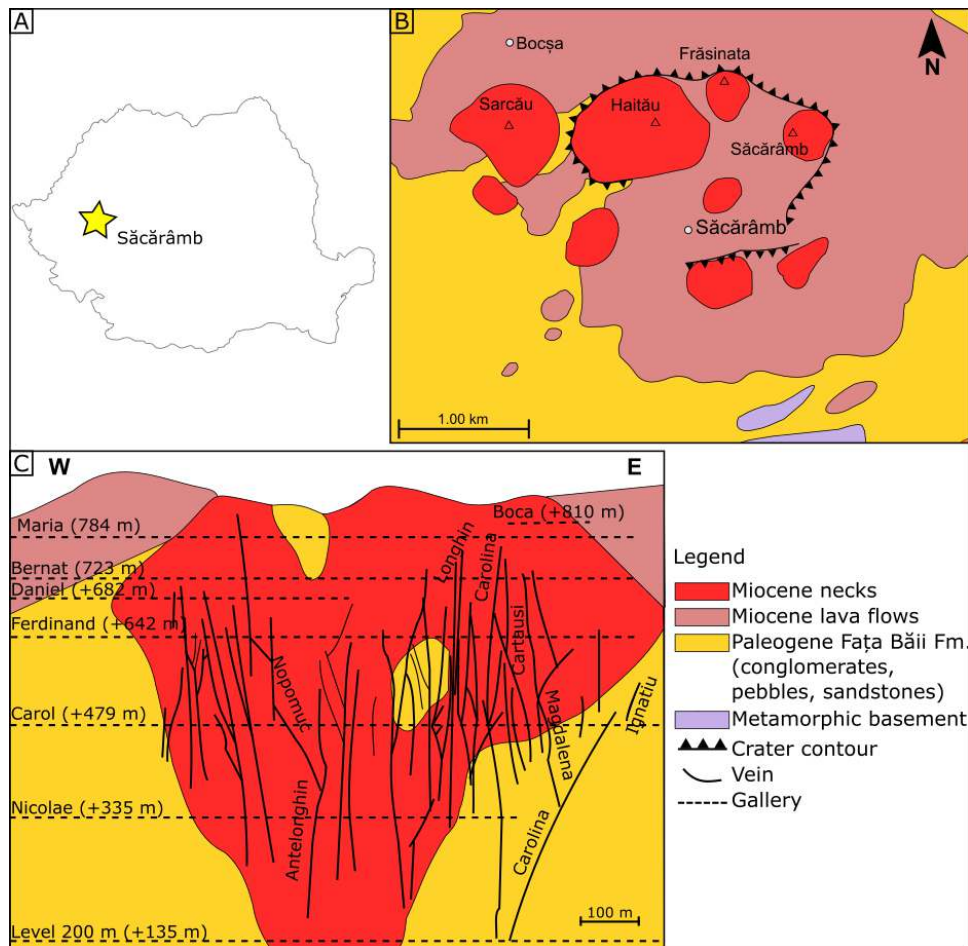
Fig. 1. Simplified geology of Săcărâmb area (a) and the location of the main veins and mining levels (Ciobanu et al., 2004 and 2008).

Reflected light optical microscopy study combined with scanning electron microscopy (SEM-EDS) and electron probe (EPMA) analyses allowed to acquire new mineralogical data on nagyagite, native tellurium and altaite from Săcărâmb ore deposit, Apuseni Mountains.

The SEM observations and SEM-EDS spectrum acquisition were made using a JEOL JSM-6360LV electron microscope with a voltage of 20 kV. The spectrum presented below all shown a carbon peak, which is due to the carbon coating of the polished section for technical reasons. The quantitative chemical data were acquired with a CAMECA SX50 device using an acceleration voltage of 25 kV, a beam current of 20 nA, with a surface of 3 x 3 micrometers of the analyzed area, and a counting time of 10 s for peaks and 5 s for background. As standard were used chalcopyrite for S and Cu; galena for Pb; cinnabar for Hg; pure metals for Au, Ag, Ge, Sb, and Te. The calculated detection limits (in wt %) are < 0.3 for Au, Ag, Pb; <0.2 for Ge, Te, Hg; and <0.1 for Cu, S, Sb. The SEM-EDS and EPMA data were gathered using the analytical infrastructure of the laboratory Géosciences Environnement Toulouse (GET – former LMTG), Observatoire Midi-Pyrénnées, Toulouse, France.

5. RESULTS

Under the microscope in plane polarized reflected light the nagyagite lamellas hosted by rhodochrosite gangue show pale gray color, medium to high reflectance and a distinct anisotropy. The nagyagite contains rare creamy-white inclusions, which are sometimes concentrated along the border of the lamellas. These inclusions have high reflectance exceeding that of nagyagite. Due to the small-size of these mineral inclusions their accurate identification by the means of optical microscope was not possible.

The mineralogy of nagyagite lamellas and of some inclusions hosted by nagyagite was validated by SEM-EDS and EPMA data. The preliminary SEM observations allowed gathering SEM-BSE images of the nagyagite lamellas hosted by rhodochrosite (Fig. 2). Each individual nagyagite lamellae have 1 to 2 cm in length and 200 to 500 micrometers in width (Fig. 2). At greater magnification and using fine contrast

33

mode it was possible to observe discrete chemical variation at the scale of nagyagite lamellae illustrated by different gray shades (Fig. 3). The variable chemistry at the scale of individual nagyagite crystal/lamellae was also confirmed by the acquired SEM-EDS spectra. As shown in Fig. 4, the nagyagite composition is variable as illustrated by the amplitude of Pb, Sb, Te and Au peaks.

Apart the creamy-white inclusions that are visible at optical microscopy scale, the SEM observations revealed the presence of small-scale black inclusions. The SEM-EDS spectrum of one such inclusion confirms its nature as native tellurium (Fig. 5). The creamy-white inclusions within nagyagite were also tested and their SEM-EDS semiquantitative chemical composition suggests its altaite composition.

Quantitative chemical analyses were carried out on nagyagite and the creamy-white inclusions, and the results are reported in Table 1. These analyses confirm that the creamy-white inclusions within nagyagite consist of altaite with an empirical formula close to the ideal one. Four point analyses were performed on a single lamellae of nagyagite (Table 1) and show slight chemical variation; however, the calculated chemical formulas are close to the ideal one.
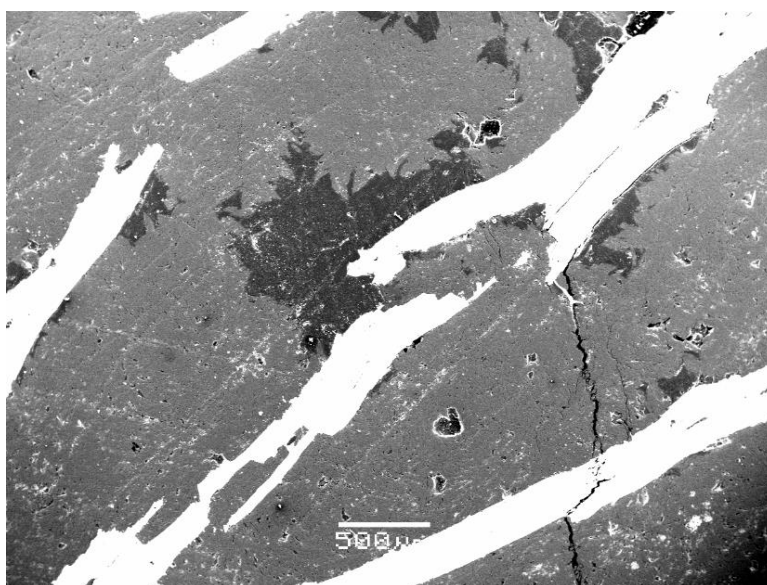
Fig. 2. Large-field SEM-BSE image of nagyagite lamellas hosted by rhodochrosite from Săcărâmb ore deposit.
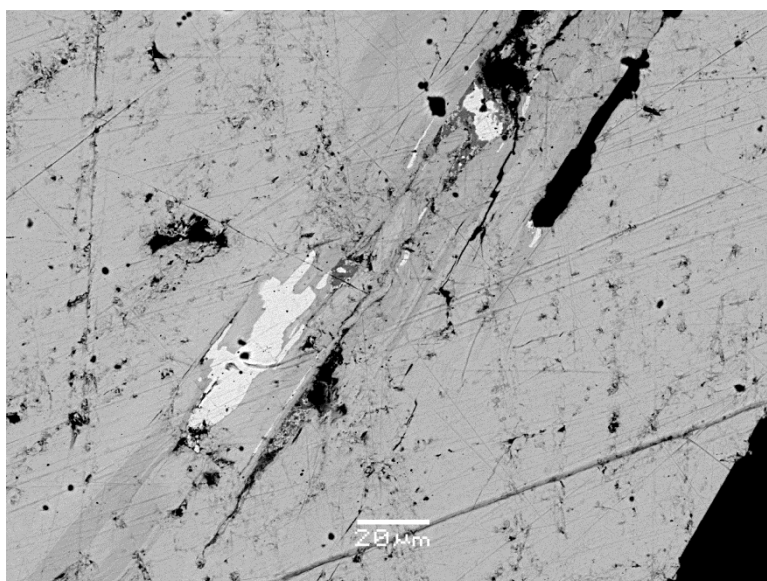
Fig. 3. Large-magnification SEM-BSE image showing the chemical composition heterogeneity of nagyagite as indicated by the existence of different gray tints. The whitish inclusions correspond to altaite and the black ones to native tellurium.
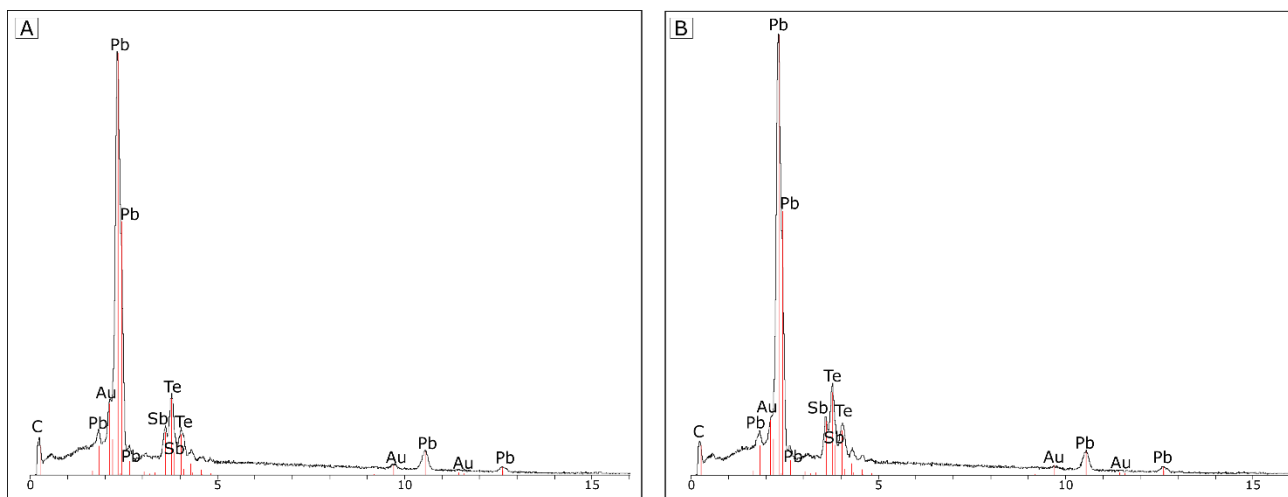
Fig. 4. SEM-EDS spectra of nagyagite from a single lamellae showing chemical composition variation for Pb, Sb, Te and Au. The left spectrum (A) corresponds to nagyagite depleted in Pb, Sb and Te and enriched in Au as compared with the right spectrum (B) that corresponds to nagyagite enriched in Pb, Sb and Te and depleted in Au.
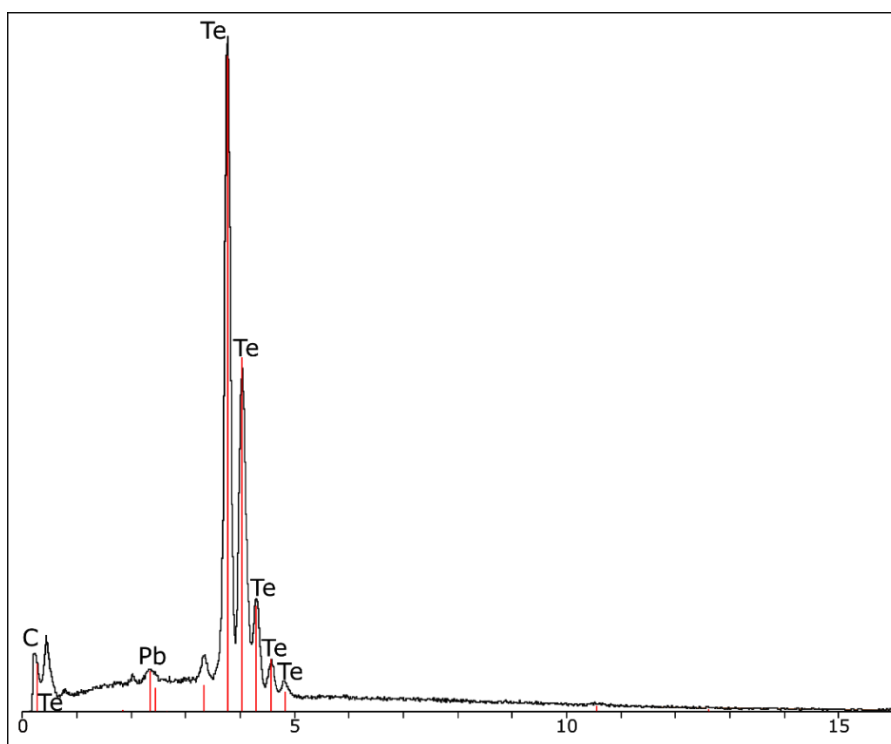
Fig. 5. SEM-EDS spectrum of native tellurium inclusion hosted by nagyagite from Săcărâmb.

Table 1. Quantitative chemical data (wt. %) for altaite and nagyagite from Săcărâmb ore deposit; "bdl" = below detection limit.

Mineral	Element (wt. %)*						Calculated chemical formula
	S	**Sb**	**Te**	**Au**	**Pb**	**Total**	
							(based on 2 *apfu*)
altaite	bdl	0.51	39.02	bdl	59.83	99.36	$(Pb_{0.97},Sb_{0.01})_{\Sigma=0.98}Te_{1.02}$
							(based on 5 *apfu*)
	11.40	8.41	17.78	6.87	56.84	101.31	$(Te_{0.80},Au_{0.20})_{\Sigma=1.00}Pb_{1.00}(Pb_{0.57},Sb_{0.40})_{\Sigma=0.97}S_{2.03}$
	11.59	8.99	17.75	6.07	56.18	100.58	$(Te_{0.79},Au_{0.18})_{\Sigma=0.97}Pb_{1.00}(Pb_{0.55},Sb_{0.42})_{\Sigma=0.97}S_{2.06}$
nagyagite	11.29	8.83	17.69	6.05	54.26	98.11	$(Te_{0.81},Au_{0.18})_{\Sigma=0.99}Pb_{1.00}(Pb_{0.53},Sb_{0.42})_{\Sigma=0.95}S_{2.06}$
	11.28	8.87	18.09	5.50	55.58	99.33	$(Te_{0.82},Au_{0.16})_{\Sigma=0.98}Pb_{1.00}(Pb_{0.56},Sb_{0.42})_{\Sigma=0.98}S_{2.04}$

*Below detection limit values were obtained for Cu, Ge, Ag, Hg in all measured points.
Observation: Arsenic (As) was not measured.

DISCUSSSION

The SEM-EDS analyses and the microprobe results confirmed the chemical heterogeneity of the nagyagite at the level of individual lamellae and allowed the identification of native tellurium closely associated to nagyagite. Ciobanu et al. (2004) previously reported the occurrence of native tellurium in three different mineral associations, *i.e.*, *i*) homogenous platelets hosted by stützite, krennerite, and sylvanite closely related to Te-bearing löllingite; *ii*) fine grains intergrown with sylvanite, rhodochrosite associated to Te-bearing loellingite; and *iii*) porous symplectite intergrowths with sylvanite and hessite in altaite, galena-altaite and along sylvanite borders. Ciobanu et al. (2008) further noticed the occurrence of native tellurium as inclusions together with hessite in the altaite and galena symplectites that replaced completely or partially the nagyagite lamellae hosted by rhodochrosite. The intimate association of native tellurium with nagyagite as mentioned by the present study was previously noticed by Dincă (2019) who described many other mineral associations of native tellurium, *e.g.*, krennerite, sylvanite, tellurantimony, coloradoite, zinkenite, and the occurrence of native tellurium on the border of tetrahedrite-tennatite veinlets.

Altaite occurs similarly to native tellurium being closely associated to nagyagite, however it is significantly more abundant. This mineral relationship was earlier reported by Ciobanu et al. (2004 and 2008) who stated that nagyagite-altaite associations is frequent, with nagyagite lamellae bordered by a more or less continuous altaite rim or having altaite inclusions. This type of nagyagite is considered by these authors as "*normal nagyagite*" or "*Nag-1*", which is depleted or contains minor As. Accordingly, the SEM-EDS analyses of nagyagite from the present study (Fig. 4) did not evidenced the presence of As.

The microprobe data for altaite (Table 1) shows significant differences from the values obtained by Ciobanu et al. (2004), in wt %, for Pb 59.83 vs. 66.00 and 64.25, and for Te 39.02 vs. 33.74 and 34.50 respectively, which shows greater deviation from the ideal values (in wt %) Pb 61.89, and Te 38.11 (Fig. 6).
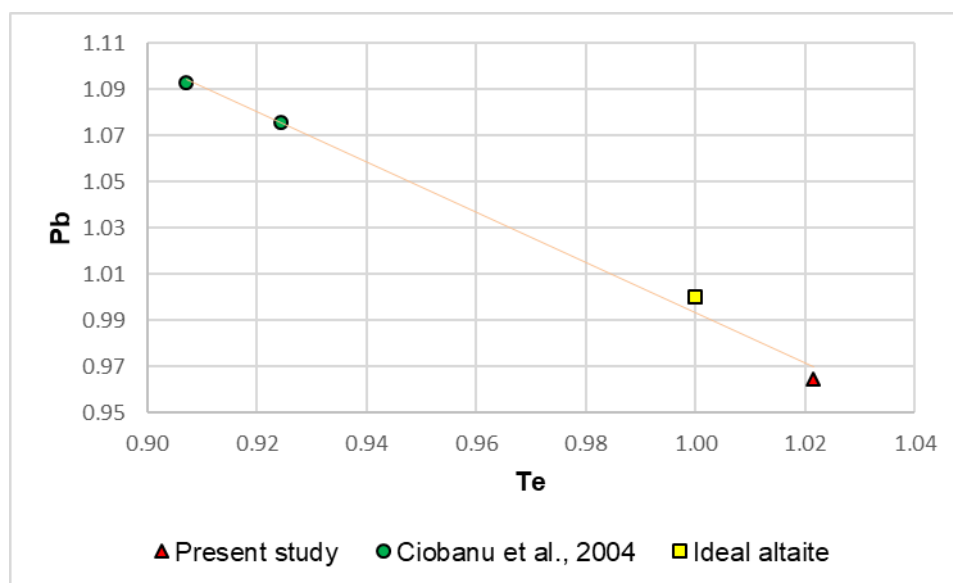
Fig. 6. Plot of different altaite compositions from the literature, the present study, and the ideal composition in terms of Pb *vs.* Te (apfu). The brown line marks a negative correlation trend.

The morphology and the mineral association of the studied nagyagite with altaite compared with the so-called "*normal nagyagite/Nag-1*" of Ciobanu et al (2004) suggests that the analysed nagyagite belongs to the same genetic group of As-poor nagyagite. However, according to Ciobanu et al. (2004) the ratio Au/(Au+Te) for the "*normal nagyagite*" is approximately 0.33, while the same ratio for the nagyagite from the present work is approximately 0.18 (Fig. 7).

Fig. 7. Plot of different nagyagite compositions (recalculated based on 5 apfu) from the literature and the present study onto ∑Pb *vs*. Au/(Au+Te) diagram (Ciobanu et al., 2004). The dotted lines mark the average values of Au/(Au+Te) ratios for the "*normal nagyagite*"and for the nagyagite from the present work; the blue line highlights the constant value for Au/(Au+Te) ratio, and the brown line marks a positive correlation trend.

The plot of the newly acquired EPMA data for nagyagite facilitates to distinguished two trends from the perspective of Pb *vs*. Au/(Au-Te) relationships (in *apfu*). The majority of the microchemical data for nagyagite from the literature indicates that for a significant Pb variation there is a merely constant Au/(Au+Te) ratio of approximately 0.3 corresponding to the blue regression line from Fig. 7. The newly acquired data for the nagyagite from Săcărâmb fills in a gap among the poor-Au nagyagite of Ciobanu et al. (2008) and together with the data of Stanley et al. (1994) and high Pb nagyagite of Ciobanu et al. (2004) delineates a positive correlation trend corresponding to the brown regression line from Fig. 7.

The content of gold in the analyzed nagyagite is ranging from 5.50 to 6.87 wt %, which is significantly smaller comnpared to the data available from the literature excepting the so-called Au-poor nagyagite of Ciobanu et al. (2008) and according to data compiled by these authors from Cioflica et al. (1993a, b) and Lupulescu, (1997) with values ranging from 3.43 to 3.64 wt %.

CONCLUSION

Nagyagite, native tellurium and altaite were identified in an ore samples with abundant rhodochrosite gangue from Săcărâmb ore deposit, South Apuseni Mountains. Native tellurium and altaite occur as small-sized inclusions in nagyagite lamellae.

The EPMA data revealed the presence of minor Sb in altaite (0.51 wt %). The microchemical data acquired for nagyagite defined the analysed mineral grain as "*normal nagyagite*" or poor As-nagyagite. In the same time its content in Au suggests its affinity to the "*Au-poor nagyagite*". The use of the Pb *vs*. Au/(Au+Te) diagram allowed to delineate two compositional trends, *i.e.*, a positive correlation for Pb > 1.5 *apfu* and a second one with constant Au/Au+Te ratio for Pb ranging from 1.15 to 1.6 *apfu*.

References:

Balintoni, I., Vlad, Ş. (1998) Tertiary magmatism in the Apuseni Mountains and related tectonic setting. Studia Univ Babes-Bolyai. Geologie IX, 1 – 11.

Berbeleac, I. (1975) Processus de metamorphisme thermique et metasomatique associe aux andesites quartziferes d'age tertiaire de Vălişoara, Monts Metalliferes. Rev. Roum. Geol., Geophys., Geogr., Geol., 19: 37-46.

Berbeleac, I., Popa, T., Ioan, M., Iliescu, D., Costea, C. (1995) Main characteristics of Neogene volcanic-subvolcanic structures and hosted ore deposits in Metalliferi Mountains. Geologica Macedonica 9, 51-60.

Bindi, L., Cipriani, C. (2004) Museumite, [Pb2(Pb,Sb)S8](Te,Au)2, a new mineral from the gold-telluride deposit of Săcărîmb, Metaliferi Mountains, western Romania. Eur. J. Mineral.

Borcoş, M., Bratosin, I., Colios, E., Ianc, R. (1972) Observaţii petrografice şi geochimice asupra vulcanitelor neogene din ciclul II de erupţie din Munţii Metaliferi. D.S. Inst. Geol., LVIII (1970-1971), 1: 86-99, Bucureşti.

Bostinescu, S. (1984) Porphyry copper systems in the South Apuseni Mountains, Romania. Annuaire de l'Institut de Géologie et Géophysique, 64: 163–174

Căpraru N. (2004) New Interpretation of the Structure of the Săcărîmb Project Area. Extendet Abstracts, IGCP-486, Alba Iulia, România.

Ciobanu C.L., Cook N.J., Damian G., Damian F., Buia G., (2004) Telluride and Sulphosalt Association at Săcărîmb. In ''Au-Ag-Telluride Deposits of the Golden Quadrilateral, Apuseni Mts., Romania. Guidebook of the International Field Workshop of IGCP Project 486 Alba Iulia, Romania'' J. Cook & C.L. Ciobanu, eds., IAGOD Guidebook Series 12: 145-186.

Ciobanu, C.L., Cook, N.J., Pring, A., Damian, G., Căpraru, N. (2008) Another look at nagyá´gite from the typelocality, Săcărîmb, Romania: Replacement,chemical variation and petrogeneticimplications. Mineralogy and Petrology, 93: 273–307.

Cioflica, G., Jude, R., Lupulescu, M., Simon, G., Damian, G. (1993a): New data on the tellurides of the Neogene ore deposits in Romania. Rom. J. Mineral. 76, suppl. 1: 11-12.

Cioflica, G., Jude, R., Lupulescu, M., Simon, G., Damian, G. (1993b) The tellurides of the Romanian Neogene ore deposits. In: Current Research in Geology Applied to Ore Deposits (P. Fenoll Hach-Ali, J. Torres-Ruiz, F. Gervilla, eds.). Proc. 2nd Biennial SGA Meeting, Granada, Spain, September 1993, 73-76.

Cook, N.J., Ciobanu C.L. (2004) Preface. In ''Au-Ag-Telluride Deposits of the Golden Quadrilateral, Apuseni Mts., Romania. Guidebook of the International Field Workshop of IGCP Project 486 Alba Iulia, Romania'' J. Cook & C.L. Ciobanu, eds., IAGOD Guidebook Series 12: 1-6.

Cook, N.J., Ciobanu, C.L., Căpraru, N., Damian, G., Cristea, P. (2005) Mineral assemblages from the vein salband at Sacarimb, Golden Quadrilateral, Romania: II. Tellurides. Geochemistry, Mineralogy and Petrology, 43: 56-63.Csontos, L. (1995): Tertiary tectonic evolution of the Intra-Carpathian area: a review. Acta Vulcano, 7: 1-13.

Csontos, L., Nagymarosy, A., Horváth, F., Kovác, W. (1992) Tertiary evolution of the Intra-Carpathian area: a model. Tectonophysics, 208: 221-241.

Csontos, L., Márton, E., Worum, G., Benkovics, I. (2002) Geodynamics of SW-Pannonian inselberg (Mecsek and Villany Mts., SW Hungary): inference from complex structural analysis. EGU Muller Special Pub. Ser. 3: 1-19. Dallmeyer, R. D., Pana, D. I., Neibauer, F., Erdmer, P. (1999): Tectonothermal evolution of the Apuseni Mountains, Romania: Resolution of Variscan versus Alpine events with 40 Ar/39 Ar ages. J. Geol., 107: 329–352.

Dincă, G. (2019) Mineralogia zăcământului de Au-Ag-Te Săcărâmb, cu privire specială asupra sulfosărurilor. Teză de doctorat, Universitatea Bucureşti, 180 p.

Dincă, G., Popescu, G.C. (2018) New sulfosalts associations from Săcărîmb, Au-Ag-Te ore deposit. Preliminary data. Romanian Journal of Mineral Deposits, 89, 1-2, 65-70.

Effenberger, H., Paar, W.H., Topa, D., Culetto, F.J.,Giester, G. (1999) Toward the crystal structure of nagyagite, [Pb(Pb,Sb)S2][(Au,Te)]. American Mineralogist, 84: 669–676.

Fodor, L., Csontos, L., Bada, G., Györfi, I., Benkovics, L. (1999) Tertiary tectonic evolution of the Pannonian Basin system and neighbouring orogens: a new synthesis of paleostress data. In Durand, B., Jolivet, L., Horváth, F., Séranne, M. (eds.): The Mediterranean Basins: Tertiary Extension within the Alpine Orogen. Geological Society of London Special Publication, 156: 295–334.

Ghiţulescu, T.P., Socolescu, M. (1941) Etude géologique et miniere des Monts Métalifčres (Quadrilatère aurifère et régions environnantes). An. Inst. Geol. Rom., XXI: 181-465, Bucureşti.

Halga, S., Ruff, R., Stefanini, B., Nicolici, A. (2010) The Rovina Valley project, Apuseni Mts., Romania: gold-copper porphyry discoveries in a historic mining district. Romanian Journal of Mineral Deposits, 84, 12-14.

Ianovici, V., Borcoş, M., Bleahu, M., Patrulius, D., Lupu, M., Dimitrescu, R., Savu, H., (1976) Geologia Munţilor Apuseni, Editura Academiei Republicii Socialiste Românâ, Bucureşti, 631 p.

Ivăşcanu, P., Kulcsar, Z., Denes, R., Baker, T., Lewis, P. (2018) Bolcana porphyry Au-Cu deposit, Apuseni Mountains, Romania: AME Roundup 2018: Core Shack Abstract Guide, p. 31.

Ivăşcanu, P., Baker, T., Lewis, P., Kulcsar, Z., Denes, R, Tămaş, C. (2019) Bolcana, Romania: Geology and discovery history of a gold rich porphyry deposit. 2019 NewGenGold Conference, Perth, 12-13 November, 2019, p. 145-160.

Kulcsar, Z., Ivăşcanu, P., Tămaş, C.G. (2019) The use of geochemical data sets on defining anomalies for targeting porphyry Au-Cu deposits - Bolcana case study, Apuseni Mountains. In Har N. (ed) Sesiunea Ştiinţifică "I.P. Voiteşti" 2019, Departamentul de Geologie, Universitatea Babeş-Bolyai, Cluj-Napoca, 34.

Leary, S., O'Connor, G., Minuţ, A., Tămaş, C., Manske, S., Howie, K. (2004) The Roşia Montană deposit. Ȋn Cook, N. J. & Ciobanu, C. L. (eds.): Gold-silver-telluride deposits of the Golden Quadrilateral, South Apuseni Mts., Romania: guidebook of the International Field Workshop of IGCP project 486, Alba Iulia, Romania, August-September 2004. IAGOD Guidebook Series, 12: 89–98.

Lupulescu, M. (1997) Nagyágite: New data and considerations. Rev. Roum. Geol. 41: 29-36.

Manske, S., Ullrich, T., Reynolds, T.J., O'Connor, G. (2004) Vein sets and hydrothermal alteration in the Cetate –Carnic area, Roşia Montană district, Romania. Romanian Journal of Mineral Deposits, 81, Special Issue, "Forth National Symposium of Economic Geology – Gold in Metaliferi Mountains", 3-5 September 2004, Alba Iulia, Romania, 122-125.

Márton, E., Vass, D., Tunyi, I. (2000) Counterclockwise rotations of the Neogene rocks in the East Slovak Basin. Geol. Carpath, 51: 159–168.

Panaiotu, C. (1998) Paleomagnetic constraints on the geodynamic history of Romania. Reports on Geodesy, 7: 205– 216, Warsaw University of Technology.

Popescu, G.C., Ilinca, G., Neacşu, A., Verdeş, G. (2013) The Gold Museum of Brad. Characterization and classification of native gold samples and of other minerals. Romanian Journal of Mineral Deposits, 86 (2), 3-122.

Royden, L.H., (1988) Late Cenozoic tectonics of the Pannonian basin system. In: Royden, L., Horvath, F. (Eds.), The Pannonian Basin: A study in Basin evolution. AAPG Memoir, vol. 45, pp. 27– 48.

Roşu, E., Szakács, A., Downes, H., Seghedi, I., Pécskay, Z., Panaiotu, C. (2001) The origin of Neogene calc-alkaline magmatism and alkaline magmas in the Apuseni Mountains, Romania: The adakite connection. Romanian Journal of Mineral Deposits, 79: 3–23, Bucharest.

Roşu, E., Seghedi, I., Downes, H., Alderton, D.H.M., Szakács, A., Pécskay, Z., Panaiotu, C., Panaiotu, E.C., Nedelcu, L. (2004a) Extension–related Miocene calc-alkaline magmatism in the Apuseni Mountains, Romania: origin of magmas. Schweizerische Mineralogische und Petrographische Mitteilungen, 84: 153–172.

Roşu, E., Udubaşa, Gh., Pécskay, Z., Panaiotu, C., Panaiotu, C.E. (2004b) Timing of Miocene – Quaternary magmatism and metallogeny in the South Apuseni Mountains, Romania. Rom. Journal Mineral Deposit: "Fourth National Symposium on Economic Geology – Gold in Metaliferi Mountains", 3-5 Sept. 2004, Alba Iulia, Romania; p. 33-38.

Savu, H., Udrescu, C., Neacsu, V., Stoian, M. (1993) The Quaternary Basalt-Andesitic Rocks of Detunata (Apuseni Mountains) and their origin. Rev. Roum. Geol., 37: 9-20.

Săndulescu, M. (1988) Cenozoic tectonic history of the Carpthians. AAPG Memoir, 45: 17-25.

Seghedi, I. (2004) Geological evolution of the Apuseni Mountains with emphasis on the Neogene magmatism – a review. In: Cook, N.J. & Ciobanu, C.L. (eds.): Au-Ag-telluride Deposits of the Golden Quadrilateral, Apuseni Mts., Romania. Guidebook of the International Field Workshop of IGCP project 486, Alba Iulia, Romania, August–September 2004. IAGOD Guidebook Series, 11: 5–23.

Seghedi, I., Bojar, A.V., Downes, H., Roşu, E., Tonarini, S., Mason, P. (2007) Generation of normal and adakite-like calc-alkaline magmas in a non-subductional enviroment: An Sr-O-H isotopic study of the Apuseni Mountains neogene magmatic province, Romania. Chemical Geology, 245: 70-88.Tămaş, C.G., Bailly, L., Ghergari, L., O'Connor, G., Minuţ, A. (2006): New occurrence of tellurides and argyrodite at Rosia Montana, Apuseni Mountains, Romania and their metallogenetic significance. Can. Min., 44/2: 689-705.

Stanley, J.C., Roberts, A.C., Harris, D.C., (1994) New data for nagyagite. Mineral. Mag. 58: 479-482.

Șimon, G., Alderton, D.H.M., Bleser, T. (1994): Arsenian nagyágite from Săcărîmb, Romania; a possible new mineral species. Mineral. Mag. 58: 473-478.

Udubaşa, G., Strusievicz, R.O., Dafin, E., Verdeş, Gr. (1992) Mineral Occurences in the Metaliferi Mountains, Romania. Romanian Journal of Mineralogy, 75: 3–35, Bucharest.

Vlad, Ș. N. (1983) Geologia zăcămintelor porphyry copper. Ed. Acad., 156 p.

Wallier, S., Rey, R., Kouzmanov, K., Pettke, T. (2006) Magmatic Fluids in the Breccia-Hosted Epithermal Au-Ag Deposit of Roşia Montană, Romania. Economic Geology, 101: 923-954.

MANGANESE, BARIUM, SULFIDE, AND URANIUM MINERALIZED BELTS WITHIN THE CAMBRIAN TULGHEŞ GROUP, BISTRIŢA MOUNTAINS, EAST CARPATHIANS, ROMÂNIA

Paulina HÎRTOPANU

University of Bucharest, Department of Mineralogy, Bd. N. Bălcescu, 1, RO-010041, Bucharest
paulinahirtopanu@hotmail.com

Abstract. The Cambrian metamorphic Tulgheş Series (TG) of Bistriţa Mts hosts four mineralized belts with line development, which are oriented NW-SE (from West to East): Manganese (MnB), Sulfide (SB), Barium (BaB), and Uranium (UB) belts. These mineralized belts have been established using the recently determined minerals and mineral varieties occurring in each belt. The interferences of mineralogical compositions of these four belts indicate a genetic link, which suggests that all were formed during the same submarine hydrothermal process on the Cambrian sea floor. The alabandite of Mn-belt occurs both in SB and BaB, the Li-minerals of MnB also occur in SB. The SB and MnB contain some Ba minerals like barite, Ba-feldspars, and cymrite, which are dominant in Ba belt. The lenses of Mn ore closely banded with barite ore in Ba-belt prove their genetic links and common evolution. The presence of Ni-Co-As sulfide/arsenide in the UB, which also occur in the MnB, SB, and BaB, indicates that the UB has mineralogical and genetic similarities with the three belts. Also, a few U-Y minerals of UB occur in MnB, BaB, and SB, as accessory minerals. Nevertheless, the UB has been tectonically strongly transformed and remobilized from its original source, which was the upper part of Tulgheş Series, TG4.

The current tectonic and structural setting of all four belts corresponds to their development and evolution in a subducted zone, a narrow active paleotrench area, reflected in their line development as belts. The submarine hydrothermal activity began in early Cambrian with Mn ore, a small amount of Ba minerals and sulfides, and continues with more Ba and a little Mn and sulfides (BaB). In the middle Cambrian the sea floor was subducted towards the N-E and the SB ore was deposited at some distance from and over the MnB and BaB, but with the same orientation. The SB contains some alabandite, baryte, Ba feldspars, and cymrite. In the upper Cambrian the hydrothermal submarine was continued with Uranium mineralization, which represents the last belt, the Uranium Belt. This was also subducted towards the NE at some distance from and over the Sulfide Belt. Nevertheless, it was tectonically strongly transformed and remobilized from its original source, which was the TG4, being subducted/ thrusting under the oldest Bretila Group, represented by Pietrosu Bistriţei porphyroide granite. This evolution of the four belts is reflected in the great thickness of thousands of meters of their host rocks, the Tulgheş Series. So, the Mn, Ba, S, and U belts evolved in the Cambrian sea floor, in a subducted zone, in a narrow active paleotrench area, reflected in their line development as belts. The four approximately paralel belts evolved from NW to SE. Therefore, the Tulgheş Series could be divided in TG1 with MnB, TG2 with BaB, TG3 with SB, and TG4 with UB.

Key words: Bistriţa Mountains, Cambrian Tulgheş Series, Mn-Ba-Sulfide-U Belts, subducted paleotrench zone, amphibolite to low green schists, submarine hydrothermal genesis.

1. Introduction

From a geological and structural point of view the Bistriţa Mountains belong to Crystalline Mezosoic Zone, a complex area, so called Eastern Central Carpathian Nappes, which represent the Eastern segment of Middle Dacides (Sandulescu, 1984). The recent geological setting of Eastern Central Nappes, now belonging to the Alpine belt, was the result of their long structural evolution through many tectogeneses cycles, between the Eurasia plate in East and the Central European plate in West. The current tectonic-structural setting of Bistriţa Mountains corresponds to its development and evolution in a subduction zone. The paleotectonic subduction is materialized in the great thickness of thousands of meters of TS (4,000-6,000m). The crystalline rocks of TS are graduallly and retrogressively metamorphosed, sometimes just with a reccurent metamorphic facies and subfacies/repeated and superimposed metamorphic events, from bottom to upper part: amphibolite facies/low amphibolite facies, retromorphosed amphibolite facies/upper green schists facies (TG1, host of MnB), green schists facies/low green schists facies (TG2, host of BaB), upper green schist/amphibolite with epidote facies (TG3, host of SB), and green schists facies/low green facies (TG4, host of UB). The all TS display a pronounced schistosity, having some similarities with burial metamorphism. During metamorphism, the wall rocks were tightly folded and microsheared. The four mineralized belts, Mn, Ba, S, and U, are situated from East to West, and from the bottom to the top inside the metamorphic rocks of Tulgheş Series (Fig. 1). The mineralogical composition of TS is rather monotone, consisting of quartz, muscovite albite, graphite, chlorite, epidote, stilpnomelane,various carbonates (aragonite, calcite, siderite, and dolomite) and with some relics of amphibole, biotite, almandine, rutile, and ilmenite. The uraniferous zircon, zircon, monazite-(Ce), allanite-(Ce), thorite, thorogumite, and smirnovskite occur as accessory.
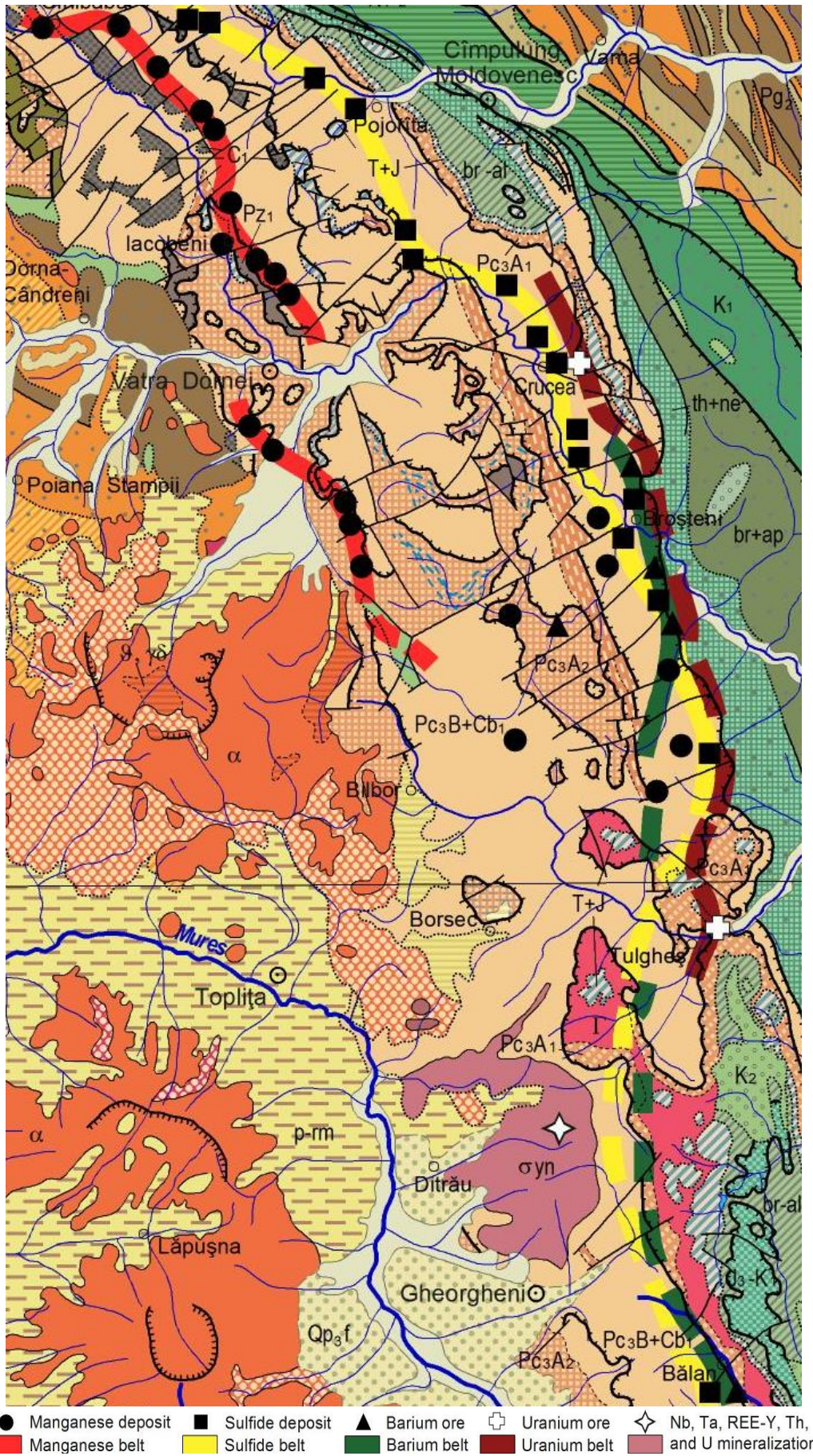
Fig. 1. Bistriţa Mts with their 4 mineralized belts, localized in the Tulgheş Series: Mn, Ba, Sulfide, U, and Ditrău rare element minerals occurrence localized in Ditrău alkaline carbonatite complex.

2. Manganese Belt

The MnB is situated in TG1, at the bottom of Tulgheş Series, whose constitutuent rocks, amphibole, biotite and almandine are strongly carbonatated (Fig. 2 left) and chloritized. It looks like a retromorphosed amphibolite. The decarbonatation reactions of the initial old rhodochrosite of the Mn ore premetamorphic bulk were the source of large CO_2 volumes of petrological importance. The intergrowth of graphite with muscovite could be seen in Fig. 2 right. The graphite could be attributed to CO_2 reduction from the fluid at moderate T and f_{O2} under that of QFM. The experimental data about graphite stability showed that high T decreases its stability field, while an increase of P increases its stability field.

The Manganese Belt is formed of more than 20 manganese deposits/occurrences, situated on two alignments along the Bistriţa Valley. The Eastern alignment comprises the following manganese deposits from North to South: Dadu, Orata, Colacu, Oiţa, Tolovanu, Nepomuceni, Arsiţa, Argestru, Căprărie, Dealul Rusului, Mândrileni, Sihăstria, Ulm, Broşteni, and Borca. The Western alignment comprises, from North to South, the following smaller manganese deposits/occurrences: Gândacu, Diaca, Puiu, Făgetel, Roşu, Sărişor, Todireni, and Neagra Şarului. The ore has lens-like form with medium dimensions, concordant with the foliation of country rocks. Initially it was most probably a continuous level, like a belt. Later the manganese ore was fragmented by metamorphism and tectonics. The characteristic feature of the ore is its banding, which is the result of metamorphism. The banding also reflects the initial sedimentation of chemical precipitation of premetamorphic material. Each band represents a petrographic type, named after the predominant mineral: spessartine, tephroite (Figs. 3 left and right), rhodonite, mangancumingtonite/ mangangrunerit, pyroxmangite, Mn-humite, johannsenite, alkali pyroxene and alkali amphibole, nambulite, natronambulite, phillosilicates with Cl (manganpyrosmalite and pyrosmalite), vein (stilpnomelane, bannisterite, ganophyllite), rhodochrosite, sulfide, oxide, and secondary manganese oxide ore types.
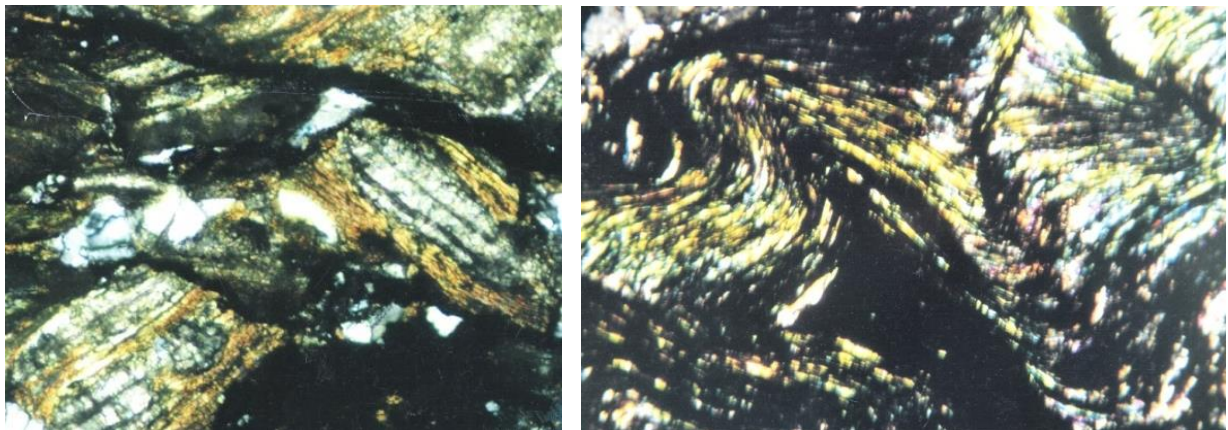
Fig. 2. Carbonatated biotite (yellow relics, cleavage), quartz (white) and graphite (black, veins), TL, N+, x35, (left); Intergrown muscovite (high birefringence, cleavage)/graphite (black), TL, N+, x30, sample BBrc3 (right).
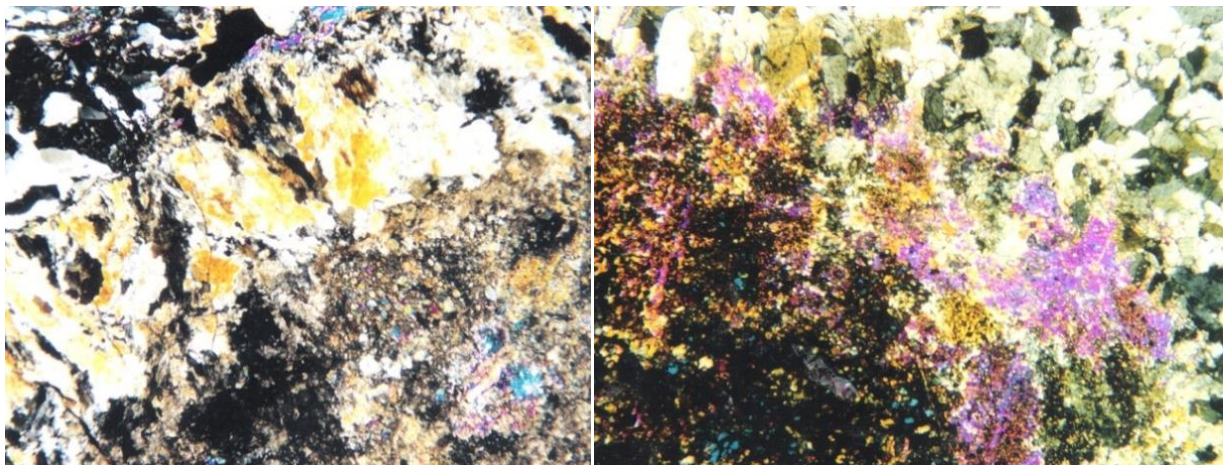
Fig. 3. Undersaturated paragenesis with no direct contact tephroite ore (bottom right corner)/quartzite country rock (top left corner), between them always there is a rhodonite band (centre, white yellow), TL, N+, x20 (left); Undersaturated paragenesis: tephroite substituted by manganpyrosmalite (bottom, left corner), rhodonite (top, right corner) and manganpyrosmalite vein between them (centre), TL, N+, x25 (right).

The mineralogical richness of the MnB, as well as its complex mineral equilibria, help us reconstruct the P, T, X, f_{CO2}, f_{O2}, f_{As}, f_{Cl}, and f_{H2O} conditions of the ore, thus completing the data on the country rock (TG1), which was strongly influenced by retromorphism and therefore more difficult to decipher. Also, it has been established that the metamorphic evolution of the Mn ore was achieved through repeated and superimposed metamorphic events, a fact explaining its complex mineralogy. The fluid phase composition (CO_2, H_2O, Cl, F, OH, As, and S) has a strong influence on the mineral transformations of MnB ore. The fluid composition and the nature of its buffering, besides the bulk X_{Mn}, X_{Mg} and X_{Fe}, in addition to P and T, control the stabilisation and transformation of old manganese oxides silicates, and carbonates into new minerals. The garnets of MnB belong to four major varieties: spessartine, spessartine-calderite, anisotropic spessartine-grossularite, and grossularite. However, there exists a transformation of one variety into another, with a change of P, T, f_{CO2}, f_{O2} conditions.

The first johannsenite occurrence in MnB is closer to the diopsid-hedenbergite. The johannsenite association (johannsenite/grossularite/Ca-rhodochrosite) (Fig. 4 left), which occurs in MnB, is certainly restricted only to high amphibolite facies in other deposits in the world. The reaction of johannsenite was probably produced at $T>600^0$ and $P>4Kb$, which are its formation conditions in other occurrences. The grossularite, ferrorhodonite (Fig. 4 right), and ferroan bustamite occur as secondary minerals, caused by a late retrograde metamorphism. The Mn olivines are represented by pure tephroite, ferroan tephroite and ferroan rich tephroite (knebelite). The absence of quartz in the olivines' association (Figs. 3 left and 3 right) rules out the existence of a medium green schists facies of their formation. Under the anhydrous conditions, where only CO_2 is present in fluid, the T formation of pure tephroite term is in accord with experimental data at $580^0\pm10^0$ and 2Kb pressure (Peters et al., 1973). Therefore, the P in tephroite ore of MnB was much higher than in experiment, then its equilibrium T was higher than 580^0C.

Based on the mangancummingtonite stability curve determined experimentally (Dasgupta et al, 1988), the substitution of pyroxmangite by mangancummingtonite/coexisting of pyroxmanite with mangancummingtonite occurs at T of $580-600^0C$ and a P of 6Kb (amphibolite facies). The chemical compositions of the two pyroxenoids, rhodonite and pyroxmangite, show the existence of a compositional miscibility gap between them. In the MnB the rhodonite never appears associated with pyroxmangite, each of them forming distinct associations, having different stability fields.

The retrograde metamorphism of pre-Alpine orogenesis caused a spectacular mineralogical change of Mn ore. This is characterized by the occurrence of zoned alkali pyroxenes and amphiboles. The aegirine, an important constituent of the Mn ore, belongs to aegirine-augite with great compositional variations, reflected by the frequent marginal and sectorial zonations (Fig. 5 left). Their great variations of chemistry (with Ti presence) and their compositional zonations are the specific features of clinopyroxenes in Mn-metamorphosed ore of the blueschists facies. The occurring conditions of MnB alkali pyroxenes and amphiboles, e.i., the $P>9Kb$ and $T<450^0C$, have been evaluated from experimental diagram Jadeite/ Glaucophane-Aegirine/Magnesioriebeckite (Wood, 1980) and from the diagram Jd-Ae-Q (Brown and Ghent, 1983), based on jadeite component of aegirine and glaucophane component of magnesioriebeckite. The alkali blue amphiboles grew zoned, concentric on nonalkali amphiboles (Fig. 5 right). The zonation reflects the change of metamorphism conditions, from the epidote amphibolites/low amphibolte facies (core of grains) to low blueschists facies (margins of grains). In the Wood experimental diagram (Wood, 1980) aegirine/magnesioriebekite-jadeite/glaucophane the coexisiting aegirine and magnesioriebekite in MnB (Figs. 6 left and 6 right) shows a $T=500^0C$ and a P=9Kb for this metamorphic event, because the jadeite/glaucophane of the aegirine/magnesioriebekite content is around 30%, which corresponds to the low blue schists facies field. The natronambulite/ nambulite/ferrigoseite/namansilite/hausmannite oxidated association have been formed contemporaneus with alkali pyroxenes and amphiboles, under high f_{O2} conditions. The stilpnomelane, bannisterite, ganophylite, cymrite, chlorite groups were formed later under green schist facies. The additional fluid components, such as Cl and As, affect the stability relations between hydrated phases and control the forming of manganpyrosmalite/ferropyrosmalite, nelenite, schalerite, and many secondary arsenates. The metamorphic evolution of Mn ore was achieved through the repetead and superimposed metamorphic events, the phenomenon which explains its complex mineralogy, each metamorphic event being a source of new minerals and mineral varieties (Hîrtopanu, 2019). The exclusive occurrence of pyrosmalites found solely in the MnB and SB is evidence of the origin of Cl deep within these deposits, in the original hydrothermal submarine solutions. A special composition of bulk rock, high activity of Cl and low oxygen fugacity are all needed for the pyrosmalites formation. Apparently, the manganpyrosmalites are retrograde phases, being formed through the substitution of the older anhydrous manganese minerals such as tephroite (Fig. 3 right), manganhumites, johannsenite, pyroxmangite, rhodonite, and rhodochrosite.
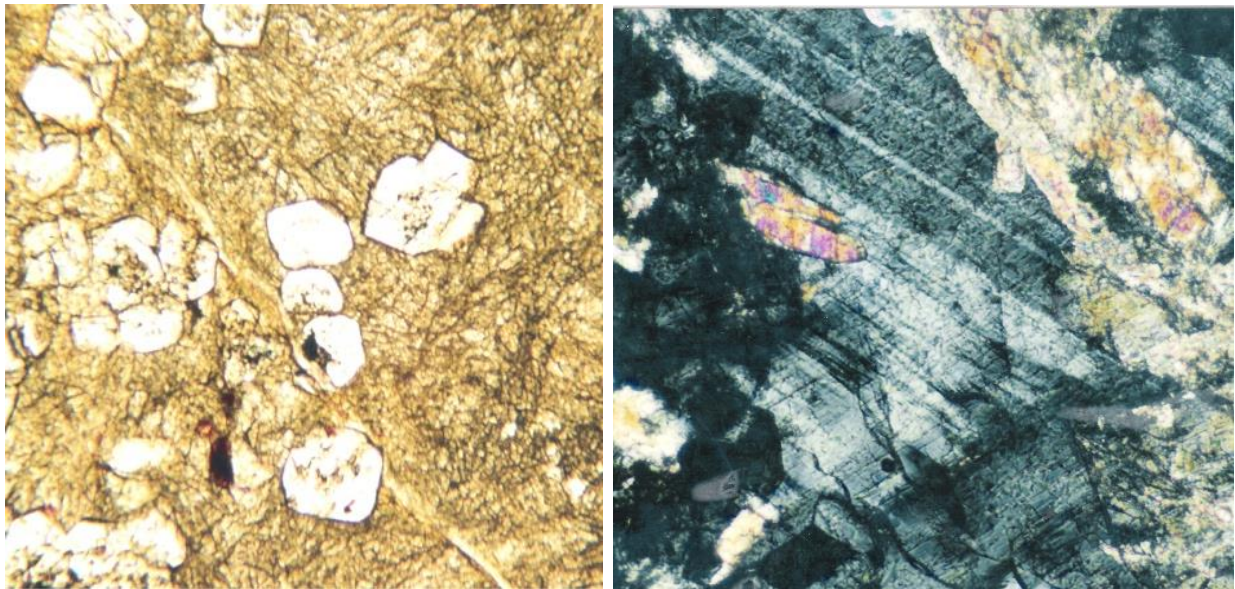
Fig. 4. Johannsenite (yellow, two cleavages), grossularite (euhedrale/rounded withe grains), and Mn-calcite (white, thin veinlets), TL, NII, x25 (left); Ferrorhodonite (large grain, centre, twinned, grey) grown on johannsenite (colored relics) and grossularite (isotrop, partiale anisotrop, black/dark grey (left), TL, N+, x30.
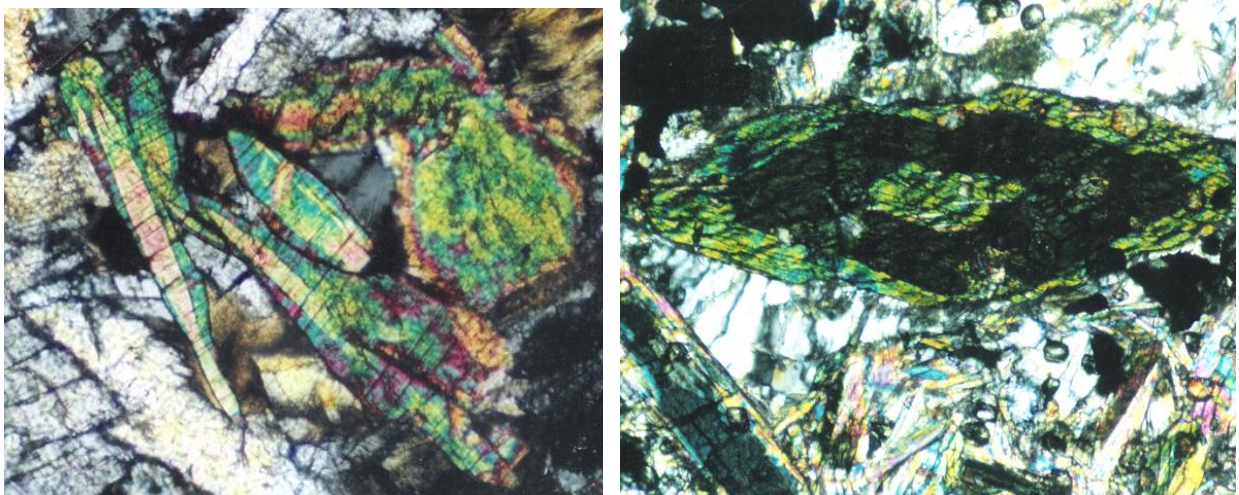
Fig. 5. Zoned aegirine (centre), nambulite (grey, left bottom corner), and ferrigoseite (top right and left corners yellow) (left) ; Zoned large amphibole crystal: mangancummingtonite (centre and marginal, green) and magnesioriebeckite (dark blue, middle of the crystal), magnetite (black), and quartz (white), TL, N+, x40.
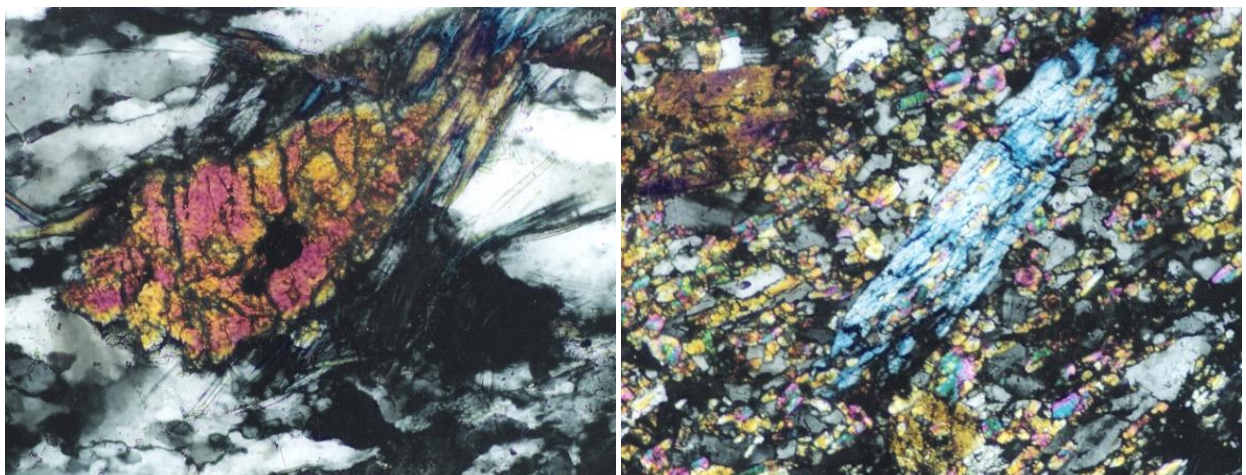
Fig. 6. Coexisting aegirine (30% jadeite, large grain, red-yellow centre) with magnesioriebeckite (30% glaucophane, blue) on its margins, in quartz (grey), TL, N+, x35 (left); Coexisting aegirine (30% jadeite, small red/yellow grains) with magnesioriebeckite (30% glaucophane, large, blue grain, centre), TL, N+, x30 (right).

3. Barium Belt

The Barium minerals are present in both the mangan and sulfide belts, but have a greater development on the alignment Holdiţa, Pârâul Caselor, Broşteni, and Borca deposits, between the Manganese Belt (at the bottom) and Sulfide Belt (at the top) and with the same NW-SE orientation lentils ore as the manganese and sulfide (Fig. 1). In the low middle Cambrian (TG2), the sea floor was subducted toward the East of MnB, and the Ba mineralizations were deposited at some distance from and over the manganese ore body. Therefore, we can draw on the geological map of the Bistriţa Mts a second belt, the Barium Belt (BaB). The occurrence of cymrite, barite, and Ba-feldspars in the deposits of Mn Belt, and also in Sulfide Belt, proves the genetic link between BaB, MnB, and SB.

The lithostratigraphical sequence with Ba mineralization of the Holdiţa deposit comprises lenses of manganese ore at the bottom, and on the top barite lenses banded by sulfide ore. The interferences of mineralogical compositions of these belts, Mn and Ba, indicate a genetic link between them. The lenses of manganese carbonate and manganese silicate ore are in some areas closely banded with barite ore. This close banding of barite and manganese ore demonstrates their common origin and evolution. The Sulfides Belt contains some Ba minerals, like barite, barium feldspars, and cymrite (Bălan, Pârâul Şarpelui, and Broşteni). The Holdiţa barite ore contains barite, Ba-feldspars (Fig.7 left), barytocalcite, benstonite, witherite, cymrite, kinoshitalite, and pyrite (Fig. 7 right). Therefore, the cymrite is also present in both the BaB (Fig. 8 left) and SB (Fig. 8 right). The alabandite, which is present in the BaB (Fig. 9 left), is present in the reduced tephroite paragenesis of the MnB (Fig. 9 right), and also in the Sulfide B (Fig. 10 left). The MnB, in its turn, has in its mineralogical composition other barium minerals, like celsian, hyalophane, barite, and cymrite as accessory minerals, proving the genetic links with barium and sulfide mineralization. This interaction of the three belts, Mn, S, and Ba, proves their genetic links and common evolution, also that they were all formed by the same submarine hydrothermal process on the Cambrian sea floor.
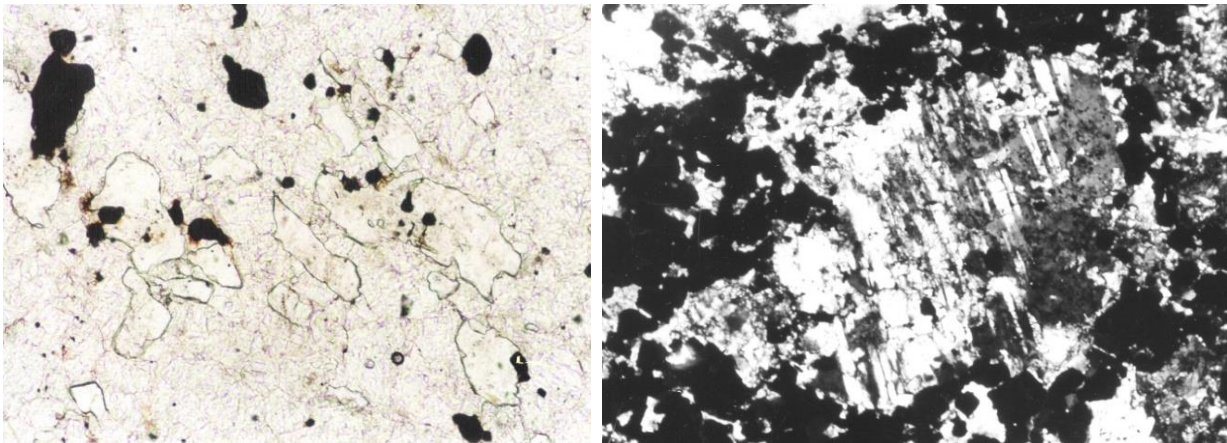
Fig. 7. Celsian (white, relics) and pyrite (black) in barite ore (pinkish white), TL, N+, x30, Barium Belt (left); Celsian (twinned, centre) and pyrite (black, around), TL, N+, x35, Sulfide belt (right).
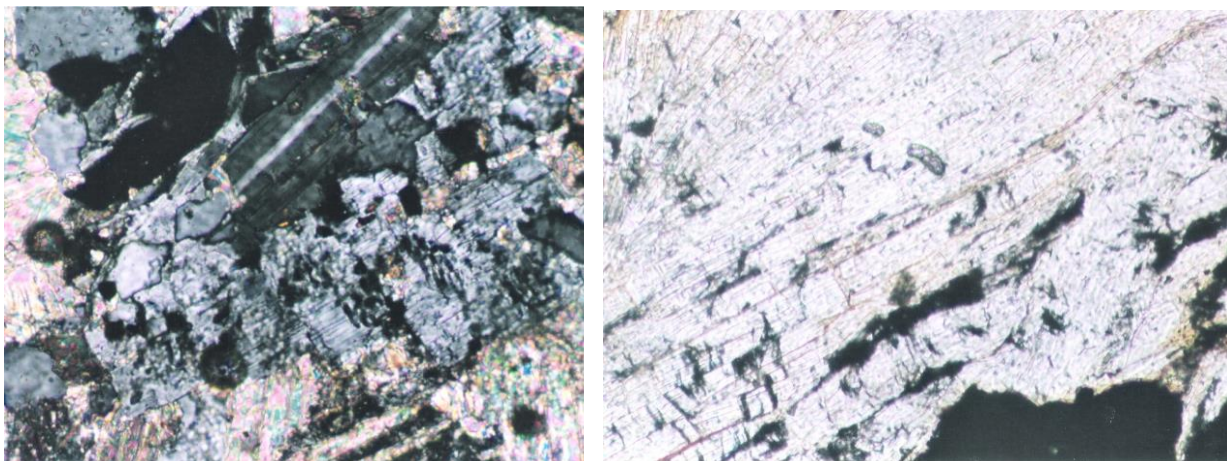
Fig. 8. Coexisting cymrite (grey, perfect cleavage) and celsian (twinned, centre), TL, N+, x30, Barium Belt (left). Cymrite (large crystals, two cleavages) and pyrite (black), TL, NII, x25, Bălan deposit, Sulfide Belt (right).
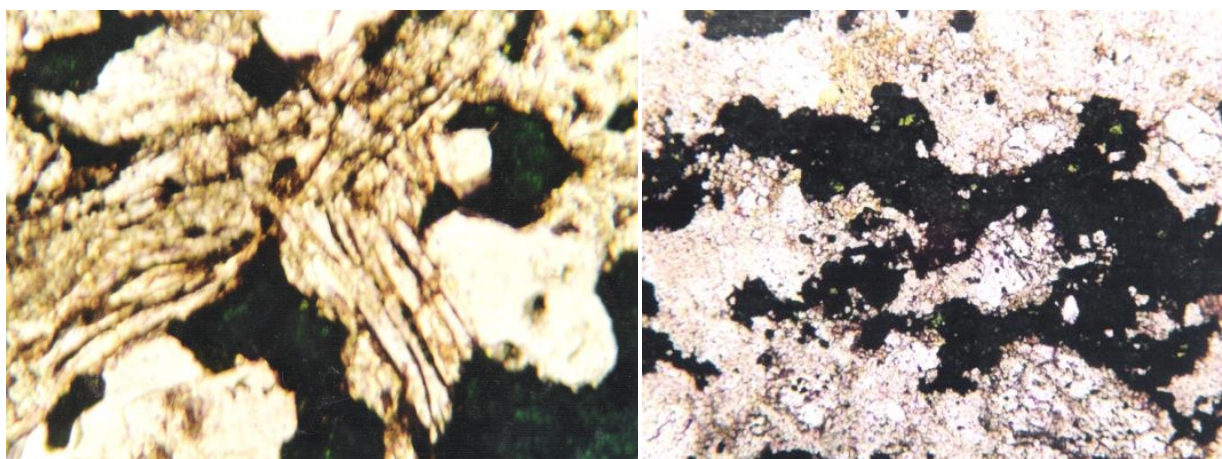
Fig. 9. Alabandite (green), kinoshitalite (large grain, light yellow) and celsian (white), TL, NII, x30, Barium Belt. Alabandite (dark green), Mn-humite (white pinkish), and rhodochrosite (white), TL, NII, x35, Mangan Belt.
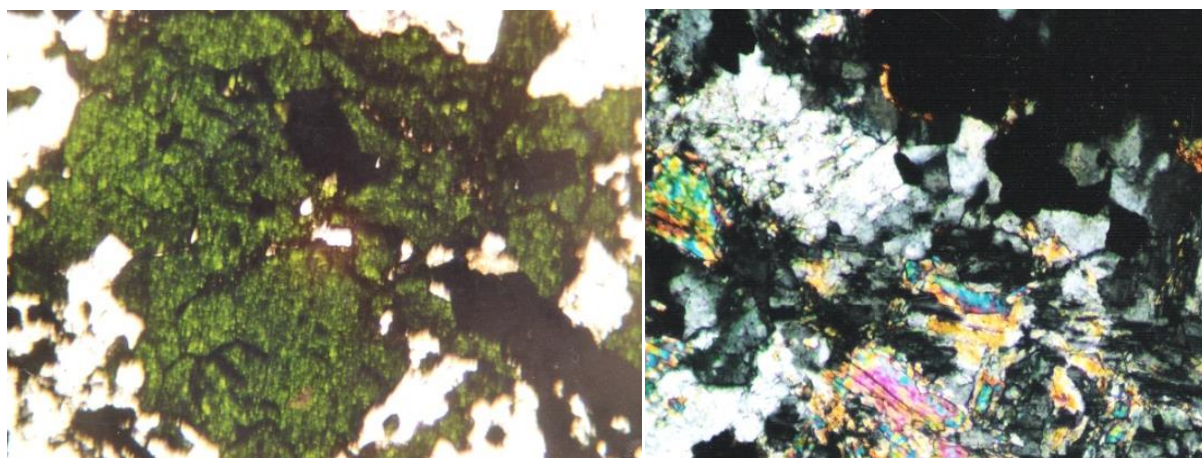
Fig. 10. Alabandite (green), celsian (white), and pyrite (black), TL, NII, x35, sample GB2, Sulfide Belt (left); Kinoshitalite (high birefringence, cleavage), celsian (white), and pyrite (black), TL, N+, x30, Ba-Belt.

The Holdița celsian contains over 90% Cn, whereas hyalophane contains under 10% Cn, which is consistent with the presence of a substantial compositional gap. The celsian has a very low K content, so hyalophane occurs only as very small unmixtures in celsian. The celsian seems to be the oldest mineral, because it is replaced by barite (Fig. 7 left) and cymrite (Fig. 8 left). The relics of celsian in cymrite may have escaped the reaction because locally P_{H2O} may have been lower than P_{fluid}, and when P_{H2O} is higher than P_{fluid}, the celsian completely disappears (Seki and Kennedy, 1964). The coexistence and phase relations of celsian and cymrite (Fig. 8 left) are of great petrological interest as a natural example of the experimentally established reaction curve celsian+H_2O=cymrite (Essene, 1967). Fluid-inclusion studies (Morro et al., 2001) indicate 350°–370°C and 1.5 kbars as conditions of their equilibration. This could be the upper limit of P–T conditions reached in Holdița barium deposit. Usually, the cymrite is formed during the late stage of low grade metamorphism, at a T of 250-300°C and a pressure 1-3 kbars (Hsu, 1994; Moro et al., 2001). Fluid inclusions within barite indicate its formation temperature between 120-240^{0}C during barite crystallization in hydrothermal system (Jamieson et al., 2016). Some cymrite relics of BaB look like they have replaced a pre-existing rectangular mineral, most likely barite (Fig. 16 right). The Holdița barite, the oldest mineral, was formed at T and P higher than that of cymrite (Hirtopanu, et al., 2008). The replacement of the barite by cymrite was experimentally demonstrated by the reaction: $BaSO_4+2OH^-$ $+A1_2O_3-2SiO_2=BaA1_2Si_2O_8 \cdot H_2O+SO^2_4$ (Hsu, 1994). The barian muscovite of Barium Belt could be formed by the dehydration of cymrite during a new stage of metamorphism. It is associated with celsian and pyrite (Fig. 10 right) and no cymrite present. The hydrothermal submarine activity begun with Mn ore with a little Ba in TG1, and continued in TG2 with more Ba and little Mn, when the seafloor was subducted toward the East. In the upper Cambrian (TG3) the seafloor was also subducted toward the East and the sulfides were deposited at some distance and over BaB/MnB. The Ba, Mn and Sulfide mineralizations evolved in Cambrian sea floor, in a subducted zone, in a narrow active paleotrench area, reflected in their line development, as belts.

4. Sulfide belt

The Sulfide Belt (SB), situated in the TG3 level of Tulgheş Series (TG), forms an alignment of 200Km of deposits situated from NW to SE, having the same orientation as MnB and BaB, being approximately parallel and at same distance: Baia Borşa, Mestecăniş, Fundul Moldovei, Pojorâta, Giumalău, Gemenea, Fagu, Puiu, Leşul Ursului, Isipoaia, Broşteni, Paltinu, and Bălan (Fig. 1). The massive sulfide lenses are mainly composed of pyrite (predominantly), sphalerite, galena, chalcopyrite, and with minor arsenopyrite, pyrrhotite, tetrahedrite (Fig.11 left), bournonite, bismutite, semseyite, jamesonite, cosalite, smaltite, molibdenite, native gold, and native bismuth, as metallic minerals, and quartz, calcite, ankerite, chlorite, muscovite, albite, and titanite, as gangue. The recent research about sulfide mineralizations have identified new minerals especially of the gangue. These new minerals determined in sulfide deposits are: celsian, hyalophane, cymrite, barian muscovite, zinnwaldite, anandite, pyrosmalite (?), and barite as important constituents of the massive sulfide ore (Hîrtopanu, 2019). The pyrite has cassiterite inclusions (Fig. 11 right). In the Puiu sulfide deposit the zinnwaldite, a Li-mica, occurs as gangue (Fig. 11 left and 11right). The Puiu sulfide deposit is situated near the Tolovanu Mn-deposit, at the top of it, where many Li minerals (natronambulite, nambulite, ferrigoseite, Li-mica, and sceondary oxide lithiophorite) occur. These new minerals, as well as the probable presence of the ferropyrosmalite, are very important in establishing the characteristic feature of submarine hydrothermal origin of sulfides, the same as for the Mn and Ba belts. The rich barite of sulfides ore from Broşteni deposit of SB occurs near the Holdiţa barite deposit of BaB, but stratigraphically at the top of it.
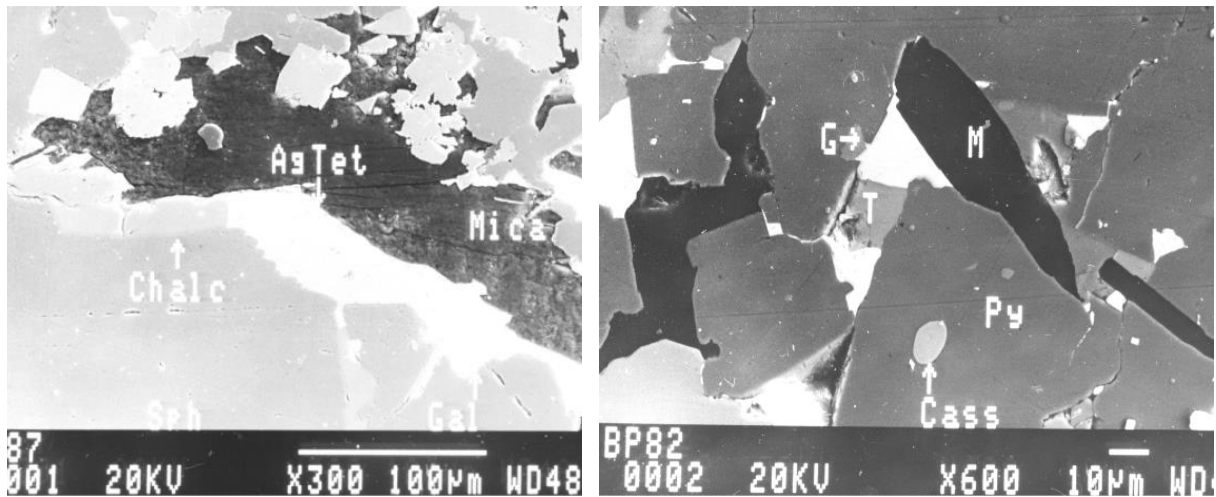
Fig. 11. Backscattered electron image of sphalerite (Sph, light grey), galena (Gal, white), chalcopyrite (Chalc, light bluish), Ag-tetrahedrite (AgTet, white), and zinnwaldite (Mica, dark grey) (left); Backscattered electron image of pyrite (Py, grey), galena (G, white), tetrahedrite (T, light grey), cassiterite (Cass, small, light blue), and zinnwaldite (M, black), Puiu sulfide deposit (right).
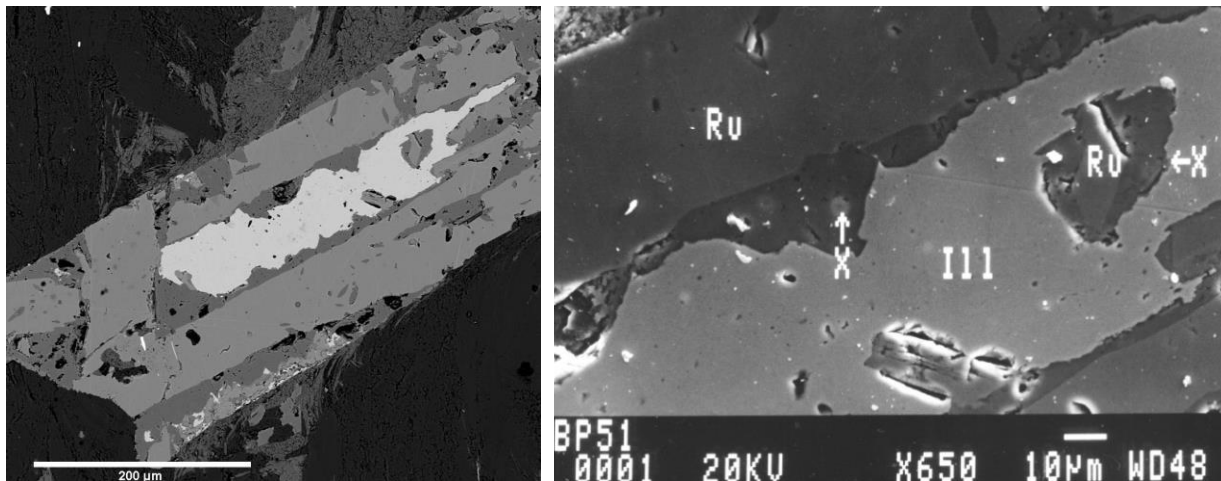
Fig. 12. Backscatterd electron image of ilmenite (white, centre, relics inside rutile), rutile (prism, light grey), siderite (dark grey, between them), and muscovite (dark grey) (left); Detailed area: ilmenite (Ill, light grey), rutile, (Ru, grey), and siderite (X, dark grey), TG3, (right).

The country rock of SB (TG3) has ilmenite relics, which are important in establishing its formation. At relatively low T the ilmenite is partially broken down into rutile and siderite, but is still a stable phase (Fig. 12 left and 12 right), as found in the TG3 rocks. At relatively high T, siderite is not stable any more and ilmenite is the only crystalline phase coexisting with rutile. The alteration of ilmenite involves the processes of oxidation and leaching, whereby iron is progressively removed to give a residual product, essentially TiO_2. These pseudomorphic transformations of ilmenite are generally associated with retromorphic processes. Therefore, the evolution of the Ti minerals is tightly linked to the evolution of metamorphic processes indicating the polymetamorphism of the formation of the contry rock (TG3) of the Sulfide Belt. The ilmenite is a mineral that persists over a long period of metamorphism between the kyanite and staurolite zone, and biotite zone. Therefore, we appreciate that the first metamorphic peak of TG3 (with Sulfide Belt) belongs to at least biotite/garnet zone of amphibolite facies.
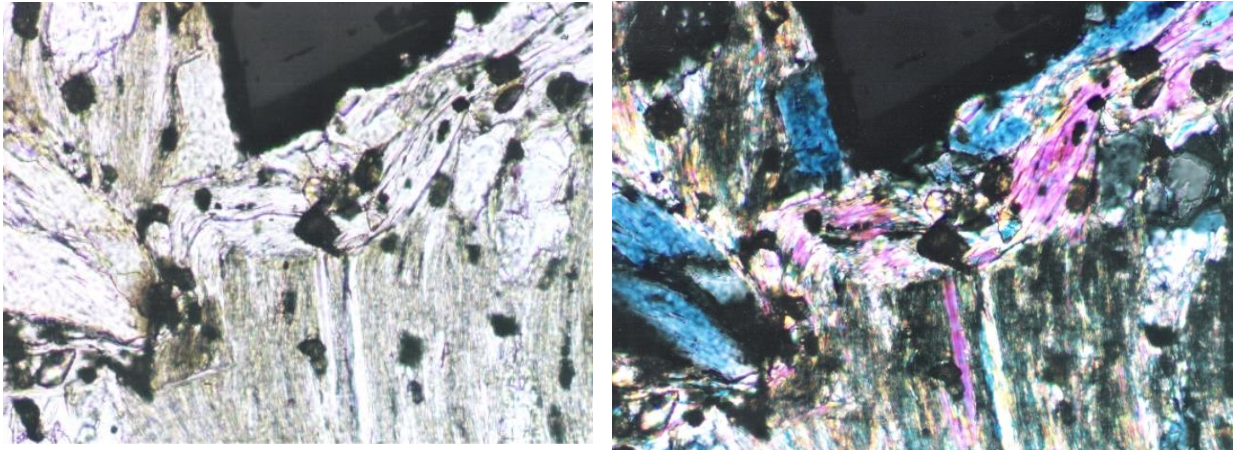
Fig. 13. Anandite (micaceous) with Ti mineral and uraniferous zircon inclusions, and zoned pyrite (top, black), TL, NII, x30 (left); The same image in N+ (right), sample Bln1, Bălan deposit, Sulfide Belt.
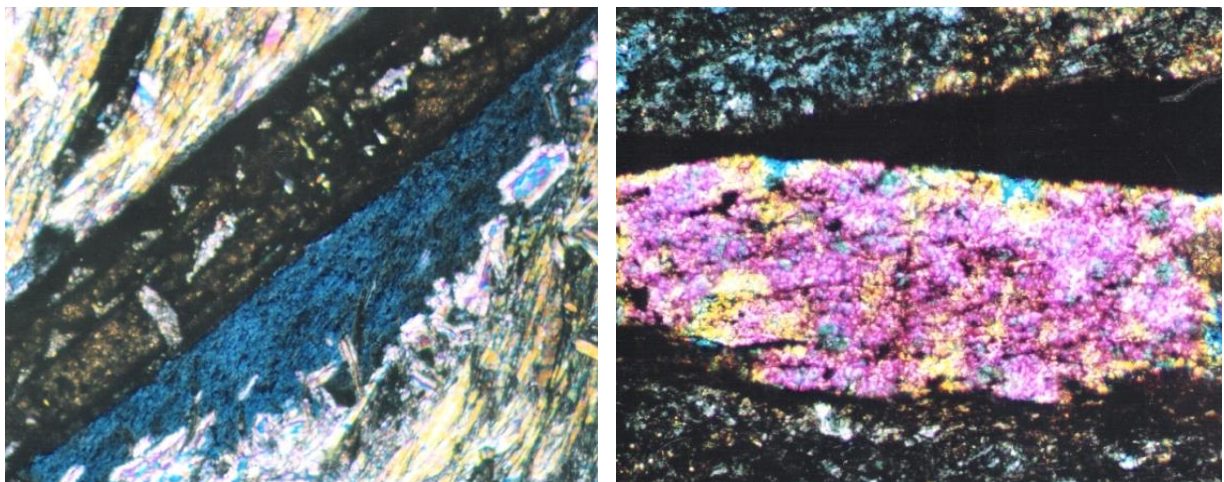
Fig. 14. Rutile (large yellow brown prism crystal), clinochlore (blue, anomaly birefringence), and muscovite (colored, cleavage), TL, N+, x25, sample Prs3, Pârâul Şarpe deposit, Sulfide Belt (left); Epidote (large crystal, high birefringence) with ilmenite around it (dark brown, black) enclosed in micaceous chloritized rock, TL, N+, x30, Pârâul Şarpelui deposit, Sulfide Belt (right).

The anandite (Figs. 13 left and 13 right), titanite (Fig. 14 left), rutile, epidote (Fig. 14 right), muscovite, zinnwaldite, albite, cymrite, quartz, and various chlorites constitutes gangue of sulfide ore.

The presence of Li minerals in the two belts, Sulfide (as zinnwaldite) and Manganese (nambulite, and natronambulite), as well as the presence of pyrosmalite minerals in both belts (pyrosmalite in SB and manganpyrosmalite MnB), demonstrates their common origin and evolution. In the barium ore, the pyrite is a constituent mineral while in the sulfide ore is predominant. The cymrite is a constituent of both sulfide (Figs. 15 left and 15 right) and barium ores (Figs. 16 left and 16 right), with some small different characteristics, being formed under some very small differences in metamorphic conditions, which are a little higher in Sulfide Belt than in Barium Belt: green schists facies for Barium Belt and low amphibolite with epidote facies for Sulfide Belt.
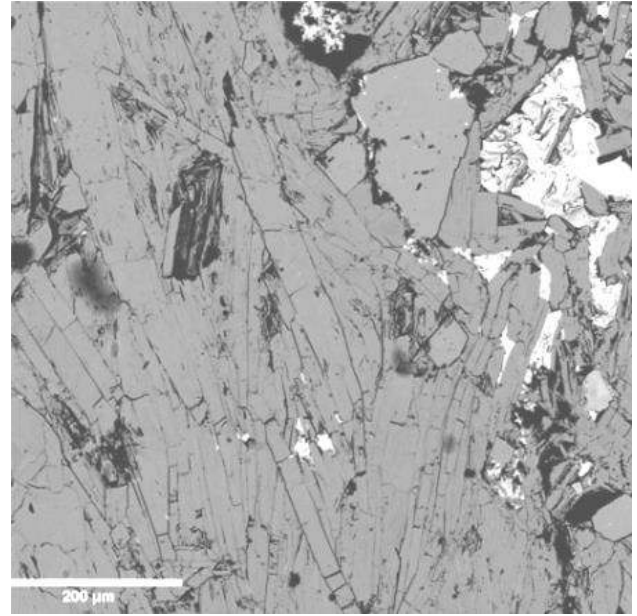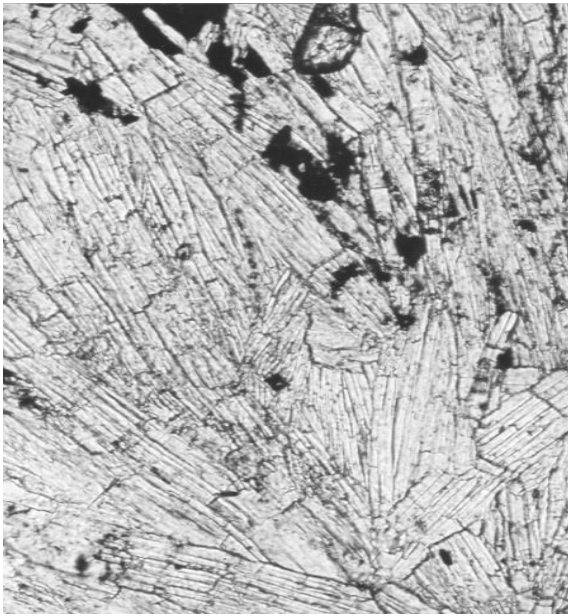
Fig. 15. Cymrite (large prisms, two cleavages), pyrite (black), and zircon (small, top), TL, NII, x30 (left); Backscattered electron image of cymrite (prisms, grey) and pyrite (white), Bălan deposit, Sulfide Belt.
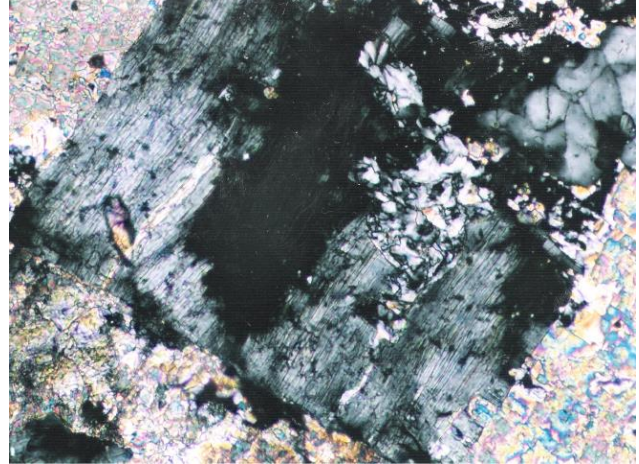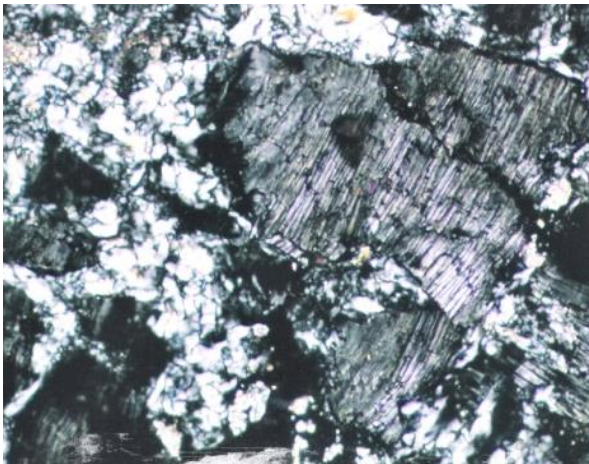
Fig. 16. Cymrite (large grey grains, perfect cleavage), partially altered, TL, N+, x30 (left); Cymrite (large quadratic shape) substituted by an amorphous mineral (black, isotrop), TL, N+, x35, Holdiţa deposit, Barium Belt.

The Bălan cymrite of Sulfide Belt presents large prisms (Fig.15 left and 15 right), while the Holdiţa cymrite has smaller grains with micaceous aspect (Fig.16 left and 16 right). Some Holdiţa cymrite become unstable, being substituted by various carbonates and an yet unidentified isotrop amorfous mineral, most probaby a Ba zeolite (Fig. 16 right). These differences in the crystal habits/general shapes of cymrite in the two belts are a result of small differences of metamorphic conditions which were, most probably, a little higher (T and P) in the Sulfide Belt ore than in that of Barium Belt. The zircon inclusions are present in both Holdiţa and Bălan cymrite (Figs. 15 left and Fig. 16 right).

The iron sulfides/massive pyrite ore of Sulfide Belt could be the expulsion into middle Cambrian seefloor, in areas such as mid-ocean ridges, of hydrothermal fluids from which metal sulfides are directly precipitating, the processes also taking place at the present-day (Vaughan and Lennie, 1991).

Vaughan (1986) suggests that the manganpyrosmalites (which are present in manganese ore of Manganese Belt, and ferropyrosmalites (which are present most probably in sulfide ore of Sulfide Belt could have a prograde metamorphic origin (from metalliferous brines) rather than a retrogressive breakdown of anhydrous Fe-Mn silicates (tephroite, rhodonite, and pyroxmangite) in areas locally enriched in water and chlorine in the later stage. The initial Cl-emichment in the old host lithologies may have occurred during seafloor hydrothermal alteration as an integral part of the syngenetic ore-forming processes for the associated base-metal mineralization (Vaughan, 1986). Therefore, in the tephroite/ manganpyrosmalite/rhodonite association of the Fig. 3 right, the manganpyrosmalite was formed there from the beginning, as old mineral, coexisting with tephroite/rhodonite along metamorphic history.

5. Uranium belt

The Crucea Uranium deposit is situated at the proximity tectonic contact of the old Precambrian Bretila Group which thrusts over the younger Cambrian Tulgheş Series. Geologically and structurally the Bretila Group belongs to a complex area, so called Eastern Central Carpathian Nappes (Săndulescu, 1984). Because of its complex tectonic setting, some host rocks of the Crucea deposit are strongly retromorphosed (Fig. 17 left) and highly carbonatated/chloritized. Some micaceous quartzites with titanite (Fig. 17 right), and quartzites with stilplomelane and accessory monazite-(Ce) and allanite-(Ce) around Crucea U-deposit belong to TG4. A few other small uranium mineralization points occur near Crucea deposit. These small occurrences and the large Tulgheş pitchblende occurrence (Tulgheş Valley, at Grinţieşu) in the south of Crucea deposit, might determine us to trace the fourth belt, the Uranium Belt (UB), situated in the East of the other three MnB, BaB, SB, on the alignment Crucea-Grintieşu (Fig. 1).
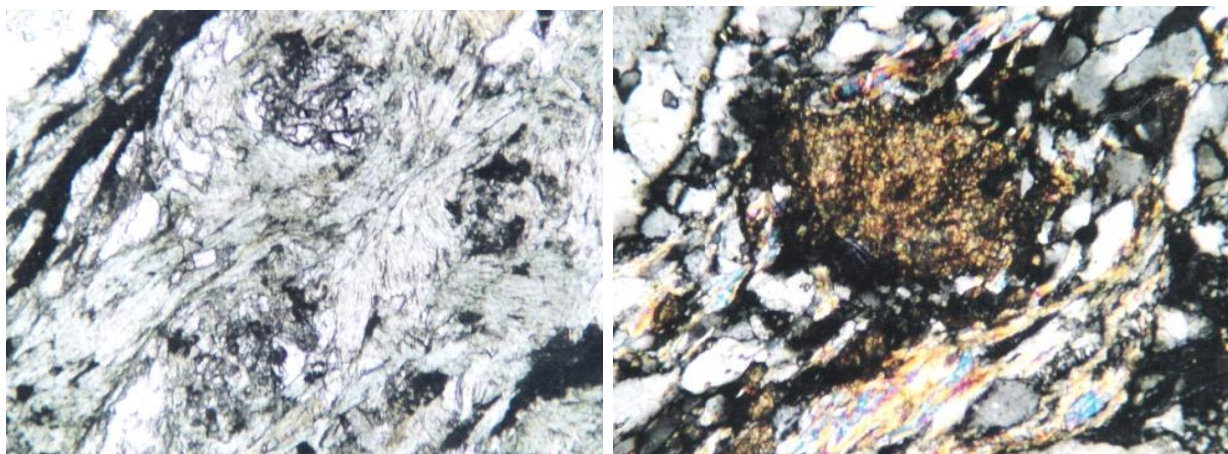
Fig. 17. Pietroşu Bistriţei porphyroide granite: almandine relics in quartz/chlorite/albite/graphite rock, TL, NII, x30. Titanite (centre), muscovite (cleavage, colored), quartz (white-grey), and albite (white), TG4 level (left);

The Uranium mineralization of Crucea deposit presents three mineralogical composition: a. the primary uranium ore is mainly constituted by uraninite/pitchblende enclosed in black carbonaceous matter (CM) as angular pure grains (Fig. 18 left) and as botryoidale band/vein (Fig. 18 right), and as vein free of CM (fig. 19 left); b. primary (Fig. 19 right) and secondary coffinite (Fig. 19 left) as veinlets, free of carbonaceous matter; c. Later uraninite mineralization as octahedral and cubic crystals, rarely dodecahedral, and a combination of these three types, especially cubes with octahedral corners (Figs. 20 and 21). The uraninite crystals have up to 0.5cm in size and more, and occur in microgeodes. All three U mineralization types are always accompanied by sulfides/arsenides, sometimes as constituent minerals (Figs. 18 left and right, and 19 right). The Grinţieşu pitchblende, known as nasturane, generally is massive, black, granular or forms veins/bands/nests with a botryoidal to reniform appearance of cm. The pitchblende is a primary, metamict, and impure variety of uraninite. It is amorphous, pitchy form of the crystalline uraninite. The Grinţieşu pitchblende is hosted by Pietroşu Bistriţei Precambrian retromorphosed porphyroid granite at its tectonic contact with TG4.

The presence of Fe-Zn-Pb-Ni-Co-As sulfide/arsenide association in the Uranium Belt, which also occurs in the Mn Belt, Ba Belt, and Sulfide Belt, indicates that the UB mineralisation was hydrothermal submarine in origin, having genetic similarities with the other three belts. But, nevertheless it was tectonically transformed and remobilized from its original source, which was the TG4 level of Tulgheş Series. The Crucea Uranium deposit sulfides/arsenides comprise three mineral associations: (1) dominated by pyrite and pyrrhotite; (2) polymetalic sulfides, dominated by Pb-Zn-Cu, represented by chalcopyrite, sphalerite, galena, bornite, and bournonite; (3) Ni-Co-As sulfides dominated by Ni-pyrrhotite, pentlandite, polydimite, gersdorffite, and rammelsbergite.Textural relations of Crucea uranium sulfide deposit data suggest that sulfides and uranium mineralization was closely intergrown being related in time and space. The gangue of this U-mineralization is constituted by calcite, siderite, dolomite, sudoite, mica, and quartz. Other sulfides, such as tetrahedrite, tennantite, marcasite, stibnite, and greenockite (Hirtopanu, 2019) were also determined at Crucea deposit, and they are also present in Sulfide Belt. The gangue of the new hydrothermal uraninite crystals ore is represented by calcite, dolomite, siderite, ankerite, and quartz crystals (Figs. 20 left and 20 right, 24 left, and 21 right).
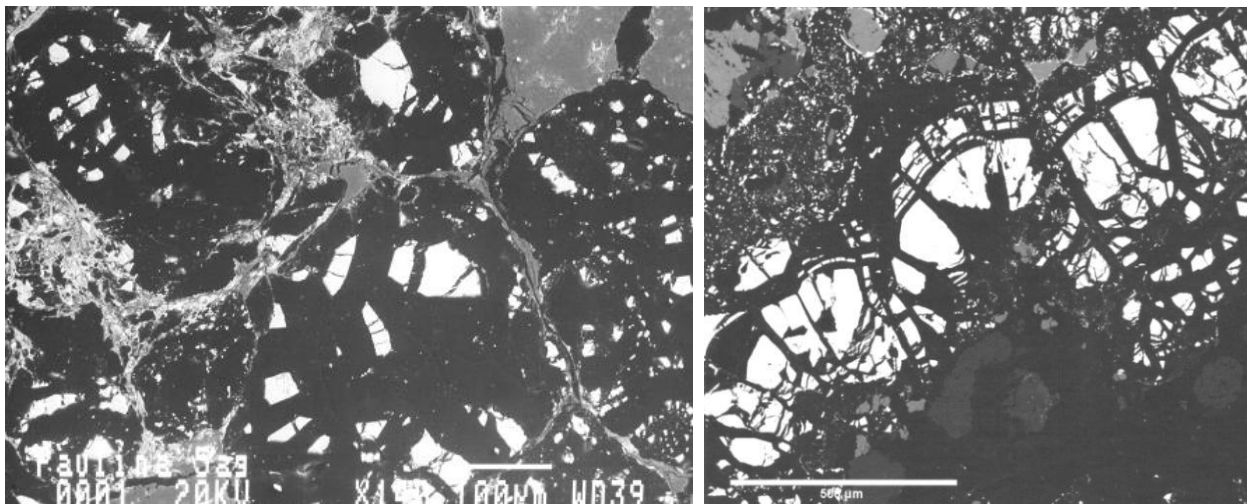
Fig. 18. Backscattered electron image of uraninite grains (bright white) in carbonaceous matter (black) and small sulfides (grey) intergrowth with coffinite (white) on veinlets (left); Backscattered electron image of botryoidal uraninite (bright white), coffinite (white, veinlets inside uraninite and around sulfides), carbonaceous matter (black), and sulfides (small grey grains, top left corner) (right).
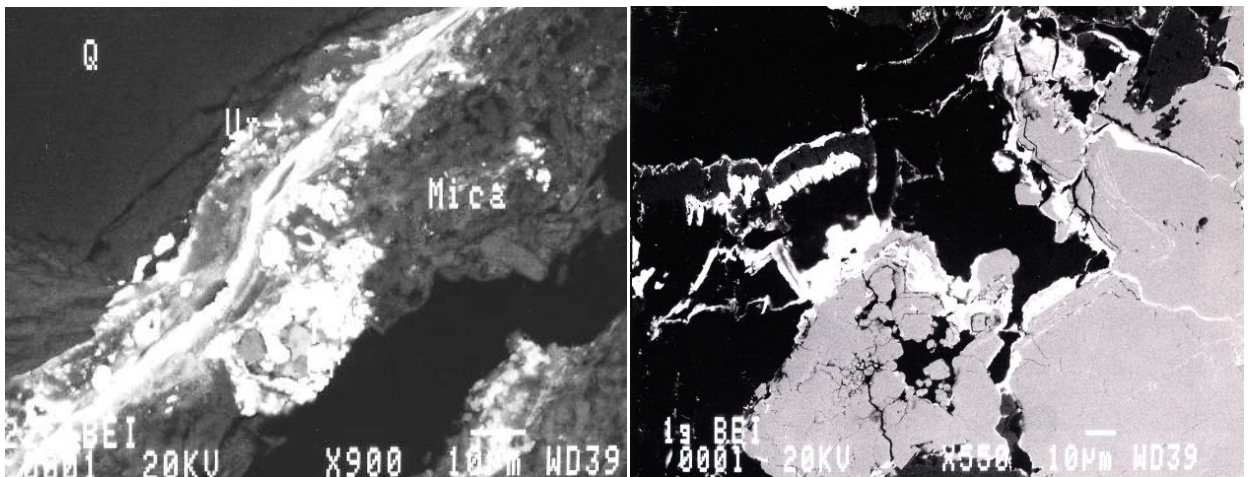
Fig. 19. Backscattered electron image of coffinitized (white, light grey) uraninite (main veinlet, braight white) uranophane (light grey inside coffinite and uraninite), mica (Mica, dark grey) and quartz (Q, black) (left); Backscattered electron image of Ni-pyrrhotite (large light grey grain) with coffinite (white, veinlets around and inside it), Fe and Mg rich carbonate (black) with coffinite inside it (right).

Fig. 20. Photo of geode/lens (20 cm long) with 0.8cm uraninite crystals in hydrothermal calcite/dolomite(white) and quartz (grey) (left); Photo of uraninite crystals of 6mm in size and/on calcite crystals as gangue (right).

52

Fig. 21. Photo of uraninite crystals of 8mm size grown on/with calcite crystals in quartz gangue (grey) (left); Photo of uraninite crystal of 7mm grown on/with calcite crystals and with sulfide impregnation (right).

The chemical composition of Crucea CM shows only C with a little S (which could come from associated sulfides), and its enclosed uraninite shows a pure composition, consisting only of Uranium. The electron microprobe analyses (Janeczek and Ewing, 1992) indicate that uraninite readily exchanges elements with the later fluids. In particular, radiogenic Pb is replaced by Ca, Si, and Fe via discrete alteration of uraninite (Janeczek and Ewing, 1992). The electron diffractogram spectra of Crucea uraninite show that the most significant substitution of uraninite leads to its conversion to coffinite, with more than 10 wt% SiO_2. The other elements that change radiogen Pb into uraninite are: P, Ca, K, Fe, Ti, Al, Mg, and Na.The P and Ca appear to be the most common substituents within coffinite, and sometimes they have high content, so probably a new mineral, named ningyoite, $UCa(PO_4)_2.1-2H_2O$, occurs in Crucea U-deposit. The character of the substitutions depends on the amount and composition of the alteration fluids, particularly their capacity for oxidation and by the characteristics of the host rock through which the fluid circulates. In Fig. 19 the backscattered electron image of Crucea Uranium ore has a polyphase evolution: U-oxide and U-silicate minerals are shown on pictures with different shades of white/gray in the uraninite /pitchblende large main vein, from uraninite (bright white, centre, high U), to anhydrous coffinite (white, around uraninite, high U, low Si), and hydrated uranophane (light grey, inside both, low U and high Si).

The U mineralization evolved in the same subduction zone as Mn, Ba and Sulfide ores. The U mineralization is a multistage type of genetic process, which implay multiple stages of dissolution and reprecipitation. The fluid-geochemical Crucea uranium formation and remobilization history has been recorded in at least 6 stages: (1) The precipitation of a urano-organic (?) and hydrothermal complexes on the Cambrian sea floor, the initial emplacement of U mineralization; (2) The metamorphism of these complexes determined the forming of CM with uraninite inside it through a reduction of mobile U^{6+} to immobile U^{4+} due to the presence of sulfides which act as reductants; (3) The tectonic pre-Alpine event, represented by the thrusting of Bretila Group over the TG4, most probably caused the strongly remobilization of U mineralization, from its original source (TG4) to nearest and under older Bretila Group; (4) The maturation of CM (now it looks like a graphite) by radioactivity caused the uranium enrichment, resulting in an increase in U minerals, especially U silicate, which form veinlets in mineral gangue, in proximity to uraninite/pitchblende ore; (5) The new appearence of a new U mineralization, such as the euhedrale uraninite crystals/group of crystals, is most probably linked with a new locally hydrothermalism, which usually happened at T <250^{0}C (Janeczek and Ewing, 1992). The later uraninite crystals are due to the younger alteration and remobilization events, rather than the primary mineralization event. This hydrothermal uraninite typically occurs as veins and in geodes. In the hydrothermal systems, the transport of hexavalent uranium (U^{6+}) occurs as soluble uranyl $(U^{6+}O_2)^{2+}$ complexes in oxidizing hydrothermal solutions along faults and cracks. The uraninite precipitation is often controlled by fluid interaction with country rocks or mixing with reducing fluids, causing physicochemical changes to a hydrothermal fluid, especially a decrease in the oxidation state of a fluid (Janeczek and Ewing, 1992). The new hydrothermal uranium ores are commonly structurally controlled and related to fracture and fault zones; 6) Under the oxidizing conditions, tetravalent uranium of uraninite and uranium silicates changes to hexavalent uranium and forms oxide, vanadate, arsenate, silicate, sulphate, and carbonate compounds, most of them bright yellow or green.

Therefore, the uraninite and uranium silicates tend to form under reducing conditions, whereas various uranyl minerals tend to form under oxidizing conditions.

6. Conclusions

The close mineralogical interbedings/interferences of Mn, Ba, Sulfide, and U ores demonstrate their common submarine hydrothermal origin, and their common evolution in a subduction tectonic framework. This evolution is reflected in the great thickness of thousands of meters of their host rocks, the Tulgheş Series. The Mn, Ba, S, and U belts evolved in the Cambrian sea floor, in a subduction zone, in a narrow active paleotrench area, reflected in their linear development as belts (Fig. 1). The hydrothermal submarine activity began with the Mn mineralization with small amount of Ba and sulfides (TG1), and more Ba and Sulfides with a little Mn (TG2) toward East and upper Mn deposits, where the seafloor was moved. In the TG3 the seafloor was subducted towards the East and the sulfides with a little barium mineralization were deposited at some distance from and over the Mn and Ba ores, but with the same orientation. Finally, in the upper Cambrian (TG4) the sea floor was more subducted towards East, and the uranium mineralizations were deposited at some distance from the sulfide belt and with the same orientation. The pre-Alpine thrusting of Bretila Group over Tulgheş Series provoked the remobilization /migration of the U ore from its original location (TG4) near and inside its new cover (Bretila Group).

The four mineralized belts indicate that a Cambrian hydrothermal submarine system have been active/reactivated from TG1 to TG4. The submarine hydrothermal activity was fluctuant, a phenomenon also occurring in the current hydrothermal submarine deposits. The Uranium Belt mineralization was hydrothermal submarine in origin, having genetic similarities with the other three belts. But, nevertheless it was tectonically strongly transformed and remobilized from its original source, which was the TG4.   The metamorphic evolution of the Mn, Ba, S, and U belts, and their host rocks, were achieved through repeated and superimposed metamorphic events, each metamorphic event being a source of new minerals.

References

Brown E.H., Ghent E.D. (1983) Mineralogy and phase relations in the blueschist facies of the Black Butte and Ball Rock area, northern California Coast Ranges. Am. Mineral., v.68, p. 365-372.

Dasgupta S., Miura H., Hariya Y. (1985) Stability of Mn-cummingtonite-an experimental study. Mineralogical Journal, v.12, p.251-259.

Essene, E.J. (1967) An occurrence of cymrite in the Franciscan Formation. Am. Mineral., 52, p.1885-90.

Lattard D., Schreyer W. (1983) Synthesis and stability of the garnet calderite in the system Fe-Mn-Si-O, Contrib. Mineral. Petrol., v. 84, p. 199-214.

Hirtopanu P. (2004) Mineralogia centurii manganifere din muntii Bistriţei. (Mineral genesis of the manganese belt in the Bistriţa Mts.). Edit. Cartea Universitară, Bucharest, 352 p.

Hirtopanu P., Andersen J.C., Chukanov N., Petrescu L. (2008) Cymrite from Bălan sulfide deposit, East Carpathians, Romania. Rom. J. Mineral Deposits, v. 83, p. 58-61.

Hirtopanu P. (2019) New minerals and mineral varieties for România. Ed. Vergiliu, Bucharest, 263 p.

Hsu L. C. (1994) Cymrite: occurrences and stability. Contrib. Mineral. Petrol., v. 118, no.3, p. 314-20.

Janeczek J., Ewing R.C. (1992) Structural formula of uraninite. J. Nucl. Mater., v. 90, p. 128-132.

Jamieson W.J., Tivey K.M., Hannington D.M., Hamsteen H.T. (2016) Precipitation and growth of barite within hydrothermal vent deposits from the Endeavour Segment, Juan de Fuca Ridge. Geochim. et Cosmochim. Acta, v. 173, p. 64-85.

Morro M.C., Fernandez A., Cembranos M.L. (2001) Celsian, (Ba,K)-feldspars, and cymrite from Sedex barite of Zamora of Spain. Can. Mineral. v. 39 (4), p. 1039-1051.

Peters Tj., Schwander H., Trommsdorff V. (1973) Assemblages tephroite, pyroxmangite, rhodochrosite, quartz: experimental data and occurrences in Rhetic Alps. Contrib. Mineral. Petrol., v. 42, p. 325-333.

Săndulescu M. (1984) Geotectonica României. Ed. Tehnică, 336 p.

Seki, Y., Kennedy G.C. (1964) Phase relations between cymrite, $BaAlSi_3O_8(OH)$, and celsian, $BaAl_2Si_2O_8$. Am. Mineral., v. 49, p. 1407-1425.

Vaughan J.P. (1986) The iron end-member of the pyrosmalite series from the Pegmont lead-zinc deposit, Queensland. V. 50, nr. 357, p. 527-531.

Vaughan J.P., Lennie A.R. (1991) The iron sulphide minerals: their role in nature. Sci.Progress, Edinburgh, v .75, nr. 3/4, p. 371-388.

Wood R.M. (1980) Compositional zoning in sodic amphiboles from blueschist facies. Miner. Mag., v. 43, p. 741-52.

THE MINING INDUSTRY, A RETROSPECTIVE OF THE 2000s: FROM THE BOOM TO THE *ENTER THE DRAGON* (I)

Antonela NEACȘU, Gheorghe C. POPESCU

University of Bucharest, 1, Nicolae Balcescu Blv. 010041 Bucharest, Romania
antonela.neacsu@gg.unibuc.ro, gheorghec.popescu@yahoo.com

Abstract: The mining activities were directed to less accessible sites and lower grades of ores, in order to satisfy a *linear* economic model. The intense consumption of metal by emerging industries *vs.* the limited amount of ore deposits in the Earth's crust generated a major crisis in the field of economic geology. The question is how long the boom of economic growth on the basis of mineral resources and especially of metal exploitation could last. The mining industry had great perspectives on the beggining of the 2000s. But the global financial crisis in the final quarter of 2008 restricted access to debt finance, with serious consequences for economic performance next years. Introducing structural changes in the 2011 industry's cost base, the financial results were not long in coming, reaching new superior values until 2013, when free cash flow for the OECD companies became negative. Free cash flow will improve again in 2014, due in large part to a decrease in capital expenditures. At the end of 2014, the market capitalization for the Top 40 was as in 2005, meaning less half of its value in 2010.

Keywords: economic model, economic geology, *critical raw materials*, mining industry trends, mining deals, future mining technology, PwC's *Mine* reports, Top 40, Industry 4.0, *resource nationalism*.

1. Introduction. The end of the mineral resources?

The global market, shaped in the 18th century by free trade and the massive movement of labour, has led to a continuous economic growth. Two hundred years later, natural resources have been treated as infinite in *economic sense* (Simon 1981, 1996), being considered *the constant and stable foundation for economic activity* (O'Neill & Khan, 2000). The economic press was, until recently, full of metaphors: 'The new Growth Evidence' (Temple, 1999), 'The Greatest Century That Ever Was: 25 Miraculous Trends of the last 100 Years' (Moore & Simon, 1999), 'Two Centuries of American Macroeconomic Growth From Exploitation of Resource Abundance to Knowledge - Driven Development'(Abramovitz & David, 2001). As part of the business, the mining industry faced a paradigm shift: the extraction activities were directed to less accessible sites and lower grades of ores, in order to satisfy a *linear* economic model, according to which stopping or at least slowing growth were inconceivable, despite eroding its own base of raw materials. As the economy and GDP grew, so did the costs of extraction and market prices of mineral resources. The intense consumption of metal by emerging industries *vs.* the limited amount of ore deposits in the Earth's crust generated a major crisis in the field of economic geology, as the famous reports of Club of Rome stated beginning to 1972. These assumptions have generally been proven wrong (Bender, 1977, 1982, Schodde, 2004), in terms of an oversupply of mineral commodities and a decrease of the price of most industrial metals until 2000 approximately. At the beginning of the 70's, exploration works were spectacularly stimulated by *the global tectonics concept*. As a consequence, in few decades, impressive new *world class deposits* (acc. to Singer, 1995) or *giant/supergiant deposits* (acc. to Laznicka, 1999) have been discovered: 90 *porphyry* Cu-Mo, 6 *porphyry* Cu-Au, 17 *porphyry* Mo, 13 epithermal Au-Ag, 7 epithermal Au, 23 SEDEX Zn-Pb-Ag, 22 VMS, 4 epithermal Pb-Zn-Ag, 4 scheelite skarn, 12 high-grade metamorphic Pb-Zn-Ag deposits. Japan (1960s-1970s), South Korea, Taiwan and Singapore (1970s-1980s) were developed a rapid industrialization related to mineral resources consumption, followed in the 1990s by China, the world's second largest Cu and Al consumer, and India, the world's largest consumer of gold (Laznicka, 2006). The continuous economic and technologic growth requires REEs (rare earth elements), RMs (rare metals) and PGEs (platinum group elements) to the point where these resources become indispensable (meaning *critical*) (Fig. 1, 4). The REEs are the ability to form small and very powerful magnets essential for smart devices and low-carbon energy electronics, wind turbines and hybrid cars. The military industry needs rare earths too. There are no substitute alternatives to these REEs (https://www.irishtimes.com/business/technology/irish-scientists-discover-how-rare-earth-mineral-is-formed-1.4439657?mode=amp), so they are considered to have *strategic* value. The United States was a significant REEs producer through the 1990s, but its production could not keep up with China's political measures looking low-priced materials, cheap labour costs and low environmental protection standards. As Deng Xiaoping prophetically said in 1992: *The Middle East has its oil, China has its rare earths* (Bradsher, 2009). China's dominance in the production of REEs was maintained after 1994 (Fig. 2): in 2010/2011

China reached a market share of around 97% of all rare earth mineral production. Outside of China, there were the US and other insignificant producers left (*e.g.,* Australia) (Schmid, 2019). The US became dependent on imports of REE-based components, since it stopped its rare earth production in 2002. As the second largest consumer of the world behind Japan, the US imported about 80% of its rare earths from China during 2015-2018 (https://www.scmp.com/economy/china-economy/article/3097847/chinas-rare-earth-export-plunge-caused-coronavirus-not).
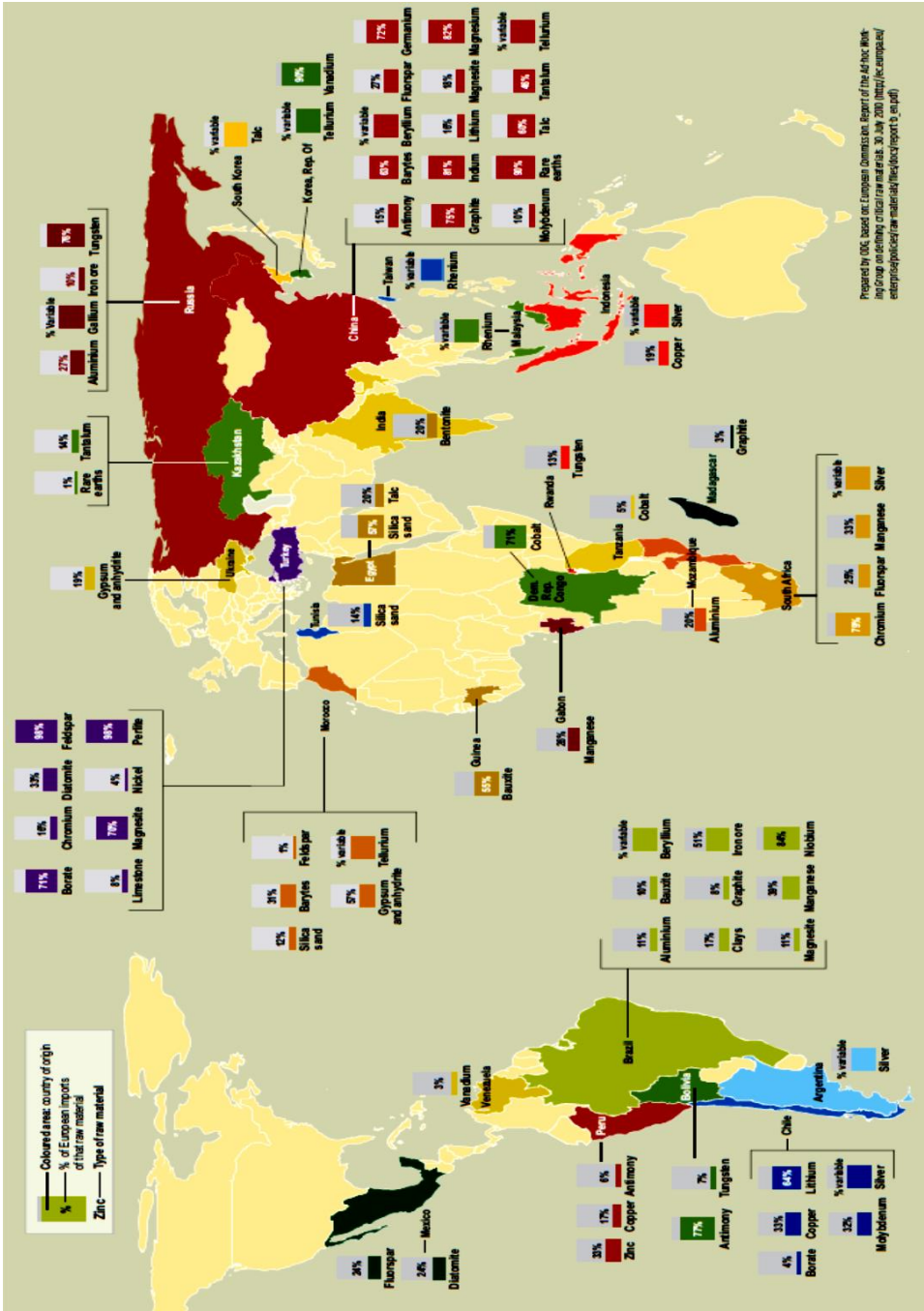
Fig. 1. The EU's dependence on critical raw materials. Source *Impunity Inc.,* 2012.

Only in 2018, the US imported a total of 18,500 tonnes, amounting to $165 million (https://comtrade.un.org/data/). Realizing the risks of depending on China for supplies, the US restarted in 2019 operations at the Mountain Pass Mine in California, with output lifted to 26,000 metric tonnes in 2019. In recent years, the EU has imported about the same amount of rare earths as the US, being among the largest consumers worldwide (Schmid, 2019). China continues to play a leading role in terms of REEs, holding 62.85% of the world mine production in 2019, and 36.66% of the world total geological reserves (https://pubs.usgs.gov/periodicals/mcs2020/mcs2020-rare-earths.pdf). There are known more than 250 REE-bearing minerals, but only three are economically viable and commercially exploited: the largest is

the carbonatite REEs Bayan Obo in China. Bastnäsite is probably the main valuable mineral for REEs in the world (https://www.irishtimes.com/business/technology/irish-scientists-discover-how-rare-earth-mineral-is-formed-1.4439657?mode=amp).
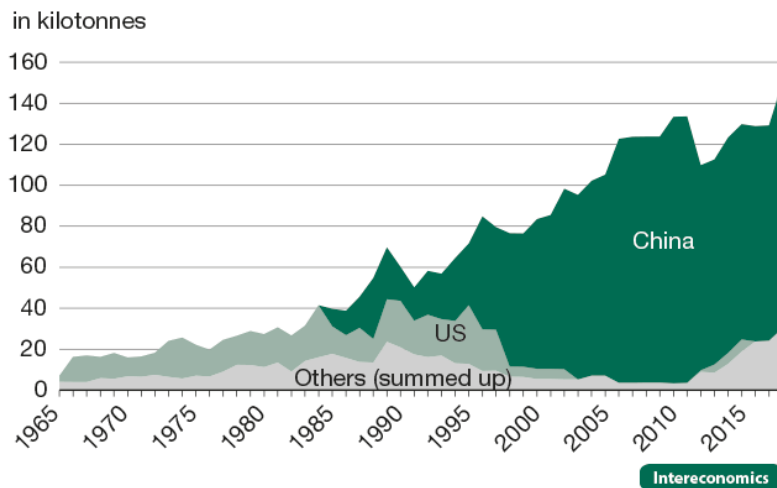
Fig. 2. Development of the REE's production market. In rare earth oxide equivalent content.
Source: *Intereconomics* 2019, based on data by USGS, available at http://minerals.usgs.gov/minerals/pubs/commodity/rare_earths/.

World Mine Production and Reserves: Reserves for Canada, Greenland, Tanzania, and South Africa were previously included with "Other countries."

	Mine production[e]		Reserves[8]
	2018	**2019**	
United States	18,000	26,000	1,400,000
Australia	21,000	21,000	[9]3,300,000
Brazil	1,100	1,000	22,000,000
Burma (Myanmar)	19,000	22,000	NA
Burundi	630	600	NA
Canada	—	—	830,000
China	[10]120,000	[10]132,000	44,000,000
Greenland	—	—	1,500,000
India	2,900	3,000	6,900,000
Madagascar	2,000	2,000	NA
Russia	2,700	2,700	12,000,000
South Africa	—	—	790,000
Tanzania	—	—	890,000
Thailand	1,000	1,800	NA
Vietnam	920	900	22,000,000
Other countries	60	—	310,000
World total (rounded)	190,000	210,000	120,000,000

U.S. Geological Survey, Mineral Commodity Summaries, January 2020

[e]Estimated. E Net exporter. NA Not available. XX Not applicable. — Zero.
[9]For Australia, Joint Ore Reserves Committee-compliant reserves were 1.9 million tons.
[10]Production quota; does not include undocumented production.

Fig. 3. REE's world mine production and reserves (https://pubs.usgs.gov/periodicals/mcs2020/mcs2020-rare-earths.pdf)

The so-called *grey gold*, coltan is one of the most hunted material ourdays (Fig. 4), used in high-tech applications, aerospace industry, and in several electronic devices. In 2006, Australia, Brazil, and Canada produced 80% of the world's coltan, but since 2018 Rwanda, the Democratic Republic of the Congo (DROC), Nigeria, Brazil and China led the top, some of them with rank as high alert (DROC), through alert (Nigeria) and high warning (Rwanda) (https://en.wikipedia.org/wiki/List_of_countries _by_Fragile_States_Index).
The world mine production for Nb-Ta has significantly increased in the past two decades, currently accounting for roughly 60,000 (Nb) and 1,200 (Ta) tonnes/year (Filella & Rodríguez-Murillo, 2017, *apud* Romero-Freire *et al.,* 2019). So, the end of the mineral resources is just fake news. The question is how long the boom of economic growth on the basis of mineral resources and especially of metal exploitation could last. Kesler (1994), Holland & Petersen (1995), Kesler & Simon (2015) warned that this was a temporary situation. So did P Krugman (see 'The myth of Asia's miracle', Foreign Affairs, 1994), and, in fact, many others, such as K Arrow, P Dasgupta, L Goulder, G Daily, P Ehrlich, G Heal, S Levin, K G Mäler, S Schneider, D Starrett, B Walker (see 'Are we consuming too much?', Journal of Economic

Perspectives, 2004): *consumption's share of output is likely to be higher than that which is prescribed by the maximize present value criterion.*
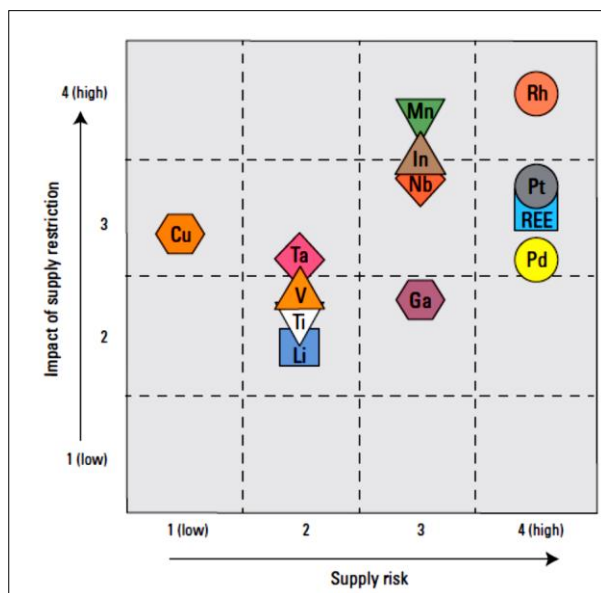
Fig. 4. Criticality matrix for RMs (Nb, Ta, Li, In, Ga, Mn, Ti, V), REEs and PGEs (Pt, Pd, Rh). They fall into the most critical zone of high supply risk and high impact of supply restriction. Source *National Research Council*, 2008, p.165 (https://pubs.usgs.gov/pp/1802/m/pp1802m.pdf)

2. The conventional economic model: development *vs* crisis

Trying to solve the problems, geologists, miners, processing engineers and mining investors have found themselves in the middle of a huge ecological crisis: *in the quantitative models (...) nature is taken to be a fixed, indestructible factor of production. The problem with the assumption is that it is wrong: nature consists of degradable resources* (Dasgupta, 2010). Among many others, another suggestive article was that of Berg & Ostry (2011) 'Inequality and unsustainable growth: Two sides of the same coin' (see Intern. Monetary Fund Staff Discussion Note, April 8, 2011). Moreover, well received by the public were the G Monbiot's articles criticizing growth as 'The Insatiable God', published by The Guardian in 2010s-2016s: the economic growth needed to stop because our society is running out of the resources that feed such growth. The exploration and mining activities have a major impact over the environment in the absence of appropriate prevention methods. The negative impact may be directly related both to the actual mining, and to supporting activities which ensure the mining logistics. So what does *an ecologically sustainable level* means? Given that economic growth is good, consumption is good, so the demand for mineral resources will continue to grow, even if they are qualitatively different from those of the earlier stages of the Industrial Revolution... Also *GDP isn't the best way to measure a good society. His alternative? The Social Progress Index, which measures things like basic human needs and opportunity* (see Green, Ideas.Ted.Com 2015). But the exponents of the conventional economic model didn't give up: *once matter-energy throughput is stabilized at an ecologically sustainable level we could presumably have significant GDP growth forever with minimal environmental costs, thanks to increasing total factor productivity* (see Worstall, Forbes 2014). Compiled from data of the World Bank, International Energy Agency, and International Council on Mining and Metals, Kesler & Simon (2015) mentioned that raw mineral production made up only a few percent of GDP in more developed countries (MDCs) (*e.g.,*the United States, the Netherlands, Sweden), reached 7 to 12% in Australia and Canada, and more than 35% in Norway. Higher percentages are more common in the BRICS, but especially in some less developed countries (LDCs), such as Papua New Guinea and Zambia, which are major copper producers, or the Persian Gulf countries that supply most of the world's oil.

Let's take a look to some of the global consequences of the conventional economic model:
• *Material growth myth.* Infinite energy demand from the exploitation of non-renewable resources.
• Linear economics – based on the continuous exploitation of resources.
• Petrostates. *Dutch Disease*
• GDP is an exact measure of welfare. GDP and demand of resources present a parallel growth.
• *Boomerang effect*: efficiency in using energy and resources accentuates growth,due to the expansion of operations and / or purchase new products; finally, an increase of demand of resources.
• The unprecedented rise of pollution, including mining wastes. Waste mining cost is not always reflected in the prices of goods.

• Inequity in mining policy
• Countries rich in mining resources have become/are becoming failed states. Overall welfare of LDCs, such as Zambia, the Democratic Republic of Congo, Tanzania, and Mongolia are highly dependent on raw-mineral prices. Mining HDCs lacking resources can get to control ore recovery activities, with maximum profit only for their citizens.
• Generating global economic crisis (*i.e.,* '70, 2008, and 2011).

3. The mining industry of the third millenium: the brilliant auspices of the begginings

The commodity prices and the market capitalization of the Top 40 are the two strongly correlated makers since 2004, when the first PricewaterhouseCoopers'*Mine* report (PwC's *Mine*) has been written. According to analyzes performed on the 40 global most important mining companies, the mining industry had exceptional economic indicators on the beggining of the 2000s.

3.1.'Enter the dragon'

This is the title of the 2005 PwC's *Mine*, where **2004** was considered *a spectacular year for the global mining industry*. All the economic indicators have risen compared to 2003: market capitalization upped 19% at $461 billion; revenue upped 39% at $184 billion; EBITDA (earnings before interest, tax, depreciation, amortization and impairments) increased 65.7% to $54.5 billion; net profit increased 111.4% to $27.9 billion; capex upped 24.3% to $22.5 billion; exploration expenditure upped 30.8% to $1.7 billion; dividends paid $8.916 million. The emergent economies were beginning to take the courage to invest in mining projects, improving their mineral and policy indexes. Only the Peruvian royalty systems declined the policy potential index from rank 19 in 2003 to 39 in 2004, according to the annual Fraser Institute Survey/*Reserves, exploration and political risk* section (data published in 2005 PwC's *Mine*), despite Peru ranked 2nd, 3rd and 7th in the production of silver, copper and gold in 2004 at the global level. The Top 40 was dominated by the founding OECD countries (Canada, United Kingdom, United States) + Australia and Japan, through 26 companies with mining projects for gold, copper and *diversifieds* (*e.g.,* Anglo American plc/UK rank 3, Barrick Gold Corp./Canada rank 7, BHP Billiton Group/Australia rank 8, Freeport Copper & Gold Inc./US rank 16, Newmont Mining Corp./US rank 30, Sumitomo Metal Mining Co. Ltd./Japan rank 37, and Xstrata plc/Switzerland rank 40 for the moment, but with an interestingevolution next years), but also for coal (Arch Coal Inc./US rank 6, Coal and Allied Industries Ltd./Australia rank 10). There were also companies from emergent OECD countries (two from Chile as Antofagasta plc rank 5, and Grupo México S.A. de C.V. rank 20), and from the BRIC group (two from Russia, *i.e.,* AK ALROSA on the first rank and MMC Norilsk Nickel rank 27, one from India (Neyveli Lignite Corp. Ltd. rank 31), and Companhia Vale do Rio Doce (CVRD) from Brazil, the future Vale S.A., rank 12). South Africa had a great influence with six companies, among which Anglo American Platinum Corp. rank 2 and AngloGold Ashanti Ltd. Peru participated with Compañía de Minas Buenaventura S.A.A. rank 11 (2005 PwC's *Mine*).

3.2.'Mine let the good times roll'

This is the slogan of 2006 PwC's *Mine* − the third annual review of global trends in **2005** mining industry, relevant for an optimistic state of mind: the 40 mining companies included in the analysis, representing over 80% of the total global industry by market capitalization, reported 59% increase in aggregate net profits, from $28 billion in 2004 to $45 billion in **2005**, in comparison with just $5 billion in 2002. These results have prompted the companies to increase the amount returned to shareholders to $16 billion in **2005**. The report showed that investor confidence in the mining industry and its prospects have continued to strengthen: in 2005 alone the industry's market capitalization increased by 72% to $791 billion; revenue increased by 25% to $222 billion; net profit margin improved to 20% from 16% in 2004; net cash inflow increased by 34% to $58 billion; capex increased by 31% to $31 billion; exploration expenditure increased by 29% to $2 billion, *etc.* As Brian Taylor, the UK Mining leader PricewaterhouseCoopers LLP, said: *we are now firmly in a mining boom and 2005 was an exceptional year by any performance measure. The key question on everyone's mind is how long this can last, but early indications suggest the results in 2006 will be even stronger* (https://pwc.blogs.com/press_room/2006/06/mining-sector-delivers-spectacular-results-for-2005.html).

3.3. The *spectacular* year 2006

Described as a *spectacular* year for the global mining industry, in **2006** net profits had increased by 64% faced to prior year, and profits were 15 times higher than in 2001. The net cash flow from operating activities was $76.7 billion, which represented 40% increase compared with 2005 (*Mining Weekly,* June 20, 2007). During **2006**, the global mining industry picked up from its rapid development in 2003-2005 (2007

PwC's *Mine*): The Top 40 increased their spending on investment activities by 83%, but the growth was under expectations, because problems as a shortage in skilled labour, depreciation of quality of equipments, lack of mining projects in safe areas, and weak innovation became pressing. Revenue growth was in line with commodity price increases (Fig. 5), being at 2.6 times the 2002 level. Governments required taxes to be paid to compensate for the removal of resource, a tendency that will be more and more relevant in our days. Net profit margin for the Top 40 maintained its almost linear growth since 2002, and was 28% compared to 5% in 2002. For the first time since 2003 its growth will begin to stop in 2007, when, in fact, it will declined with 26%. The **2006** Top 40 included companies interested in the same mineral resources as in 2004 and 2005, noting the growing demand for gold (Agnico Eagle Mines Ltd./Canada rank 1, Anglo
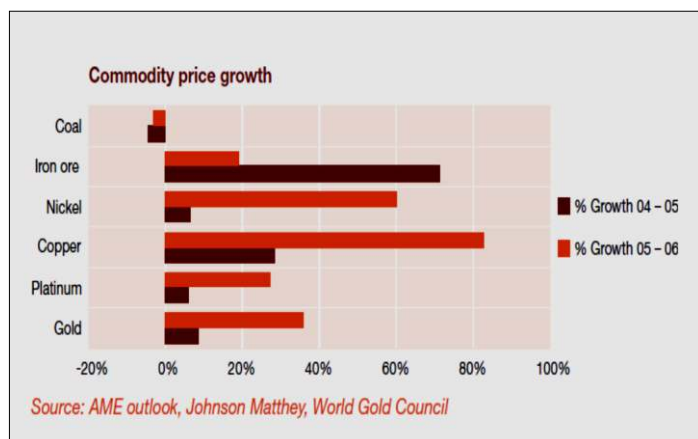
Fig. 5. Commodity prices in 2004-2006. The average prices have increased not only for nickel, copper, platinum, and gold, but also for silver (58%), aluminum (34%), cobalt (84%), uranium (106 %) and zinc (138%), acc. 2007 PwC's *Mine*

American plc/UK rank 4, three South African companies AngloGold Ashanti Ltd. rank 5, Gold Fields Limited rank 16 and Harmony Gold Mining Company Limited rank 18, and Xstrata/Switzerland upped to rank 37 from rank 40 in just a year), PGE (two South African companies Anglo Platinum Ltd. rank 3 and Impala Platinum Holdings Limited rank 19), copper (two Chilean companies Antofagasta plc. rank 6 and Corporacion Nacional del Cobre de Chile (Codelco) rank 14, Freeport-McMoRan Copper & Gold Incorporate/US rank 15, KGHM Polska Miedz S.A. rank 22), nickel (MMC Norilsk Nickel/Russia upped to rank 26), and zinc (Zinifex Ltd./Australia entered the Top 40 on the last rank). Coal demand has declined, but still found two important companies, *i.e.,* China Shenhua Energy Company Ltd. rank 10, and Coal & Allied Industries Limited/Australia rank 11. The number of non-OECD companies increased at 16 in **2006**, in comparison with 11 in 2004: six from South Africa, three from China, three from Russia, two from India, one both from Brazil (Companhia Vale do Rio Doce (CVRD), rank 12), and Poland. In **2006**, a number of mega deals had been sealed: Companhia Vale do Rio Doce leading the way when it bought Inco (2007 PwC's *Mine*).

3.4. Riding the wave

*The industry has entered **2007** on a very high note and companies' fortunes will depend on how they ride the wave* (*Mining Weekly,* June 20, 2007)*.* Recorded production costs increased significantly in **2007**, which led, among others, to a reorientation of Top 40 to operate solely in emerging markets with cheaper input costs. Thus, no less than 13 companies from emerging countries were found in **2007** Top 40, some of them constantly active until ourdays: China Shenhua Energy Company Ltd. rank 9, MMC Norilsk Nickel/Russia rank 28, and Vale/Brazil with a significant drop with 24 ranks. A meteoric entering of two Indonesian companies could be observed, such as PT International Nickel Indonesia Tbk on rank 32. Antofagasta became a British company and advanced to rank 4, so Chile was present only with Codelco rank 10. BHP Billiton Group, which will dominate the Top 40 after 2013, remained on rank 8 as an Australian company. Anglo American plc/UK recorded the highest revenue figure in 2006, being on 1st rank in **2007** Top 40. The market capitalization was of $9.1 billion for all companies of the Top, 36% belonging to emerging companies from the BRICs (including/Hong Kong), Indonesia and South America, in comparison with 14% in 2003. There are five South African companies in **2007** Top 40, including Anglo Platinum Ltd. rank 2 and AngloGold Ashanti rank 3. As will be seen, the participation of emerging countries will be increasingly relevant in the coming years, as the appetite for geopolitical risk will change, and UK, US, Australia, South Africa, *etc.*, will list companies operating solely in African and Asian territories. As with prior years, copper remained the dominant source of revenue for the Top 40, accounting for 28% of the total revenue, followed by coal, iron (12%) nickel (10%), and gold (9%). With a relative weaker

performance than last years, a number of gold companies expected better times and higher prices (2008 PwC's *Mine*). The *hedge funds* were more active in the mining industry, acting as a catalyst for boosting investments for short-term profits, as was the case, for example, in 2006. They would continue to play a role in the sector as high cash flows and easily accessible funds were making mining companies attractive targets (*Mining Weekly,* June 20, 2007). Overall, the year **2007** did not look bad for global mining industry, since net investing cash flows have increased 88% from 2006 and have exceeded net operating cash flows for the first time since 2003. Global capital markets had an increased confidence for the mining industry, with proceeds from share issues increasing by 100% from 2006. Revenue was 3.3 times and net profit was 20 times that of 2002, but EBITDA margins have stabilized for the first time after a continuous grown since 2002, and net profit margins have fallen for the first time since 2002 (2008 PwC's *Mine*). The rise in operating, labour, power, equipment, property and plant costs reflected both a significant reinvestment in the industry in **2007**, but also resource constraints, skills shortage, problems related to productivity factor, water shortage issue, the unprecedented rise of pollution and other environmental problems (2008 PwC's *Mine*).

4. Against the background of the global crisis: 2008-2010

The onset of the global financial crisis in the final quarter of **2008** was reflected to ongoing market and commodity prices and in restricted access to debt finance. These two years were characterized by a deal activity centered in North America, Asia-Pacific and South of Asia, but driven by Canada, China and Australia. Still the emerging countries were less affected, doubling the returns of companies in comparison with traditional mining countries. Against the background of the global crisis, the share of *hedge funds* increased as a store of wealth.

In **2008** prices fell to a level close to 2004, as well as the market cap, and, after a significant recovery, the two markers have a continuous downturn from 2011 to 2015 (Fig. 15), acc. to 2017 PwC Analysis. The total value of mining M&A (Mergers & Acquisitions) had seriously decreased, from $153.4 billion in **2008** to $77.1 billion in **2009**. Coal assets were attractive, particularly due to the continuous demand for coal from China, the total deal value increasing from approx.16% in **2008** to 27% in **2009**. Chinese acquisitions accounted 7.4% of all deals in **2009**, oriented to the Australian companies' assets with the aim of securing long term supply. However, China was the third as importance with $1.3 billion of deals, after Canada ($12.1 billion) and United States ($8.7 billion) (acc. to 2009 PwC's Annual Review *Mining Deals*). The share of *hedge funds* increased in gold and precious metals'assets, the contribution to deal value ranging from 17% in **2008** to 24% in **2009**.

There are some interesting details in the **2009** Top 40: AngloGold Ashanti Ltd./South Africa, Antofagasta plc/UK, Barick Gold Corp./Canada and BHP Billiton Ltd./BHP Billiton plc/Australia/UK continued their advancement, being on rank 2, 3, 4 and 5 respectively, while Anglo American plc/UK remained the first. To observe the increased share of traditional mining countries in an attempt to return to the boom for global mining industry: 28 OECD companies (+ Mexico and Chile), three from South Africa, 8 from the BRIC countries and one from Peru (2010 PwC's *Mine*). From now on, although Canada, Australia, USA and UK will remain the main actors in the global mining industry, the BRICs and other emergent countries will play an increasingly important role. The market capitalization of the Top was $6.5 billion in **2009**. The P/E ratio was *unusually high* due to huge earnings impacted by impairment and lower commodity prices, as 2010 PwC's *Mine* emphasized. In **2010** this ratio declined as profit growth has exceeded the increase in market capitalization (Fig. 6). The market capitalization was $11 billion, due to the larger gains of smaller companies, and the net assets remained at 35% of market capitalization, demonstrating not an undervalued industry, but an increasing by the profits that the mining industry has generated in **2010** (2011 PwC's *Mine*).

The **2010** Top 40 was comprised of 22 OECD companies and 18 emerging market companies, including those from the BRICs (plus Hong Kong), South Africa, Poland and Peru. Anglo American plc/UK, AngloGold Ashanti Ltd./South Africa, Antofagasta plc/UK, Barick Gold Corp./Canada and BHP Billiton Ltd./BHP Billiton plc/Australia/UK went down one place in the **2010** Top 40, being on rank 2, 3, 4, 5, and 6, while Anglo-Eagle Mines Ltd./Canada, not included in 2009 analysis, upped to the first rank. The newly listed and the largest new entrant was Coal India (rank 10). There was a cumulative 32% increase in revenues, 72% increase in adjusted EBITDA and an increase in net profit of 156%. From 2007, the emerging market players more than doubled the returns of companies in comparison with traditional mining countries (Fig. 7). Silver Wheaton Corp./Canada (rank 35) had the highest one-year TSR (Total Shareholder Return) of the **2010** Top 40 (2011 PwC's *Mine*), and continued successfully in **2011** Top 40 (rank 33). South Africa becomes officially an emerging country in 2010 by the BRICS founding, but, excepting the

2011 Top 40 edition, in all the others it is considered a traditional mining power, as the OECD's countries are.

Fig. 6. The P/E ratio. 2011 PwC's *Mine*
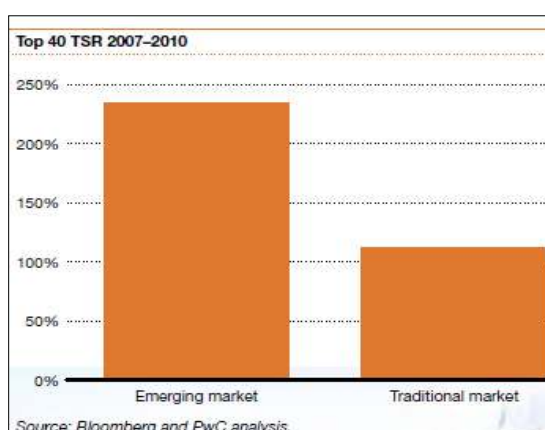
Fig. 7. Total Shareholder Return Data (TSR) 2007-2010. 2011 PwC's *Mine*

$ billion	2010	2009	2008	2007	2006	2005	2004	2003	2002
Aggregated income statement									
Revenue	435	325	349	312	249	222	184	110	93
Operating expenses	246	217	208	176	141	141	129	81	72
Adjusted EBITDA	189	108	141	136	108	81	55	29	21
Amortisation, depreciation and impairment	34	31	57	19	12	16	15	10	9
Income tax expense	38	22	21	32	27	16	9	4	2
Net profit	110	49	57	80	66	45	28	12	6
Increase/(decrease) in revenue	34%	(7%)	12%	25%	12%	21%	67%	18%	-
Increase/(decrease) in adjusted EBITDA	75%	(23%)	4%	26%	33%	47%	90%	38%	-
Year on year increase/(decrease) in net profit	124%	(14%)	(29%)	21%	47%	61%	133%	100%	-
Adjusted EBITDA margin	43%	33%	40%	44%	43%	36%	30%	26%	23%
Net profit margin	25%	15%	16%	26%	27%	20%	15%	11%	6%

Fig. 8. Nine-year trends 2002-2010 for the Top 40 (2011 PwC's *Mine*)

The 2011 PwC's *Mine* showed the 2002-2010 trends in the global mining industries, with a severe drop of revenue, net profit and adjusted EBITDA in 2009 (Fig. 8), together with a decrease of exploration spend, meaning a focus on the brownfield exploration. Despite of record revenue and an increase by 124% of net profit in **2010** to above $100 billion, also despite of the highest level of adjusted EBITDA, margins are impacted by the continuous increased operating expenses: at 43%, the **2010** adjusted EBITDA margin is no higher than *the excellent years* 2006 and 2007, whilst the commodity prices increased every year. Costs and the price of key inputs (already mentioned above) have remained high because of the financial crisis. In **2010** investing cash flows were only 58% of operating cash flows, compared to an average of 94% for 2003-2009. Operating cash flows increased to their highest level since 2003, by 65% over 2009. For the first time since 2005 financing cash flow was a net outflow, with a net of $35 billion being repaid to lenders or returned to shareholders (2011 PwC's *Mine*).

According to Metals Economics Group's *World Exploration Trends 2011*, the total global spend reached $12.1 billion in **2010**, up from $8.4 billion in **2009**: gold and base metals dominated exploration expenditure in **2010**, comprising approx. 85% of the total, gold alone accounted more than half of the total planned spending, the first time since 1999. As 2011 PwC's *Mine* stated, an uniform increase in copper reserves across the Top were attribute to Ivanhoe Mines Ltd./Canada (rank 21) and UK/Australian Rio Tinto plc/Rio Tinto Ltd.'s massive Oyu Tolgoi project in Mongolia (rank 32), to Freeport – McMoRan Copper & Gold Inc./US (rank 15) in North America, and also to a mining cluster program developed by the Chilean government, BHP Billiton and Codelco (Chile). The production of bauxite remained relatively stable, although BHP Billiton and Rio Tinto have reduced part of their ore reserves, following the changes in Brazilian environmental laws.

5. 'The growing disconnect'

This is the suggestive title of 2012 PwC's *Mine*, announcing structural changes in the **2011** industry's cost base, although the financial results hit new superior values: revenue increased 26% to over

$700 billion, net profit upped 21% to $133 billion, operating cash flows grew 34% to $174 billion, investing cash flows grew 92%, total assets was above $1 trillion and grew a further 13%, the Top 40 returned 156% more to shareholders than in 2010, including by way of dividends. Despite these last shareholder distributions, falling stock prices showed that investors expected larger cash returns in **2011**. A record level of net profit was generated by high commodity prices (Fig. 9), but margins remained flat because of higher costs (Fig. 11). One of the lowest levels of P/E ratios for the Top 40 (Fig. 10) suggested that miners were faced with investor confidence suspicions (2012 PwC's *Mine*).
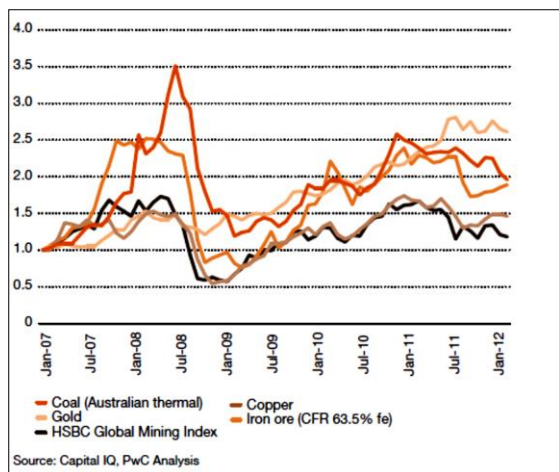
Fig. 9. Monthly average coal and some metals prices, HSBC Global Mining Index 2007=1(PwC's 2012 *Mine*)
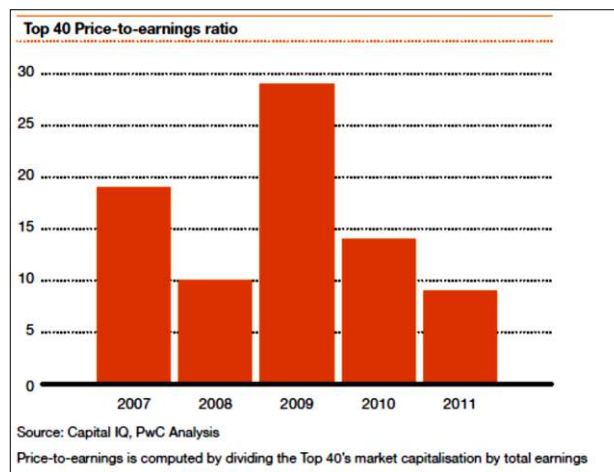
Fig. 10. P/E ratio resulting from the Top 40's market capitalization by total earnings (PwC's 2012 *Mine*)

The already mentioned structural changes in the industry's cost base is referring to the rise of costs of production, seen as inevitable in the future because of the decline of mineable grade deposits, generating more waste that needs to be mined and processed for the same amount of a commodity, and of course, because of more and more less accessible mining sites. At the end of **2011**, the total market capitalization for the Top 40 was of $1.2 trillion, compared with $1.6 trillion at the end of 2010. There were only six companies that posted positive movements in **2011**: three gold companies and other three related or focused on emerging markets.
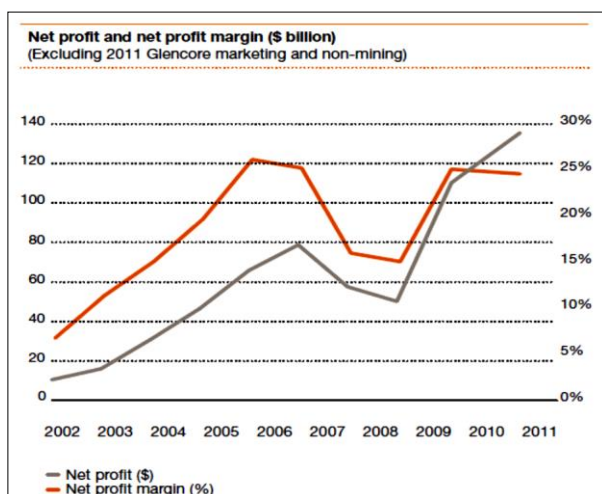
Fig. 11. Net profit and net profit margin ($ billion) (excluding 2011 Glencore marketing and non-mining). 2012 PwC's *Mine*
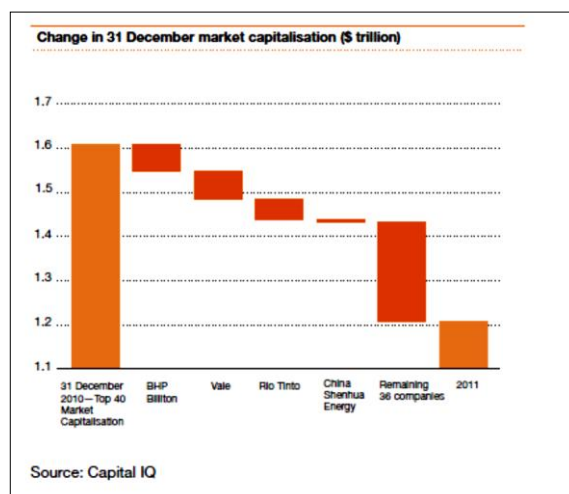
Fig. 12. The 2011 Top 4 companies by market capitalization. 2012 PwC's *Mine*

The Top 4 companies by market capitalization represented 38% of the Top 40 (Fig. 12) (2012 PwC's *Mine*). Excepting metallurgical coal, diamonds and zinc, the copper, gold, platinum, iron ore, nickel, bauxite and thermal coal production continued to grow in **2011**, with the special contribution of the same Top 5 companies as in 2009, and the other 12 companies from the BRICS (including Hong Kong and South Africa), as China Shenhua Energy Company rank 7 and Coal India Ltd. rank 8.

By market capitalization, emerging market companies constitute 38% of the Top 40 in 2011, up from 35% in 2010 − the highest level ever seen during the period 2002-2011. Diamonds didn't generate the expected profits for BHP Billiton and Rio Tinto, in contrast with Anglo American holding up to 85% interest in De Beers, and Botswana Government Company holding the 15%. Glencore joined the Top 40 on rank 15, following its IPO (Initial Public Offering) in **2011**, which was a turning point for the economic and market parameters of the Top: according to 2012 PwC's *Mine*, when included, revenue increased 65% over 2010, in comparison with only 24% when excluded.
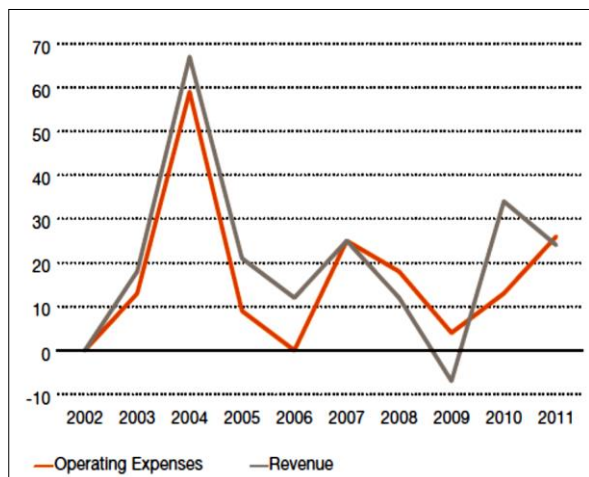
Fig. 13. Revenue and operating expenses between 2002 and 2011. 2012 PwC's *Mine*

The adjusted EBITDA margin fell to 32% − the lowest ever seen in *Mine* since 2004, and the net profit margins were to 19% when including, compared to 42%, and 25% respectively when excluding **2011** Glencore marketing and non-mining. For the first time since 2007, a strange situation related to the changes in net profit and net profit margin could be seen (Fig. 11): the net profit margin decreased while net profit was up. In **2011** was maintained the trend from 2007-2009 global financial crisis, meaning that operating expenses exceeded revenue growth (Fig. 13). But, there were different causes: during the global crisis, the commodity prices strongly declined, opposite to 2010 an especially to 2011, when commodity prices strongly increased, but the operating costs surged.

Only 15 companies from the **2011** Top 40 have been included in all prior editions of *Mine*, four companies returned to the Top after missing out in 2009 and 2010 (*e.g.,* Goldcorp), and two companies, which had been included in every edition of *Mine,* were simply leave the top: Consol Energy, because of weakening US coal demand, and Cameco, because of declined uranium demand after Fukushima nuclear disaster in March 2011 (2012 PwC's *Mine*).

6. 'Down, but not out': 2012-2013

In the March 2013 PwC's *Mine* report 'Down, but not out', looking for a review of global mining deals in 2012 and an outlook of 2013, it is mentioned that **2012** *was far from the most active year for mining mergers and acquisitions (M&A)*. The value of mining deals dropped in 2012, but not so dramatically as in 2009. *The deal of the year* was the merger between Switzerland - based Glencore International plc and United Kingdom - based Xstrata plc to form Glencore Xstrata plc/UK, one of the world's largest diversifieds mining companies, that will climb to 14th rank in 2013 Top 40. This merger deal value was close half to that of 2012 M&A total value (Fig. 14). Many leading companies of the last years' top, as Barrick Gold, BHP Billiton, Anglo American and RioTinto have revealed that they remain in the market only to sell. China had surpassed the US, being the world's biggest trading nation in **2012**, and consequently, a larger Chinese demand for commodities was expected, including an increasing appetite for mining investment. By the way, Shandong Gold's acquisition of Australian Focus Minerals and Zijin Mining's acquisition of Australian Norton Gold Fields drew attention to China's interest in global gold assets. Copper, zinc, silver and gold had improved their prices, after the unfortunate 2011. Copper and gold accounted for half of the **2012** Top 20 deals. If coal was the 2011 dominant commodity accounting for 26% of deal value, followed by copper with 23% and gold with 13%, in **2012** copper increased at 30% and gold at 27%, excluding the Glencore − Xstrata merger. The demand for copper allowed DROC to enter the 2012 Top 20, with two companies (the joint venture between La Compagnie miniere de Sakania Spr, Frontier Sprl and Roan Prospecting & Mining SPRL with South African Kolwezi Ltd. rank 9, and Camrose Resources Daletona Properties Limited rank 19), together with the well-known Inmet Mining Corp. Canada rank 2 and Anglo American Sur S.A. /UK, Chile rank 3. Iron ore was present in the **2012** Top 20 deals, due to the steelmakers: the world's fourth - largest steelmaker POSCO (South Korea) was part of a consortium

Fig. 14. Global mining M&A volume and aggregate value, acc. S&P Capital IQ, PwC Analysis. In 2013 PwC's *Mine*

that bought a 15% stake in ArcelorMittal Mines Canada Inc., and Anglo American increased its stake in South African Kumba Iron Ore Ltd. to just fewer than 70%, from previously 4.5%. After the Fukushima nuclear disaster in March 2011, there was a globally strong decline of uranium demand, but Japan step by step restarted its nuclear plants and China continued its nuclear power plant built out, leading to a slowly return of uranium prices. That's how the Canadian Denison Mines Corp. offered a stock-swap deal for Fission Energy Corp., and Russian state uranium company ARMZ proposed to take Canada's Uranium One Inc. On the other hand, the European interest for uranium has dropped, several governments seeking to sell stake of their own nuclear fuel vendor Ureco, the second world's larger. Critical resources enjoyed the **2012** Top 20 deals, by Neo Material Technologies Inc./Canada (rank 8) and Talison Lithium Limited/Australia (rank 14) (2013 PwC's *Mine*).

Looking to the year **2013**, the coal and metal prices fell significantly from 2012 (*e.g.*, (-9%) copper and coal, (-28%) gold), excepting iron ore: 6%. The price of gold has fallen after a continuous rise in 90s and 2000s, a trend that has continued through an absolute minimum of the last 10 years in 2016 (https://goldprice.org/gold-price-history.html). The profitability of the mining industry was at its lowest level since 2000. 2014 PwC's *Mine* reported that despite the decline in liquidity and a net debt up by 42%, a decrease of EBITDA of only 8% (see part II of this article, with data from 2019 PwC's *Mine*), and also a small increase of dividend yield of 4% had recorded in **2013** (Fig. 19). The operating costs increased by 4%, which will become a feature of the coming years, according to PwC's *Mine* reports. The Top 40's aggregate net profit sank $52 billion (72%) to a decade low $20 billion (*their deepest aggregate net profit depth in a decade,* as 2014 PwC's *Mine* noted); gold companies were responsible for $20 billion of net losses. Five gold companies fell out of the Top 40 in **2013**. The market capitalization fell by approx. $280 billion, meaning 23% (Fig. 15). 23% decrease in investing cash flows had as consequence that, for the first time, OECD's free cash flow was negative, at $(-6) billion in 2013, in comparison with that of the BRICS companies (Fig.16) (2014 PwC's *Mine*). Again, for the first time, most of the Top belonged to emerging market companies, accounting for 53% in December **2013**. The total net profits of them were $24 billion in aggregate, compared to a cumulative net loss of $4 billion for companies in developed markets, impacted particularly by impairments. Additionally, another unwanted $57 billion record impairment was recognized by the Top 40 during **2013**, after the prior year record of $40 billion: therefore, impairment charges were up 43% (2014 PwC's *Mine*).

The BRICS represent about 42% of the world's population, 23% of GDP, 30% of the territory and 18% of the global trade (according to http://brics2019.itamaraty.gov.br/en/about-brics/what-is-brics). In the **2013** Top 40, the emergent market companies were mainly from the BRICs in the end of December (2015

PwC's *Mine*) and, for the first time since 2003, none from South Africa: Vale/Brazil rank 3, the Russian Uralkali rank 17, MMC Norilsk Nickel rank 10, ALROSA rank 29, India (2 companies, including Coal India Ltd. rank 8), 6 companies from China & Honk Kong (China Shenhua Energy Company Limited rank 5, China Coal Energy Company Ltd. rank 23, Inner Mongolia Yitai Coal Company Ltd. rank 25, *etc.*), 3 companies from China (*e.g.,* Inner Mongolia Baotou Steel Rare-Earth Hi-Tech Co. Ltd. rank 36). The others were Saudi Arabian Mining Company (Ma'aden) rank 28, and KGHM Polska Miedz Spolka Akcyjna rank 30.
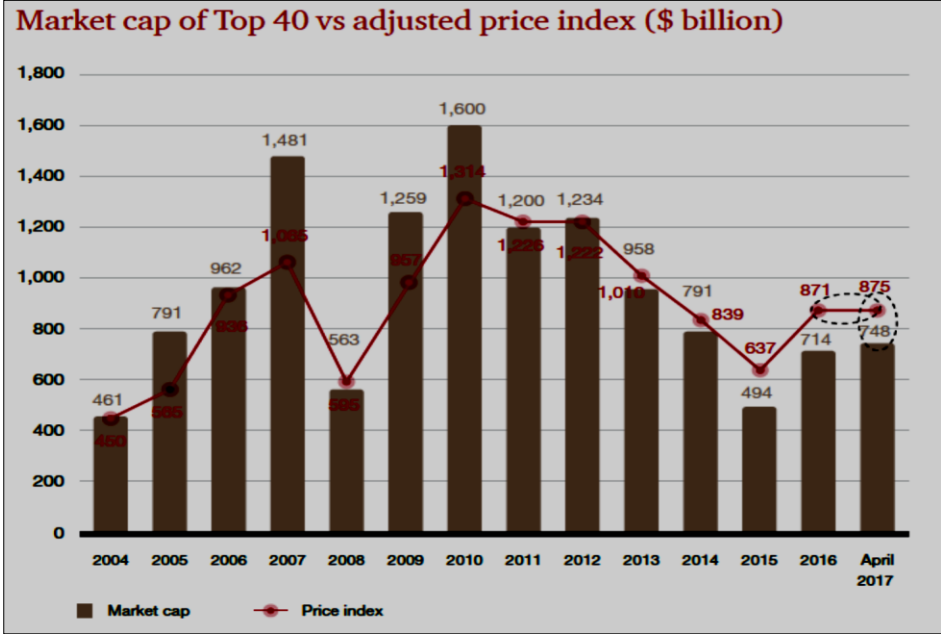
Fig. 15. Market capitalization of the Top 40 companies *vs.* an adjusted price index for a basket of commodities including copper, coal, nickel, zinc, gold, silver and iron ore. Source: PwC Analysis. 2017 PwC's *Mine*
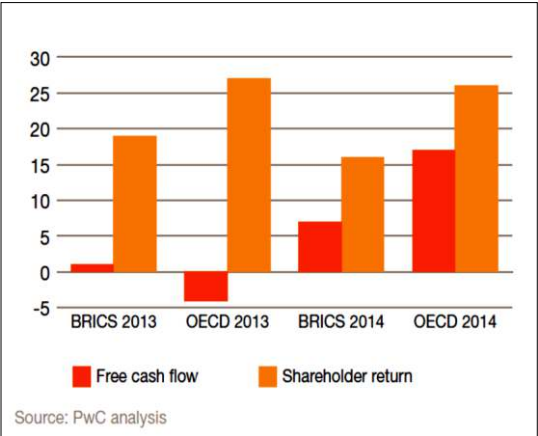
Fig. 16. Top 40 free cash flow and shareholder returns, acc. PwC Analysis. 2015 PwC's *Mine*
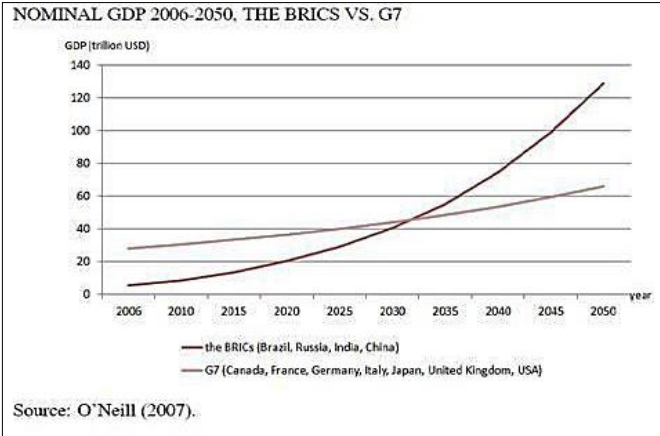
Fig. 17. The BRICs *vs.* the G7 economies in 2032 (O'Neill, 2007)

As 2014 PwC's mentioned: *2013 was a year that forced miners to realign expectations*. In the case of the BRICS, primary products and resource based manufactures represent the majority of the exports, which partially could explain their determination for investing in mining projects, *vs.* a decrease of the already mining investment values for the development countries. As O'Neill (2007) forecasted (Fig. 17), the BRICs (in 2007 without South Africa) as a group will overtake the G7 economies in 2032, so an increase of their influence in the global mining industry was expected. The same assumption will be found in the 2015 PwC's *Mine: BRICS companies tend to focus on mining in emerging markets exclusively, whereas OECD companies tend to have more diverse global portfolios*. Indeed, the OECD *diversifieds* represented 51% of the total market capitalization of the Top 40 during **2013**, up 5% from 2012. With two new top entries as Saudi Arabian Mining and the Sumitomo Metal Mining Company/Japan, they have reduced their portfolio

by divesting noncore commodities, a majority related to energy and assets outside of core mining (*e.g.,* BHP Billiton, Rio Tinto, Vale, Glencore, Barrick, Fortescue, Cameco, Newmont, Freeport − McMoRan, ALROSA). So, they spent 11% less during **2013.** But the gold companies were under the greatest pressure because of the falling prices. They were forced to make significant improvements in 2014, for adapt to the new market realities. Thus far in 2014, Barrick reported that it has reduced all-in sustaining costs by 11% to $833/oz as compared to the same point in 2013. Similarly, Newmont has reported that it reduced gold all-in sustaining costs in the first quarter of 2014 by $82 million, compared to the same period of 2013, forecasting to save $600-$700 million by 2016. Gold reserves fell 8%, from 468 million ounces at the 2012 reporting year-end to 431 million ounces at the 2013 reporting year-end. Over the 2010-2013 period, reserve price assumptions increased by more than 25%. The fall in gold prices during **2013** saw the weighted average price assumption fall by approximately 10% between 2012 and 2013. The highest price assumption fell from $1,500/oz to $1,350/oz. The lowest remained unchanged at $950/oz. On the opposite side, Chinese investors showed their continued interest in the mining industry, preparing the consortium led by China Minmetals Corporation for acquiring Las Bambas mine in April 2014 from Glencore Xstrata (2014 PwC's *Mine*).

Interesting is that production growth continued in **2013** from prior year across most commodities (8% copper, 4% iron ore and potash, 2% coal and gold), despite falling prices and fears of many mining CEOs. Fortescue Mining contributed two thirds of the net increase in production during 2013 in advance of reaching its long-awaited target iron ore production volume of 155 million tonnes in March 2014.

The impact of acquisitions and debt restructuring have led to an increase for only four companies of **2013** Top 40, in that as share prices trended differently to the overall mining market: Freeport − McMoRan (copper), Fortescue Metals (iron ore), First Quantum Minerals (copper and gold) and Polyus Gold (gold) (2014 PwC's *Mine*).

2013 was especially the year in which the issue of innovation was highlighted as somewhat left behind: *compared to other industries, mining is very conservative in terms of Research and development (R&D) investment. Only nine mining companies are included in a recent survey of the world's top 2,000 companies by R&D investment* (2014 PwC's *Mine*). Two years of negative trends will cause companies to become more aware that innovation could be the key of enhance the profitability and productivity, trying to address labour shortages and costs, and investing in technologies required in more difficult conditions (*i.e.,* declining grades, remote locations, deep mining).

Another problem was related to the risk of operating in emerging markets, in the sense of *resource nationalism:* a trend of governments looking to maximize returns from their national resources was and will be continuously accentuated, leading to imposing windfall taxes or other measures to more actively manage their natural resources (2014 PwC's *Mine*).

However, the Top 5 was very similar in the next two years (2013-2014), with BHP Billiton Plc/ BHP Billiton Ltd. UK/Australia rank 1, Rio Tinto plc/ Rio Tinto Ltd. UK/Australia rank 2, Vale S.A. Brazil rank 3, Glencore plc/UK rank 4 and China Shenhua Energy Company Limited China/HK rank 5 in 2013 (2015 PwC's *Mine*), and an exchange of ranks between Vale and China Shenhua Energy Company Limited in 2014 (2016 PwC's *Mine*).

7. 2014: BRICS companies taking risks, OECD companies focusing on capital discipline

According to 2015 PwC's *Mine*, the negative tendencies have continued in **2014**, when the return on capital employed (ROCE) fell to its lowest level since 2003, just over 9%, down from 9.5% in 2013 (Fig. 21), proving the challenges in mining industry of getting new expansion projects approved: BRICS companies seemed more willing to take risks, OECD companies focused on capital discipline: *We are afraid of greenfields (...). Greenfields are risky. Greenfields do have capital overruns* (Ivan Glasenberg, CEO, Glencore Xstrata, March 2013) (2014 PwC's *Mine*).

Commodity prices continued to decline during that year (iron ore, coal, and copper prices fell 50%, 26% and 11%), but also in the first four months of 2015 (a further 12%, 5% and 6%, respectively) (Fig. 18). Gold prices remained relatively stable.
The outlook for base metals was better, especially for copper, zinc, and aluminum, meaning that supply for these commodities has led to either a stabilization, or increase in prices. Nickel gained about 15% due mainly to supply issues (*e.g.,* ban on exports of unprocessed ore in Indonesia). Consequently, the **2014** Top 40 lost $156 billion (about 16%) of their combined market value in the first half of the year, largely due to iron ore miners and *diversifieds*. A good explanation could be an oversupply and a negative short-term demand outlook, but also a 7% slowdown in economic growth of China, with a serious impact in terms of global commodity demand, especially for iron ore and metallurgical coal. Copper remained the largest

revenue contributor to the Top, despite the price dropped from $3.40/lb to $2.90/lb during **2014**. World mine copper production increased 2.6%. Very good productions from Glencore's African mines and Rio Tinto's Oyu Tolgoi mine were offset by reduced output from Freeport's operations in Indonesia, where export restrictions and labour-related issues led to disruptions, and finally to the biggest production decline (21%). Growth was strongest in Congo (13.4%), but the largest producer remained Chile, which accounted for more than 30% of global production ($5.8 million tonnes) (2015 US Geological Survey Data, in 2015 PwC's *Mine*).

EBITDA for the **2014** Top 40 was down 5% (see part II of this article, with data from 2019 PwC's *Mine*), because the decline in commodity prices has not been offset by a reduction in operating costs, and production increases were mitigated, to a certain extent, accounting for a concurrent increase in operating costs. The market capitalization for the Top 40 was $791 billion at the end of 2014, as in 2005, and about less half of its value in 2010 (Fig. 15), meaning a drop of 16% from $947 billion at the end of 2013. The average dividend yield for the Top increased to 5% in 2014 from 4.3% in 2013 (Fig. 19). This was the highest dividend yield in the history of *Mine*, where the 10-year average (2004-2014) was 2.8%. The dividend yield was 6% for iron ore at BHP Billiton, Rio Tinto, and Vale, in order to maintain their dividend policies. Net profit of the Top 40 rose to $45 billion in **2014** from $21 billion in 2013, meaning a 114% increase. Although net profit increased, when adjusted for impairments, a decline in adjusted net profit of 9% from 2013 has been obtain, being of $72 billion in **2014.** Also the P/E ratio strongly decreased in **2014**, becoming negative in 2015 (see part II of this article, with data from 2017 PwC's *Mine*). Free cash flow has improved especially for the OECD companies, from negative value (-$3 billion) in 2013, to more than $16 billion in 2014 (Fig. 16), due in large part to a decrease in capital expenditures (2015 PwC's *Mine*). Shareholder return fell by more than $2 billion for the BRICS companies, instead of $1 billion for the OECD companies in 2014 (Fig. 16).
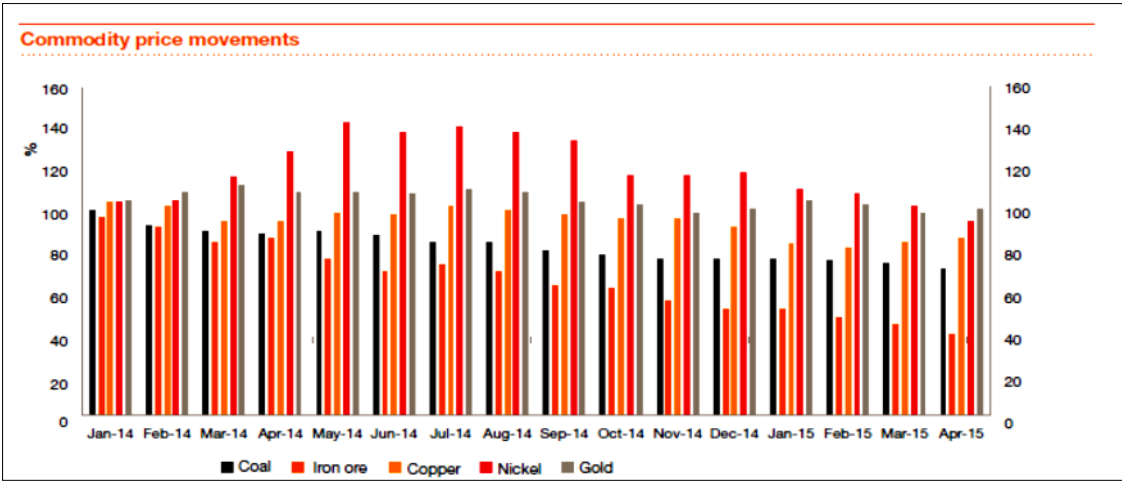
Fig. 18. Prices of some commodities in 2014 and first four months of 2015, World Bank. In 2015 PwC's *Mine*
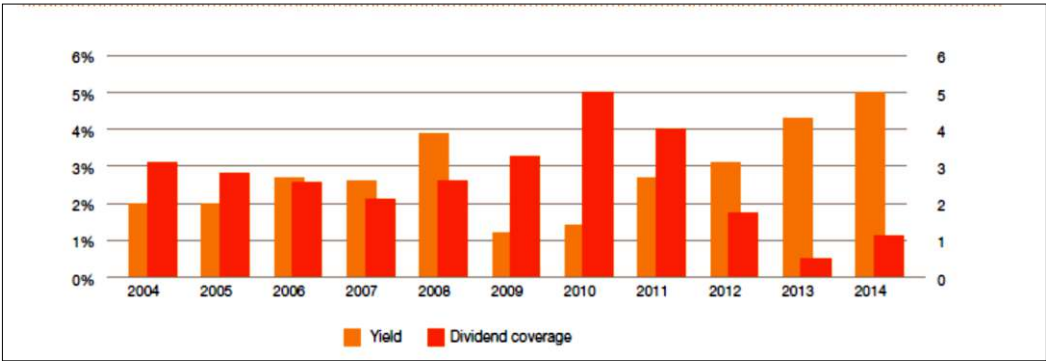
Fig. 19. Dividend coverage and yield between 2004 and 2014. Net profit excluding impairment. Source PwC analysis. In 2015 PwC's *Mine*

companies slashed capital expenditure by 23%, which is 9% higher than of the BRICS companies. This demonstrated that amid a crisis of confidence in the global mining sector, the BRICS markets were growing

excessively compared to the OECD markets. After reducing capital expenditure, a slowdown in capital velocity was expected (Fig. 20). There were 22 OECD companies (including from Mexico) in the Top, 17 companies from the BRIC's (among which 9 from China/China − HK), and one from Saudi Arabia. 59% of the BRIC companies improved in value, compared to 22% of the OECD's. In other words, a 21% drop in value of the OECD's and only 7% of the BRICS companies: $137 billion versus $19 billion, respectively. Three Chinese companies, Zijin Mining (gold) rank 17, China Coal rank 14, and Yanzhou Coal rank 26 had impressive gains, each of more than 30% compared to prior years. Mergers between OECD and BRICS companies were also finding, such as UK/Russia in the case of Polyus Gold International Limited, or South Africa/United States/Australia for AngloGold Ashanti Ltd. Meantime placed on rank 11, MMC Norilsk Nickel/Russia will advance to the rank 5 in 2015.
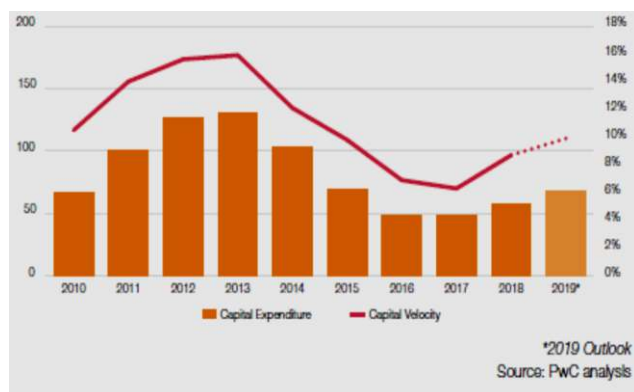
Fig. 20. Capital velocity compared to capital expenditure, acc. PwC Analysis. 2019 PwC's *Mine*
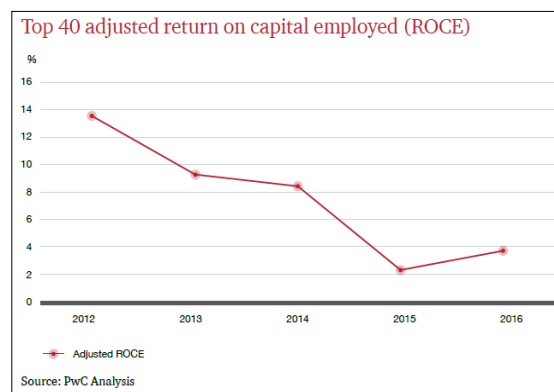
Fig. 21. ROCE movements, acc. PwC Analysis. PwC's *Mine*, June 2017

Conclusions

The intense consumption of metal by modern industries encouraged the exploration activities wordwide, also stimulated by the principles of the global tectonics. New WCD's have been discovered, allowing to map in few decades *giant/supergiant* metallogenic provinces. The current economic model, based on increasingly advanced technologies requires REEs (rare earth elements), RMs (rare metals) and PGEs (platinum group elements), also called *critical*. So, the end of the mineral resources, claimed since few decades, is only fake news. Fueling the global economy, mineral resources led both to boom and crisis. On a hand, our modern world could not exist without mineral resources, on the other hand the geological reserves are limited and their exploitation generates ecological problems. Therefore, the mining industry is required to follow a path of balance that brings prosperity through mineral resources, with minimal envionmental consequences.

The 2002-2010 trends in the global mining industries, where **2004** was considered *a spectacular year,* **2005** *an exceptional year* and **2006** and **2007** *excellent years for the global mining industry,* due to positive evolution of the economic indicators, also included a severe drop of revenue, net profit and adjusted EBITDA in **2009**, together with a decrease of exploration spend. Against the background of the global crisis, the share of *hedge funds* increased in gold and precious metals'assets as a store of wealth, the contribution to deal value ranging from 17% in **2008** to 24% in **2009**. Despite of record revenue and an increase by 124% of net profit in **2010,** a continuous increased operating expenses have been reported. Costs and the price of key inputs have remained high because of the 2007-2009 financial crisis. In **2010** investing cash flows were only 58% of operating cash flows, compared to an average of 94% for 2003-2009. The emergent economies were beginning to take the courage to invest in mining projects, improving their mineral and policy indexes. *The growing disconnect* of **2011** announced structural changes in the industry's cost base, although the financial results hit new superior values: revenue increased 26%, operating cash flows grew 34%, investing cash flows grew 92%. A record level of net profit was generated by high commodity prices, but margins remained flat because of higher costs. Miners were faced with investor confidence suspicions. In **2011** was maintained the trend from 2007-2009 global financial crisis, meaning that operating expenses exceeded revenue growth. But, there were different causes: during the global crisis, the commodity prices strongly declined, opposite to 2010 an especially to 2011, when commodity prices strongly increased, but the operating costs surged. Coal was the **2011** dominant commodity accounting for 26% of deal value, followed by copper with 23% and gold with 13%. **2012** *was far from the most active year for mining mergers and acquisitions (M&A),* whose values had dropped

dramatically anyway in 2009. Copper and gold accounted for half of the **2012** Top 20 deals, excluding the Glencore − Xstrata merger. The demand for copper allowed DROC to enter the **2012** Top 20, with two companies. Iron ore was present in the Top 20 deals, due to the steelmakers. In **2013**, the profitability of the mining industry was at its lowest level since 2000. The price of gold has fallen after a continuous rise in 90s and 2000s. The operating costs increased by 4%, which will become a feature of the coming years. The Top 40's aggregate net profit recorded *their deepest depth in a decade*; gold companies were responsible for $20 billion of net losses. The market capitalization fell 23%. For the first time, OECD's free cash flow was negative, and most of the Top belonged to emerging market companies, accounting for 53% in December **2013**. As a consequence, in **2014** *the BRICS companies taking risks,* and *OECD companies focusing on capital discipline*. In **2014**, when the return on capital employed (ROCE) fell to its lowest level since 2003, the commodity prices continued to decline, excepting gold. At the end of 2014, the market capitalization for the Top 40 was as in 2005, and about less half of its value in 2010. On the contrary, the average dividend yield for the Top increased to 5% in 2014, the highest dividend yield in the history of *Mine*. Free cash flow has improved especially for the OECD companies, from negative value in 2013, to more than $16 billion in **2014**, due in large part to a decrease in capital expenditures.

References

Abramovitz M., David PA (2001) Two centuries of American macroeconomic growth from exploitation of resource abundance to knowledge - driven development. In Stanford Inst. for Economic Policy Research Discussion Paper. ©Moses Abramovitz and Paul A. David. 216 p. https://siepr.stanford.edu/sites/default/files/publications/01-05_0.pdf

Arrow K, Dasgupta P, Goulder L, Daily G, Ehrlich P, Heal G, Levin S, Karl-Göran Mäler K-G, Schneider S, Starrett D, Walker B (2004) Are we consuming too much? Journal of Economic Perspectives, v. 18, no.3, p. 147-142. https://pubs.aeaweb.org/doi/pdfplus/10.1257/0895330042162377

Bender F (1977) An Earth Scientist's view of metallic resources. In: F Bender ed, Mineral Raw Materials. Schweizerbart, Stuttgart, p. 117-136.

Bender F (1982) Significant energy raw materials for everyone? In: Resources for the Twenty-First Century. U.S. Geol. Surv. Prof. Paper 1193, p. 104-155.

Berg AG, Ostry JD (2011) Inequality and unsustainable growth: Two sides of the same coin. In: Intern. Monetary Fund Staff Discussion Note, April 8, 2011, 21 p. https://www.imf.org/external/pubs/ft/sdn/2011/sdn1108.pdf

Bradsher K (2009) China tightens grip on rare minerals, The New York Times, 31 August 2009. http://www.nytimes.com/2009/09/01/business/global/01minerals.html

Dasgupta P (2010) Nature's role in sustaining economic development. Philosophical Transactions of the Royal Society. B Biol Sci., v. 365, iss. 1537, p. 5-11. https://royalsocietypublishing.org/doi/pdf/10.1098/rstb.2009.0231

Green M (2015) Why we shouldn't judge a country by its GDP. In Ideas.Ted.Com, Apr 22, 2015 https://ideas.ted.com/why-we-shouldnt-judge-a-country-by-its-gdp/

Holland HD, Petersen U (1995) Living dangerously. The Earth, its resources and the environment. Princeton University Press, 600 p.

Kesler SE (1994) Mineral resources, economics and the environment. Macmillan College Publishing Company, Inc. New York, 396 p.

Kesler SE & Simon AC (2015) Mineral resources, economics and the environment. Cambridge University Press, 434 p.

Krugman P (1994) The myth of Asia's miracle. Foreign Affairs, Nov./Dec. 1994, v. 73, no.6, p. 62-78. http://www.brmandel.com/uploads/3/2/4/5/3245755/myth_of_asias-miracle.pdf

Laznicka P (1995) Quantitative relationships among giant deposits of metals. Economic Geology 94(4), p. 455-473.

Laznicka P (2006) Giant metallic deposits. Future sources of industrial metals. Springer-Verlag Berlin Heidelberg, 732 p.

Moore S, Simon JL (1999) The greatest century that ever was: 25 miraculous trends of the last 100 years. In: Policy Analysis 364. https://www.cato.org/sites/cato.org/files/pubs/pdf/pa364.pdf

O'Neill J. (2007) BRICs and beyond, Goldman Sachs Economic Research Group. New York: Goldman-Sachs, 268 p. https://www.goldmansachs.com/insights/archive/archive-pdfs/brics-book/brics-full-book.pdf

O'Neill RV, Khan JR (2000) Homo Economus as a keystone species, BioScience 50, iss. 4, pp. 333-337. https://academic.oup.com/bioscience/article/50/4/333/270746

Romero-Freire Ana, Santos-Echeandía J, Neira Patricia & Cobelo-García A (2019) Less-studied technology -critical   elements (Nb, Ta, Ga, In, Ge, Te). In: The Marine Environment: Review on their concentrations in water and organisms. https://www.frontiersin.org/articles/10.3389/fmars.2019.00532/full

Schmid M (2019) Rare earths in the trade dispute between the US and China: a déjà vu. Intereconomics, v. 54, no. 6, p. 378–388. https://ihttps://www.intereconomics.eu/contents/year/2019/number/6/ article/rare-earths-in-the-trade-dispute-between-the-us-and-china-a-deja-vu.

Schodde RC (2004) Discovery performance of the western world gold industry over the period 1985-2003. PACRIM 2004 Proceedings, Adelaide. Aus IMM, pp 367-380.

Simon JL (1996) The Ultimate Resource 2, Princeton University Press; Revised ed., 778 p.

Singer DA (1995) World class base and precious metal deposits − A quantitative analysis. Economic Geology, v. 90, pp. 88-104

Temple J (1999) The new growth evidence. In: *J of Economic Literature*, American Economic Association, v. 37, iss. 1, pp. 112-156. https://pubs.aeaweb.org/doi/pdfplus/10.1257/jel.37.1.112

Worstall T (2014) In response to Herman Daly. *Forbe*s, Dec. 12. https://www.forbes.com/sites/timworstall/2014/12/12/in-response-to-herman-daly/?sh=7d33e3c728d6

https://www.irishtimes.com/business/technology/irish-scientists-discover-how-rare-earth-mineral-is-formed-1.4439657?mode=amp

https://www.scmp.com/economy/china-economy/article/3097847/chinas-rare-earth-export-plunge-caused-coronavirus-not

Impunity Inc., 2012: Reflections of the super- rights and super – powers of corporate capital. https://www.tni.org/files/download/impunity_inc_0.pdf

https://comtrade.un.org/data/

https://pubs.usgs.gov/periodicals/mcs2020/mcs2020-rare-earths.pdf

Intereconomics 2019, v.54, no.6. http://minerals.usgs.gov/minerals/pubs/commodity/rare_earths/

https://pubs.usgs.gov/periodicals/mcs2020/mcs2020-rare-earths.pdf

Fragile States Index 2013-2020. https://en.wikipedia.org/wiki/List_of_countries_by_Fragile_States_Index

National Research Council, 2008, p.165. https://pubs.usgs.gov/pp/1802/m/pp1802m.pdf

http://brics2019.itamaraty.gov.br/en/about-brics/what-is-brics

https://goldprice.org/gold-price-history.html

2005 PwC's *Mine.* https://allafrica.com/download/resource/main/main/idatcs/00010686:f24b1f4d4abc9aae8722d2e8484c1612.pdf

https://pwc.blogs.com/press_room/2006/06/mining-sector-delivers-spectacular-results-for-2005.html

2007 PwC's *Mine.* https://www.pwc.co.za/en/assets/pdf/pwc-mining-review-07.pdf

Mining Weekly. https://www.miningweekly.com/article/mining-sector-increasingly-attractive-to-private-equity-pwc-2007-06-20

2008 PwC's *Mine.* https://www.pwc.co.za/en/assets/pdf/pwc-mining-survey-08.pdf

2009 PwC's Annual Review *Mining Deals.* https://pwc.blogs.com/files/mining-deals-2009.pdf

2010 PwC's *Mine.* https://www.pwc.co.uk/assets/pdf/mine-back-to-the-boom.pdf

2011 PwC's *Mine.* https://www.pwc.com/cl/es/publicaciones/assets/mine-2011.pdf

World Exploration Trends 2011. A special report from Metals Economics Group for the PDAC International Convention. http://www.mcilvainecompany.com/industryforecast/mining/overview/MEG%20Exploration%20trends.pdf

2012 PwC's *Mine.* http://download.pwc.com/gx/mining/pwc-mine-2012.pdf

2013 PwC's *Mine.* https://www.pwc.com/gx/en/mining/publications/assets/pwc-mine-a-confidence-crisis.pdf

2014 PwC's *Mine.* https://www.pwc.com/gx/en/mining/publications/assets/pwc-mine-2014-realigning-expectations.pdf

2015 PwC's *Mine.* https://www.pwc.com/cl/es/publicaciones/assets/mine-report_06-2015.pdf

2016 PwC's *Mine.* https://www.pwc.com/gx/en/mining/pdf/mine-2016.pdf

2017 PwC's *Mine.* https://www.pwc.com/gx/en/mining/assets/mine-2017-pwc.pdf

2019 PwC's *Mine.* https://www.pwc.com/mx/es/publicaciones/archivo/2019/06/20190604-pwc-mx-mine-report- 2019.pdf

THE MINING INDUSTRY, A RETROSPECTIVE OF THE 2000s: FROM THE BOOM TO THE *ENTER THE DRAGON* (II)

Antonela NEACȘU, Gheorghe C. POPESCU

University of Bucharest, 1, Nicolae Balcescu Blv. 010041 Bucharest, Romania
antonela.neacsu@gg.unibuc.ro, gheorghec.popescu@yahoo.com

Abstract: Starting with 2015 the mining industry continued to face major difficulties because of the slower global growth. The mining industry has become an increasingly difficult operating system, as the annual PricewaterhouseCoopers'*Mine* reports emphasized. An acceleration of the downward trend that began in 2012 meant that market caps do not exceeded net assets for the traditional companies of the Top in 2015. The commodities price declined to an *insurmountable* level in 2015, as well as ROCE, marking a new negative record in the history of *Mine*. The first quarter of 2016 was a restart for the mining industry, in a sense of rising of market cap and price index, profitability and a significant rise in free cash flow for the Top 40. Since 2017, revenues, EBITDA and market cap rose, but capital expenditure was lowest since 2006 and capital velocity was at the lowest rate since 2003. Until 2018, there was a generally low level of exploration, excepting copper, nickel, lithium and cobalt projects. A lift in operating cash flow has allowed the Top 40 to increase both capital expenditure and shareholders distribution in 2018. Net profit upped and most commodities increased average prices until the end of the year, when appeared decreases caused by economic uncertainty. In that context, miners worked to develop a modern, sustainable and safety mining, in order to obtain a solid financial performance during 2019. The year of the virus would follow.

Keywords: *critical elements, speciality metals*, mining deals, PwC's *Mine* reports, *economic colonialism, consumer sentiment,* global mining market size, culture of innovation in mining, challenges in mining, culture of involvement during the pandemic.

1. Mining industry, a difficult operating system

The mining industry has become an increasingly difficult operating system, as the annual PricewaterhouseCoopers'*Mine* (PwC's *Mine*) reports emphasized. Despite the brilliant auspices of the beginning of the 2000s, according to analyzes performed on the 40 global most important mining companies, none remained unaffected by the economic crisis of the first decade of the new millennium.

1.1. 'Slower, lower, weaker but not defeated'

The year **2015**: as expected, the mining industry continued to face major difficulties due to slower global growth. The Top had impairments of $53 billion and it have written-off the equivalent of 32% of capex spent since 2010 (Fig. 1). As a result, capital velocity has decreased to 10.6% (see part I of this article, with data from 2019 PwC's *Mine*). The adjusted return on capital employed (ROCE) has strongly declined to approx. 2% (see part I of this article, with data from 2017 PwC's *Mine*), reaching a new negative record in the history of *Mine*. During 2015, the Top 40 showed a decline in market capitalization of 37% from 2014, meaning $297 billion lost (see part I of this article, with data from 2017 PwC's *Mine*), with many of the established members of the Top 40 marked below their book values for the first time since 2004. This was the year when market caps do not exceeded net assets, at least for the traditional companies of the Top (Fig. 3). EBITDA slumped by 39% (Fig. 10). Dividends were cut. When adjusted for impairment, the P/E ratio became negative in **2015** (Fig. 6) (2017 PwC's *Mine*). Excepting gold, revenue by commodity decreased in 2015 in comparison with prior year for iron, coal, copper and others (Fig. 4). The revenues of the Top in **2015** declined to $539 billion from $678 billion in 2014, being an acceleration of the downward trend that began in 2012 (Fig. 10). The commodities price declined to an *insurmountable* level (as 2016 PwC's *Mine* stated) (Fig. 2): nickel had the worst performance, dropping by 41%, followed by iron 40%, and gold 14%. Production values were generally higher than in 2014, excepting potash and thermal coal (Fig. 5). Thermal coal was marginalized, although the Asian emerging companies were driven import demand past years. One of the explanations was that some of coal production companies (*e.g.,* Peabody *Inc.*, Arch Coal) filed for bankruptcy in **2015**. Another explanation was, of course, the pressure of non-conventional energy sources, as the lithium's rise. According to 2016 PwC's *Mine*, Deutsche Bank forecasted in 2015 that the global lithium supply market will triple over the next ten years. The new 2014 entry in Top 40 on rank 31 was the Chinese Sichuan Tianqi Lithium, one of the only nine companies of the **2015** Top 40 showed increases in market capitalization. A notable exception is Canada, where despite lower prices for most mineral commodities, the total value of mineral production in **2015** was of $42.8 billion, only slightly lower

(2.6%) than the 2014 value of $43.9 billion. The excess supply for most minerals was partly offset by favorable exchange rates, as is highlighted in Mining Sector Performance Report 2006-2015 of Canada (https://www.nrcan.gc.ca/sites/www.nrcan.gc.ca/files/mineralsmetals/pdf/mms-smm/MSRP_report_access _EN.pdf). There is no new China on the horizon, the authors of the 2016 PwC's Mine hastened to note, instead acknowledging the performance of India and ASEAN countries in 2015 and next years (Fig. 7).
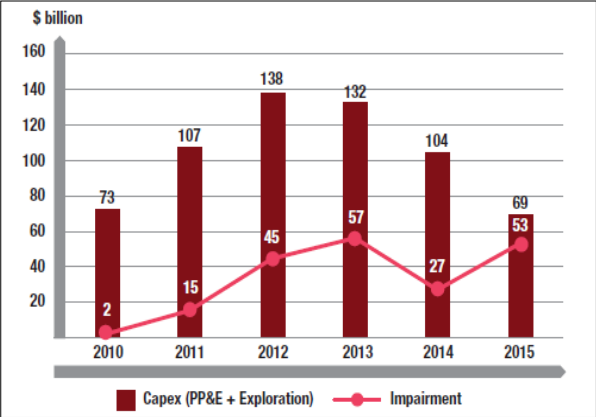
Fig. 1. Capex *vs.* impairment. Source PwC analysis. 2016 PwC's *Mine*
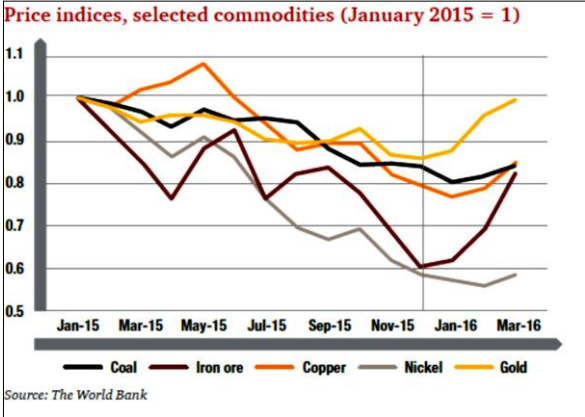
Fig. 2. Price indices of some commodities during 2015 and first three months of 2016, acc. The World Bank. In 2016 PwC's *Mine*

However, studying the 2016 *Mine* report, only nine companies of the **2015** Top 40 showed increases in market capitalization: from these, four were gold companies, and three are Chinese non-ferrous metal companies. The Top recognized 18 emerging companies (excluding those involving in mergers with OECD's, such as Russian and South African companies), from which 12 are Chinese companies, with four new entrants. China consumed more than 40% of the world's copper supply and was nearly 70% of global iron ore demand. AngloGold Ashanti Ltd. South Africa/United States/Australia has remerged in the **2015** Top 40 (rank 30) for the first time since 2013.
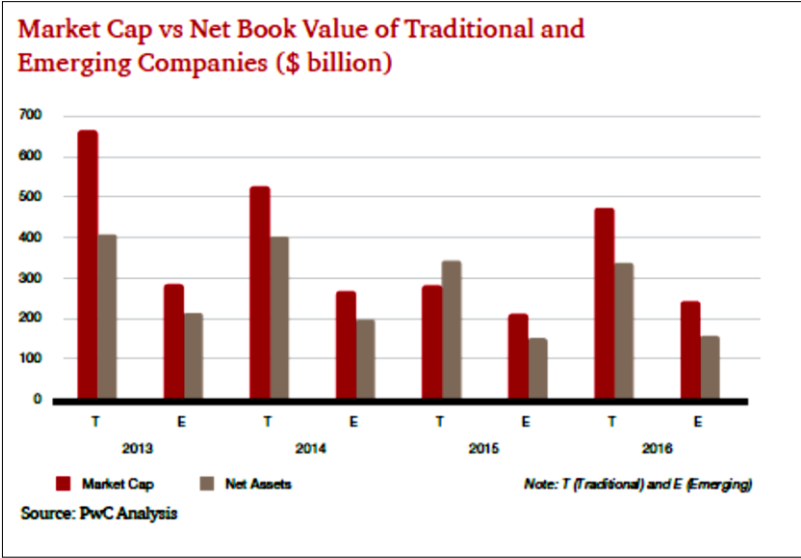
Fig. 3. Market cap *vs*. net book value in the 2013-2016 period ($ billion), acc. PwC Analysis. 2017 PwC's *Mine*

Dominated by the emerging companies, the **2015** Top 5 included three companies of the past two years Top 5, with BHP Billiton Plc/ BHP Billiton Ltd. UK/Australia rank 1, Rio Tinto plc/Rio Tinto Ltd. UK/Australia rank 2, China Shenhua Energy Company Limited China/HK rank 3, and two new participants, as Coal India Ltd. rank 4, and MMC Norilsk rank 5 (2016 PwC's *Mine*).
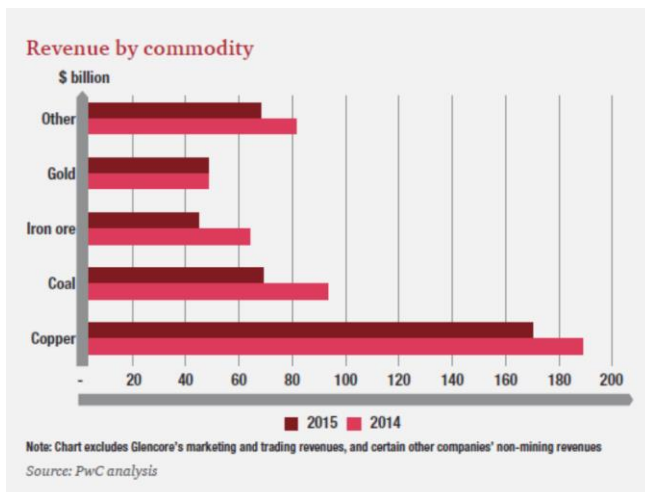
Fig. 4. Revenue by commodity 2014 vs. 2015, acc. PwC analysis. 2016 PwC's *Mine*
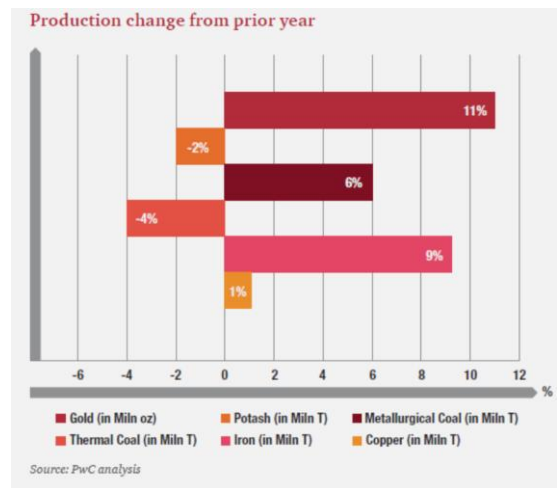
Fig. 5. Production changes in 2015, acc. PwC analysis. 2016 PwC's *Mine*

1.2. 'Recovering from race to the bottom'. Raising lithium and cobalt

Recovering from 2015's race to the bottom, the members of the Top 40 paused and drew breath in 2016, according to 2017 PwC's *Mine*. The first quarter of **2016** was a restart for the mining industry, in a sense of rising of market cap and price index (see part I of this article, with data from 2017 PwC's *Mine*): the market cap of the Top 40 increased by 45% to $714 billion, as in 2014 approximately (Fig. 8). Also the profitability has returned to the Top, with an aggregate net profit of $20 billion, as compared to an aggregate loss of $28 billion in 2015. There was a significant rise in free cash flow, up to $40 billion from $13 billion.
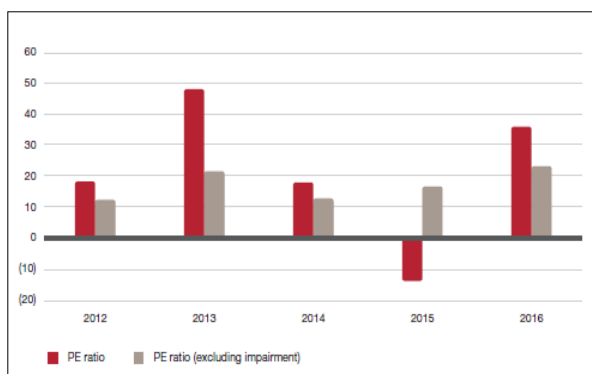
Fig. 6. Top 40 price to earnings ratio before and after adjusting for impairment in mining industry between 2011 and 2016. 2017 PwC's *Mine*
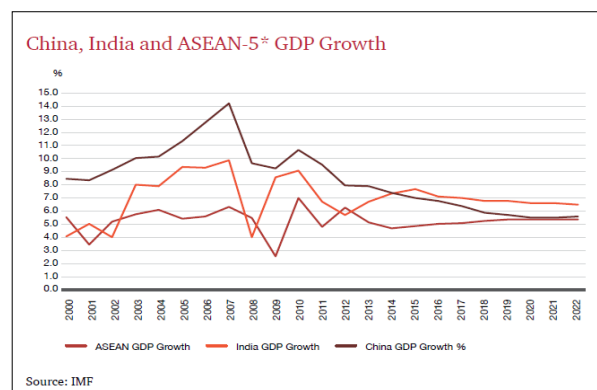
Fig. 7. The performance of India and ASEAN countries in terms of GDP Growth.2017 PwC's *Mine*

After significant losses in 2015 (Fig. 6), the earnings excluding impairment charges of the Top 40 companies increased slowly in **2016**, and the P/E ratios has become again positive. P/E ratio is an indicator of the market's view of expected profitability: the higher is P/E, the higher is the investors' availability to pay a greater price for a stock's future earnings.The positive gap of approx. $220 billion represents the first increase since 2010, in terms of market caps exceeding net assets (Fig. 3). It was supported by the $204 billion of impairments booked since 2010.

ROCE had the most dramatic fall in 2015 (to just over 2%) since 2004, but in **2016** it rose slightly approaching 4%. One of the problematic parameter was capex, which fell dramatically with 41%, to a new low record of $50 billion (see part I of this article, with data from 2017 PwC's *Mine*). This meant too few greenfield mining projects. Valuations have climbed, especially for the traditional companies, gaining an additional $34 billion. Among the traditional companies, four companies represented almost 50% of the increase in overall market capitalization: BHP Billiton Ltd. Australia/UK rank 1 in 2016 Top 40, Rio Tinto Ltd. Australia/UK rank 2, Glencore plc/Switzerland rank 3, Vale S.A./ Brazil rank 5. China, India and the ASEAN countries (Indonesia, Malaysia, The Philippines, Thailand, and Vietnam) had great economic opportunities in **2016**, being top destinations for mining projects, with important consequences as far as

GDP growth was concerned (Fig. 7). A more and more demand for cobalt and lithium was reported, as a consequence of the technology and energy sector development, targeted being DROC and China.

The recovery of mining in 2016 was possible rather due to investor trust, than the commodity prices. During **2016**, the spot commodity prices were relatively flat to a small increase, excepting maybe of iron ore (Fig. 9), which must have influenced the movements in Top 40, since four companies of Top 5 have exposure to iron ore (as it was already mentioned above).

Otherwise, the mining businesses were subtle influenced in **2016** by the Brexit vote, the elections of USA and the escalation of tensions on the Korean Peninsula. The political events have always caused market volatility, with consequences on the daily reporting of the commodity price fluctuations, and further, on the predictions about the state of mining industry. The *Trump bump* appeared to offer a solution to the so called *war on coal* in the US. But, as it is known today, its effects on increased prices was too small and for short terms.
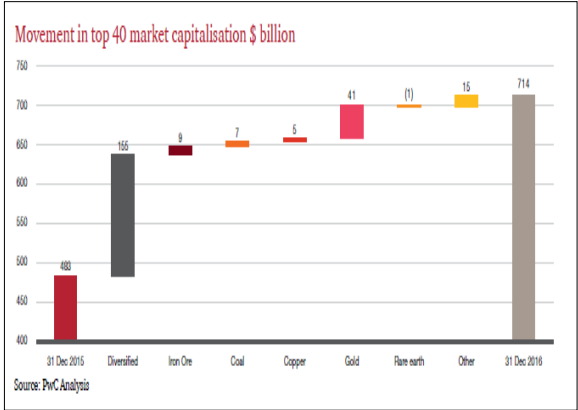
Fig. 8. Movement in Top 40 market capitalization, acc. PwC's Analysis. 2017 PwC's *Mine*
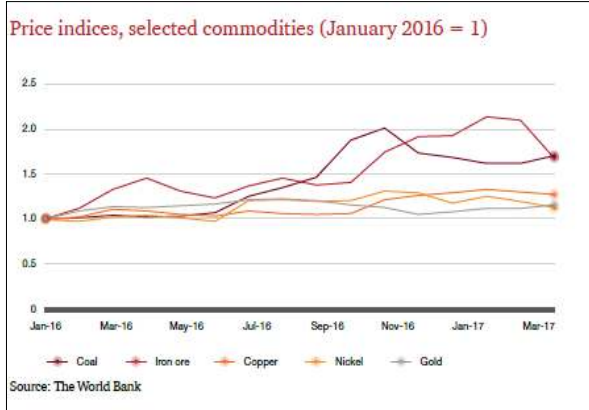
Fig. 9. Commodity process in 2016 and first three months of 2017, acc. The World Bank. 2017 PwC's *Mine*

Similarly, iron ore prices did not increase due to an US infrastructure boom, but rather due to the Chinese financing. According to the US Energy Information Administration's 2016 *International Energy Outlook* (see 2017 Pwc's *Mine)*, the Asian coal-fired capacity will double by 2040, based on important demands from China, India, Indonesia, Bangladesh, and Vietnam. This trend is reflected also by the constant presence in the last decade's Top 40 of Coal India Ltd. (rank 4 in 2015, 6 in 2016, 10 in 2017 and 2018, 8 in 2019), Shaanxi Coal Industry (new entry in 2014, rank 21 in 2015, 32 in 2016, 23 in 2017, 23 in 2018, 19 in 2019), China Coal Energy Company Ltd. (rank 12 in 2015, 25 in 2016, 29 in 2017, 2018 and 2019), but also by the 2018 new entry PT Bayan Resources Tbk Indonesia (rank 40 in 2019). Also the demand for metallurgical coal seems to remain strong over the long term, especially due to the Asian consumption of steel.

Lithium and cobalt demands were continuously growth during past decade, as batteries producing continued to develop. Most of the world's lithium reserves extend in Latin America (Bolivia, Argentina, Chile), but China, sixth-placed on the list, controlled the majority of the world's raw material refining. In terms of the lithium-ion battery supply chain, in 2020 China controls 77% of the world's cell capacity (acc. BloombergNEF, in https://www.nsenergybusiness.com/features/six-largest-lithium-reserves-world/) and 60% of the world's component manufacturing. Tianqi Lithium Industries, Inc. (former Sichuan Tianqi Lithium, new entry in 2014 Top 40) was the only pure-play lithium producer in **2016** Top 40 (rank 31 in 2015, rank 38 in 2016). Today, none is more popular than the lithium-ion battery and none of lithium-ion battery with titanium, manganese, phosphate or nickel provides the same amount of energy density that cobalt does. Additionally, cobalt is one of the essential components of smartphones, tablets and laptops, allowing them to become slimmer and not heat up, and to retain the same battery life. Analysts predicted cobalt demand to shrink in 2020 in part driven by weak vehicle sales. HSBC Global Research expected global cobalt demand to drop 10% year over year until to 113,000 tonnes in 2020, but to surge 21% in 2021 to about 138,000 tonnes and continue to climb through 2022 and 2023. In the same paradigm, by 2023 the electric vehicles will account for 34% of cobalt demand, up from 24% in 2019 (quoted from July 28, 2020 *Press Release:* Benchmark Mineral Intelligence). That is way cobalt is one of the most hunted commodities, and DRC is the target for the cheapest one: it produces over 60% of the world's cobalt, and holds about 40% of the world's untapped resources of cobalt. Most of mines are still located in Katanga. The American,
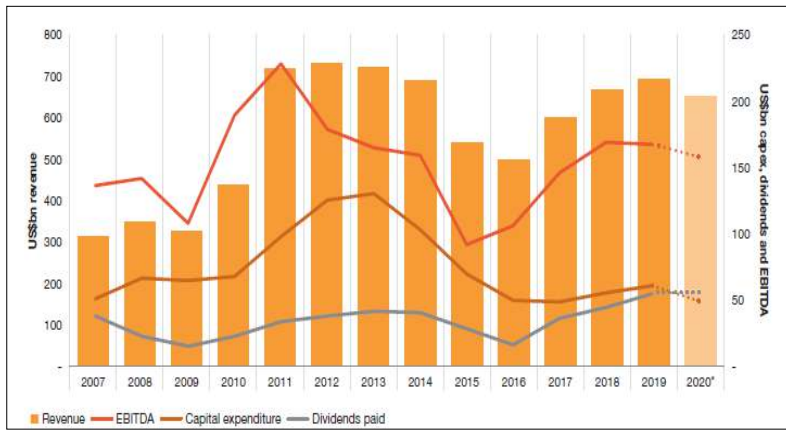
Fig. 10. Top 40 mining companies performance trends, acc. Annual reports, PwC Analysis. In 2019 PwC's *Mine*

European and Chinese corporations are the most interested in cobalt exploration and exploitation activities in DRC. In **2016**, Glencore was the world's largest miner of cobalt, acquiring full ownership of the Mutanda Mining SARL and the Katanga mine (both copper-cobalt) in the DRC, hoping to become the world's largest cobalt producer (see 2017 and 2018 PwC's *Mine*). After only four years, in February 2020, Glencore announced that it planned to increase its exports by the end of the year, from 27,000 tonnes in 2019 to 39,000 tonnes. Over 80% of the country's exports represent mineral commodities (see https://www.worldbank.org/en/country/drc/overview), so some of the economic analysts are afraid that *the rush* for Congolese mineral resources, especially for cobalt and copper, could institute a new form of *economic colonialism* (acc. to https://www.arcgis.com/apps/Cascade/index.html?appid=3cedc4c7ef40422e9bbb1edbec5d83c6).

There were 23 *traditional* companies in **2016** Top 40 (including AngloGold Ashanti Ltd./South Africa and Anglo American plc UK/South Africa, two companies from Mexico, and one each from Saudi Arabia and Channel Islands) and 17 emerging companies (eleven Chinese's (± Hong Kong), three from Russia, two from India, and one from Brazil). **2016** Top 5 included three first *traditional* companies, as BHP Billiton Ltd. Australia/UK, Rio Tinto Ltd. Australia/UK, and Glencore plc/Switzerland, followed by China Shenhua Energy Company Limited, and Vale S.A./Brazil. *Diversifieds* and gold companies dominated more than half of the Top 40. As top movers, Alrosa re-emerged in the Top since 2015 landed on rank 17 in 2016, Fortescue Metals upped from rank 40 in 2015 to rank 15 in 2016, Anglo American plc climbed from rank 27 in 2015 to rank 9 in 2016, and the 2015 new entry China Molybdenum Co. Ltd. landed on rank 29 in 2016.

1.3. *A stellar performance*

If 2016 was a year of pause and relax after recovering, **2017** *was a remarkable year* for the Top 40 members (2018 PwC's *Mine*)*:* in comparison with 2016, revenues rose by 23% to $600 billion, from $489 billion, EBITDA upped with 38%, from $106 billion to $146 billion in 2017, market cap upped with 30%, reaching $926 billion, from $714 billion in 2016. Capital expenditure showed a plateau configuration since 2016 (Fig. 10), being lowest since 2006, *i.e.,* $48 billion. Barely in 2018 capex increased for the first time in five years, albeit still below since 2013. The capital velocity was at the lowest rate since 2003. Other than sustaining capital expenditure, the new above $500 million projects approved during **2017** were limited to a couple of copper projects. There was a generally low level of exploration, but also encouraging signs of turnaround, as S&P Global Intelligence reported: exploration activity was globally upped with 15% from 2016, to $8.4 billion in **2017** (2018 PwC's *Mine*). Dividends were high level in 2017 (Fig. 10), increased by 125%, from $16 billion in 2016 to $36 billion. As it has already observed, also in the worst times of 2000s for mining, they were paid, meaning that maintaining confidence has always been a major concern in industry.

The global annual GDP has begun to grow, meaning that the mining industry could develop thanks to new demands on the back of economic global recovery (Fig. 11).

A stellar performance looking to financial results in **2017** was possible by focusing on cost saving and productivity, and also by adding a favorable market in terms of price increasing for mineral products (Fig. 12). The Top 40 represented approx. 50% of global production for iron ore, copper, manganese, cobalt and PGM's.

So, while *the future looks bright* for the Top 40, *long-term success is by no means assured*: 32% of operating costs is represented by labour costs for the Top 40 companies, being expected a decrease of employees in the future, especially through technology advances. **2017** was the year of the record increase in tax contributions: the Top 40 tax expense increased by 81%, with cash taxes paid to governments increasing by 67%. Through the boom cycles of 2008 and 2012, mining companies had the wise to deploy excess

capital back into the industry. Thus, after a long expectation, in 2017 shareholders have realized returns from the industry's asset base (Fig. 13). Improving their financial position, companies of the Top 40 have obtained a gearing comparable to the 10 year Top 40 average of 30% (Fig. 14), demonstrating a better degree of funding by shareholders versus creditors.
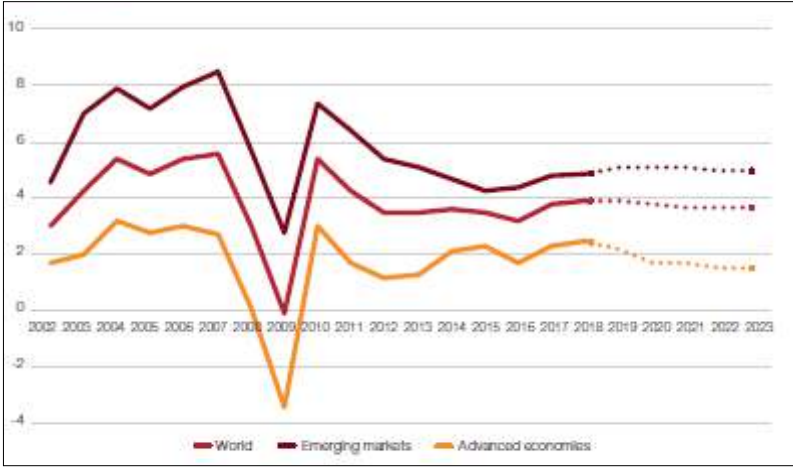
Fig. 11. GDP growth, acc. IMF, PwC Analysis. 2018 PwC's *Mine*
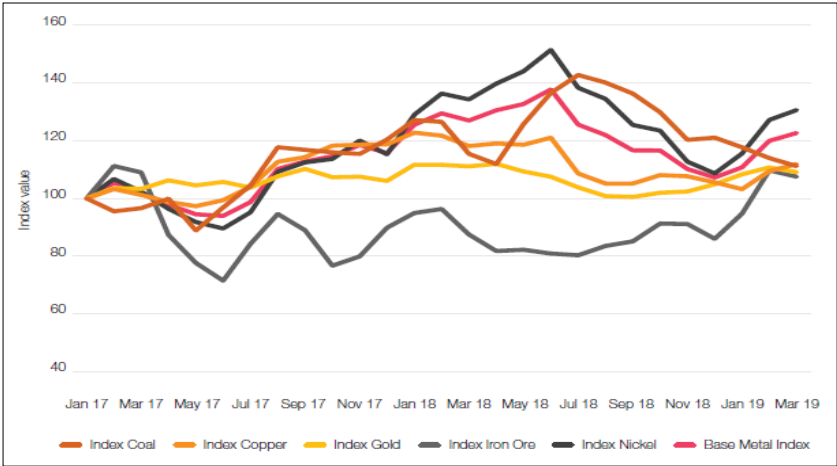
Fig. 12. Price index for key commodities, acc. World Bank. 2019 PwC *Mine*
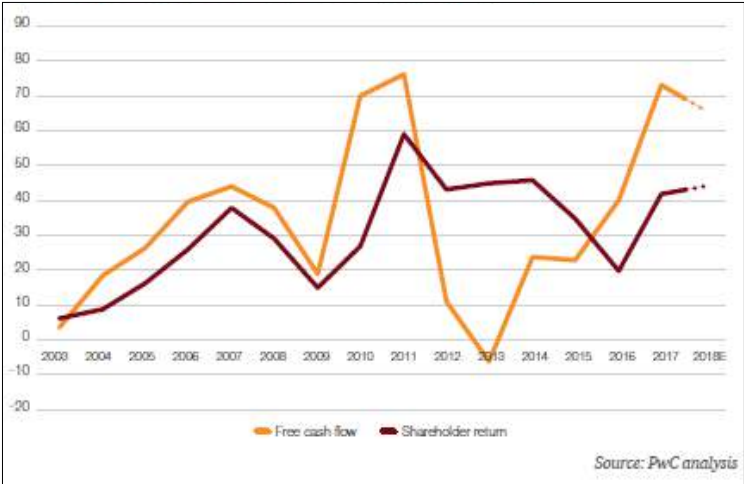
Fig. 13. Free cash flow and shareholder returns ($ billion), acc. PwC Analysis. In 2018 PwC's *Mine*

The Top 5 companies owned in **2017** 47% of total market capitalization, and they were the same as in 2016, and, as it will be seen, also in 2018. **2017** Top 40 included 23 *traditional* companies (including those from Mexico and South African share in Anglo American plc) and 17 emerging companies: ten from China (±Hong Kong), two from Russia (from which MMC Norilsk Nickel rank 6 and Alrosa rank 31), two from India (with Coal India Ltd. falling on rank 10), Vale S.A. /Brazil (rank 5), one each from Poland and Saudi Arabia (the last numbered prior years as *traditional*). Due the strong copper prices, two new entrants enjoyed the Top 40 in 2016: KGHM Polska Miedz Spółka Akcyjna rank 39 and Kaz Minerals plc/UK rank 40 in **2017** (2018 PwC *Mine*). They replaced AngloGold Ashanti Ltd. and Zhongjin Gold Corp. Ltd, who have been seriously affected by the suppressed gold price in **2017** (Fig. 17). Thus, it was recorded a reduction in the number of gold companies to eight and an increase of copper companies to six, amid the same dominance of diversifieds' companies, 13 on the list in 2017. The most active mover was China Molybdenum Co. Ltd., which climbed 18 spots to rank 11 in **2017** Top 40, as a result of acquisition of Anglo American's Niobium and Phosphate business. The Russian Polyus Gold International Ltd. became a British company (2018 PwC *Mine*).
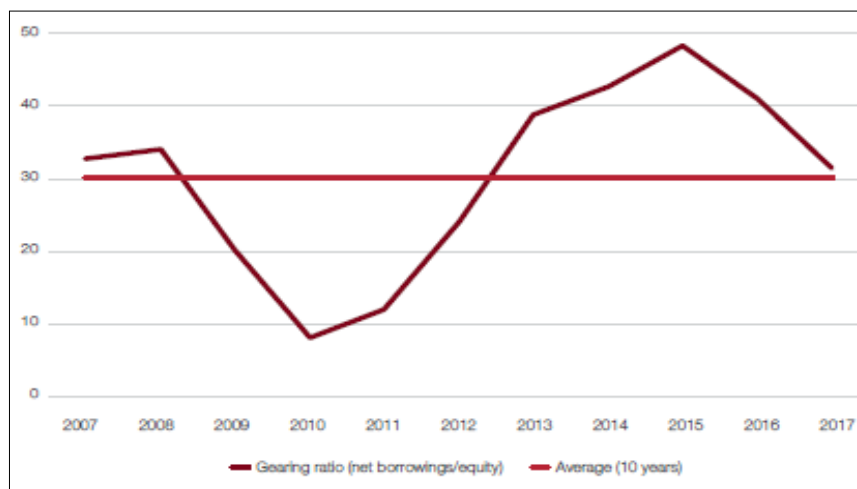
Fig. 14. Gearing ratio and average from 2007 to 2017, acc. PwC Analysis. In 2018 PwC's *Mine*

1.4. From digital and Industry 4.0 *to change consumer sentiment.* Building a culture of innovation in mining

Continuing the **2018**'s analysis on the global mining industry, things were looking better and better, as the 2019 PwC's *Mine* reported. But also questions about the industry's future appeared. **2018** Top 40 mining companies' revenue upped with 8% to $683 billion from 632 billion in 2017, with record dividends paid to shareholders of $43 billion, with EBITDA of $165 billion, upped with 4%; M&A activity upped 137% to 30 billion (due the activity in the gold sector), and capex upped for the first time since 2013 (Fig. 10).

But there was a soft 12% increase over 2017 to $57 billion, which means that miners were cautious: 48% of spending was for ongoing projects, and few new ones were initiated and approved in 2018. Free cash flow upped 12%, from $69 to $77 billion.

A lift in operating cash flow with 12% has allowed the Top 40 to increase both capital expenditure and shareholders distribution in **2018**. Net profit upped with 2%, from $65 to $66 billion. Most commodities increased average prices until the end of 2018 (Fig. 12), when appeared decreases caused by economic uncertainty. Production increased on average by 2%. A declined market cap with 18%, to $757 billion on the end of December 2018, an increased of costs with 8.6% driven largely by commodity-based input costs, a modest growth in production, and a decreased of the value distributed to government and employees with 43% (Fig. 15), here are the minuses in **2018**.

As the report mentioned, *mining requires far more than good financial performance to continue to create and realize value in a sustainable manner (...) the under-performance is connected with the risk and uncertainties of a changing world and the market perception about the mining industry's ability to respond.* The regulatory and political challenges were not absent that year, when were marked by *volatility and uncertainty*: the US–China trade disputes and upheaval in the Eurozone, taxation, environment politics, investment and labour, all put pressure onthe mining industry.
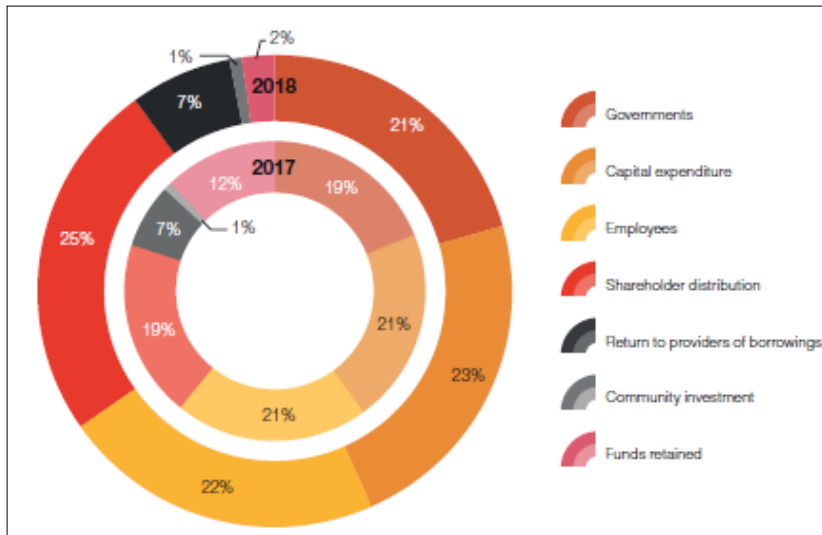
Fig. 15. Top 40 value distribution in 2017 and 2018, acc. Annual reports, PwC analysis. 2019 PwC's *Mine*

As we have already mentioned from the beginning of this article, there are expected for miners to learn from digital and Industry 4.0 and to develop a modern, sustainable and safety mining, in order *to change consumer sentiment* (2019 PwC's *Mine*). It is discussed about building a culture of innovation in mining, about technology in the context of the whole supply chain. For example, Rio Tinto and Alcoa formed a new venture with Apple to create the world's first carbon-free aluminium smelting process. RCS Global has partnered with a number of organizations to use blockchain technology to trace and validate ethically sourced cobalt. Such efforts could include coal companies investing in technologies for carbon capture and storage (as coal contributes 38% to global electricity generation), or platinum group metal (PGM) miners working on the commercialization of hydrogen fuel cells. A **2018** study by PwC's Global Digital Impact Centre found that companies who achieve digital technology earn higher revenues and lower their costs over time (2019 PwC's *Mine*).

Copper, coal and iron ore were the main commodities of the **2018** Top 40 in terms of revenue (Fig. 16). The price of copper upped 6%, revenue upped 12%. Over half of the Top 40 produced 55% of global copper production, both as primary or as by- or co-product. Despite that year after year copper production grew approx. with 7% for the Top, a decline in production is expected in the future, as declining grades and higher costs. For the coal, the price upped 21%, revenue upped 12%: the difference between revenue and price growth is explained by coal offtake agreements, which are not at spot. *The IEA, Coal 2018* forecasts highlighted that the coal demand will continue in the near to medium term, due to above average economic growth in China, India and South East Asia. In the long term, renewable energy will reshape the energy mix, and coal consumption is expected to plateau from 2023. In 2018, the price of iron ore downed 3% (Fig. 12), because the increase in iron ore production caught up with demand. Top 40 productions of iron ore increased due to Australian

Fig. 16. Top 40 revenue-based commodities in 2018 and 2019, acc. Annual reports, PwC analysis. 2020 PwC's *Mine*

and Brazilian producers, explaining why revenue upped 2%. The increase of transactions (M&A) in **2018** was driven by the gold sector, coal, but also by securing supply of battery metals. Gold transactions increased from 8% of the total Top 40 deal value in 2017 to 25% in 2018, meaning with $7 billion, and with $14 billion so far in 2019. Barrick Gold. Corp. merged with Randgold Resources ($6.5 billion) *to create industry-leading gold company with the greatest concentration of Tier One Gold Assets in the*

industry (https://www.barrick.com/news/news-details/2018/Barrick-and-Randgold-Combine-to-Create-Industry-Leading-Gold-investment-Vehicle/ default.aspx). Freeport and Rio Tinto sold for $3.9 billion a portion of the Grasberg Mine to Indonesia Asahan Aluminium (Persero), because of Indonesia's divestment regulations. $4.1 billion was the Tianqui's acquisition of 24% in Sociedad Química y Minera de Chile S.A. from Nutrien Ltd, to secure enough raw materials for China's push for lithium (2019 PwC's *Mine*).

The **2018** Top 5 is the same as in 2016 and 2017, including in terms of hierarchy, and as in 2019, excepting the hierarchy of the last three participants: BHP Group Ltd. Australia/UK, Rio Tinto Ltd. Australia/UK, Glencore plc/Switzerland, China Shenhua Energy Company Limited, and Vale S.A./Brazil. The top 5 made up 50% of total 2018 Top 40 market capitalization, including 22 *traditional* companies (*i.e.*, OECD's companies, Mexic, South Africa), 16 emerging companies (10 from China and China/Hong Kong, with China Molybdenum Co. Ltd. rank 11, Tianqi Lithium Industries, Inc. rank 33 and China Northern Rare Earth rank 37 among them), MMC Norilsk Nickel rank 6, Alrosa rank 31, Coal India Ltd. rank 10, Saudi Arabian Mining Co. (Ma'aden) rank 15, and KGHM Polska Miedz Spólka Akcyjna rank 39, *etc.*), one new entry from Indonesia (PT Bayan Resources Tbk), and one new entry from Russia/UK (Polymetal International plc). The dominance of Top 40 gold companies increased to ten, coal companies increased to six and *diversifieds* still accounted for 13. There were three new gold entrants: Kirkland Lake Gold Ltd, AngloGold Ashanti Ltd. and Polymetal International plc. Together with PT Bayan Resources Tbk. (coal), they replaced Potash Corp. (who had just become part of Nutrien), Randgold Resources (which merged with Barrick Gold Corp.), National Mineral Development Corp., and KAZ Minerals.

1.5. Confirmed expectations in 2019. *Speciality metals.* **The rise of gold**

There were great expectations from **2019**, in terms of mining evolution. For the most part, they have been confirmed: faced to prior year, revenue upped 4% to $692 billion, largely a result of rising commodity prices (Fig. 12), EBITDA flatted at $168 billion, PBT (profit before tax) downed 11% to $89 billion, dividends paid up 25% to $55 billion, market capitalization upped 19% to $898 billion, capex upped 11% to $61 billion (Fig. 10). Free cash flows declined marginally as a result of increased investment in capital expenditure, from $80 billion to $69 billion (2020 PwC's *Mine*). So, solid financial performance and prudent capital expenditure were acquired in 2019, allowing the world's Top 40 miners to face the deep and unforeseen crisis caused by the pandemic with Covid-19.

Coal's contribution to Top 40's revenue remained steady over 2019, while iron ore grew of approx. $130/tonne. However, the tragic tailings dam collapse at Brumadinho has cut back supply in the first half of 2019. Also the US-China trade war continued to disturb commodity demands. Both these events, together with ongoing cost pressures and asset impairments totalizing $14 billion, including the Rio Tinto's $3.5 billion write-down on the Oyu Tolgoi copper project, contributed to lower profitability of Top 40. Consequently, revenue gained did not translate into PBT, which declined in aggregate by 11% over 2018 to 2019. Working capital level has decreased by $4 billion compared to 2018. An interesting economic parameter is operating expenses, which increased with 5% over 2018 to 2019, but decreased with 6% over 2019 to 2020. At the end of 2019, the Top 40 had $88 billion in cash holdings and gearing of 31% (2020 PwC's *Mine*).

During **2019**, Newmont acquisition of Goldcorp *Inc.* was a 13.1 billion business. Following Barrick Gold's acquisition of Randgold Resources the number of notable transactions has risen, including Northern Star and Saracen acquiring Barrick and Newmont's Kalgoorlie operations, Kirkland Lake's proposal to buy Detour Gold and Evolution Mining acquiring the Red Lake gold complex from Newmont Goldcorp. (http://www.bakersteelglobalfunds.com/wp-content/uploads/2020/01/The-Natural-Resources-Sector-in-2020-Baker-Steel-January-2020.pdf). Investor sentiment towards gold has been improving gradually, since its price reached its cyclical low in 2015 (Fig. 17). The enterprise value of mega gold deals was $19.2 billion at the end of December 2019 (June 2020 PwC's *Mine*). Investors have returned to gold because of demand for portfolio diversification (*gold is an effective portfolio diversifier*), strong equity market gains, low volatility and historically low bond yields (http://www.bakersteelglobalfunds.com/wp-content/uploads/2020/01/The-Natural-Resources-Sector-in-2020-Baker-Steel-January-2020.pdf).

The gold prices have risen over to 2018 to 2019, and mainly over 2019 to 2020 and during 2020, but gold deals were less frequent with 33% in 2020, in comparison with 2019, in terms of the first four months of every year. Gold miners have learned from the 2010's mistakes, *trying to avoid the pitfalls of pursuing large cash and debt-backed deals in a rising price environment* (quoted from 2020 PwC's *Mine*). In the context of improving macroeconomic factors and market conditions for the precious metals sector, both gold and silver appeared to outperform during 2020 (Fig. 18, 19): *2019 has seen gold and the dollar rally together. We expect to see a mixed conditions for the dollar in 2020 and potentially a rise in volatility*

driven by the impeachment proceedings and Presidential Election, as well as a continuation of the geopolitical tension and trade confrontation which has been such a dominant theme of recent years (quoted from http://www.bakersteelglobalfunds.com/wp-content/uploads/2020/01/The-Natural-Resources-Sector-in-2020-Baker-Steel-January-2020.pdf).

Fig. 17. Thirty year gold price history https://goldprice.org/gold-price-history.html

Fig. 18. Gold and the US dollar rise during 2019   **Fig. 19.** Gold/silver ratio since 1997 to 2020
(both figs. acc. to Bloomberg, 2019 December 31. http://www.bakersteelglobalfunds.com/wp-content/uploads/2020/01/The-Natural-Resources-Sector-in-2020-Baker-Steel-January-2020.pdf)

Another long-term outlook which appeared much brighter after 2019 is about the so-called *speciality metals* (Fig. 20), involved in the development of new technologies, electric vehicles (EVs), battery and in the adoption of green energy. The most performing was the PGMs group, especially palladium, which benefitted from continued strong support of South African mining policy, and nickel, whose prices gained significantly due to record low inventories and concerns over restricted supply from Indonesia. On the other hand, vanadium, lithium, cobalt and graphite faced driven declined. For example, the lower than expected demands a result of Chinese EVs subsidy cuts together with oversupply from loss-making Australian mines have weaken the lithium market. But 2020 appeared positive as demand picks up due to rising European EVs sales. Also battery-related metals, especially lithium and cobalt, saw rapid price gains since 2015, followed by oversupply and declined demands (Fig. 21).

The **2019** Top 40 had 12 companies in precious metals, coal companies decreased to five and *diversifieds* still accounted for 13. Speaking of Top 5, who made up 45% of total Top 40 revenue, is the same since 2016 in terms of participants, but with Vale rising two ranks and Glencore and China Shenhua Energy descending one rank: BHP Group Ltd. Australia/UK, Rio Tinto Ltd. Australia/UK, Vale S.A./Brazil, Glencore plc/Switzerland, and China Shenhua Energy Company Limited. The Top included 23 *traditional* companies (OECD's + Mexico + South Africa) and 16 from emerging countries (9 from China and Hong Kong, 3 from Russia, 2 from India, one from Brazil and one from Saudi Arabia). The four new entrants in the Top (Hindustan Zinc/India, Impala Platinum and Sibanye Stillwater/South Africa, and

Kinross Gold/Canada) replaced companies whose market capitalizations have declined in 2019: Goldcorp (acquired by Newmont), PT Bayan Resources Tbk. (coal), KGHM Polska Miedz Spólka Akcyjna (copper) and China Northern Rare Earth (Group) High-Tech Co. Ltd.
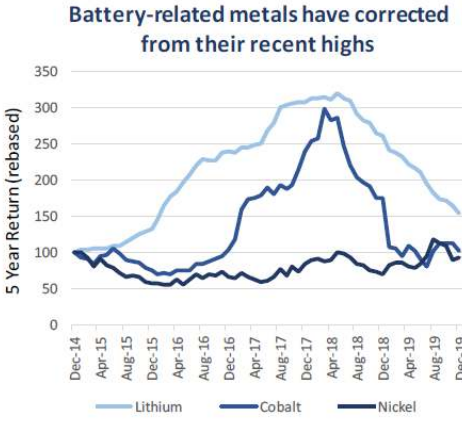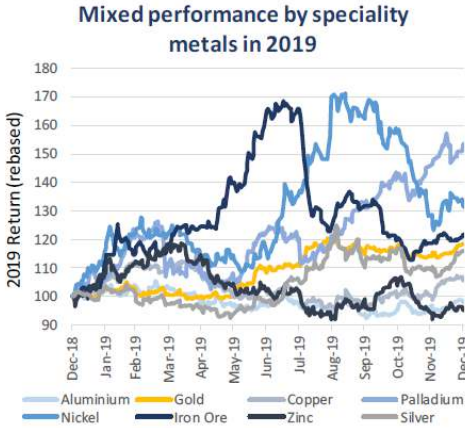
Fig. 20. *Speciality metals* return in 2019   **Fig. 21.** Battery-related metals' return over last 5 years (both figs. acc. to Bloomberg, 2019 December 31, http://www.bakersteelglobalfunds.com/wp-content/uploads/2020/01/The-Natural-Resources-Sector-in-2020-Baker-Steel-January-2020.pdf

The investor sentiment and concerns over global economic growth will be accentuated in 2020, as far as uncertainness over the US − China trade war and geopolitical tension globally. The recovery of mining industry from the past few years of unfulfillments has been unexpected slow. There are warehouse inventories to industrial metals still undervalued and lagged behind general equity markets over 2015 (http://www.bakersteelglobalfunds.com/wp-content/uploads/2020/01/The-Natural-Resources-Sector-in-2020-Baker-Steel-January-2020.pdf).

2. A strong outlook for metals and miners in 2020

That is the conclusion of the Baker Steel's Investment Team in January 2020. Looking to the June 2020 PwC's *Mine* (Fig. 22), it is anticipated that the 6% fall in revenue and also in EBITDA will reach to $649 billion, and to $157 billion respectively, until December 2020. Cash flow from operations was forecast with reference to EBITDA, with no material movement in working capital expected by the end of 2020. Investing cash flows include capex, which is expected to reduce approx. 20%. The report recommended that miners should prioritize production over capital spending in 2020, because it will be difficult to mobilize and procure labour and equipment to remote sites safely in the pandemic context. IMF has predicted a 3% global contraction in 2020, meaning a serious negative impact on economy worldwide.

3. Keep operating through the COVID-19 crisis

As it is known, mining has managed to continue to operate through the COVID-19 crisis, with the hope that the Top 40 will be relatively moderate affected until the end of 2020. The June 2020 PwC's *Mine* mentioned that more than $380 million had been pledged by the Top 40 for COVID-19 relief. Certain input costs were foreseen to decline (*e.g.,* fuel), but they were offset by higher operating costs (remote workforces, monitoring and controlling operations from outside the mine site setting), expected rather to arise because of social distancing measures and stay-at-home orders for people who were unable to work.

A global mining revenue reduction in the first half of 2020 was driven by falling prices, especially to thermal coal and copper, whose contribution was over $20 billion. Copper, nickel, and zinc prices have fallen by double-digit percentage points since December 2019 until the middle of this year (June 2020 PwC's *Mine*). Conversely, the gold price rose continuously during 2020: gold futures for April delivery jumped as much as 1.9% to $1,704.30/oz, the highest for a most-active contract since December 2012 (https://www.mining.com/web/gold-slides-below-1700-as-investors-look-everywhere-for-cash/). Some analysts expect gold to keep climbing, giving to miners the advantage of the recovery of share price in first half of 2020 (*e.g.,* Newcrest announced in May A$1 billion capital rise, acc. June 2020 PwC's *Mine*). In this way, new gold projects could be approved. For example, in March 2020 the US Bureau of Land Management accepted West Kirkland Mining's mine plan of operation for the Hasbrouck gold project in Nevada (https://www.mining.com/hasbrouck-gold-projects-operation-plan-approved/). In December 2020,

Fig. 22. 2020 Top 40 financial performance. June 2020 PwC's *Mine*

US$bn	2020 outlook	2019	2018	% change 2019 to 2020	% change 2018 to 2019
Revenue	649	692	667	-6%	4%
Operating expenses	(484)	(515)	(491)	-6%	5%
Other operating income/(expenses)	(8)	(9)	(7)	-13%	33%
EBITDA	**157**	**168**	**169**	**-6%**	**-1%**
Depreciation and amortisation	(55)	(50)	(47)	9%	8%
Impairment reversal/(expense)	(14)	(14)	(9)	3%	53%
Net finance costs	(14)	(14)	(13)	-2%	12%
Profit before tax	**75**	**89**	**100**	**-17%**	**-11%**
Income tax expense	(23)	(29)	(26)	-19%	9%
Net profit	**51**	**61**	**74**	**-15%**	**-18%**
Profitability measures					
EBITDA margin	24%	24%	25%		
Net profit margin	8%	9%	11%		
Return on capital employed		11%	10%		
Return on equity		11%	14%		

Kirkland Lake announced its largest exploration program since acquiring the Fosterville mine (Australia) in 2016: the 2021 exploration will follow up on existing drill results that included the intersection of quartz with visible gold, found in large concentrations and at exceptional grades in multiple locations (https://www.mining.com/kirkland-lake-sets-1-3-1-4-moz-production-target-for-2021/).

Barrick Gold notified in March **2020** (https://www.mining.com/barrick-boosts-inventory-of-key-commodities-due-to-coronavirus/) that it was increasing its inventory of *key commodities* to above normal levels in response to the global spread of coronavirus. The world's second-largest gold miner mentioned that *placed and forecast orders remain unchanged and supplies to mines have not been affected*. For the gold miners, their companies were more able to execute deals, but also were in greater demand: *e.g.,* in June 2020 (https://www.whitecase.com/publications/insight/mining-metals-covid-19-world-underlying-resilience-masks-esg-concerns), Zijin Mining agreed to buy Guyana Goldfields to expand its mining portfolio, and South Africa's top gold miner, Harmony Gold, agreed to purchase AngloGold Ashanti's operations in the country.

Iron ore miners achieved record production levels throughout the global lockdown, holding above $80/tonne. Despite uncertainty regarding Brazil mining in 2020, iron ore prices have risen (Fig. 23), recording US$100/tonne in June, and allowing the sector to revert. On December 18, iron ore traded at the highest level since October 2011, upped 78% in 2020 (https://www.mining.com/iron-ore-price-leaps-to-highest-since-2011/).

In terms of 2020 production, weaker results in diamonds and thermal coal were mostly offset by increases in copper and iron ore, resulting in minimal net impact over global production value (June 2020 PwC's *Mine*). According De Beers, the world's top diamond producer by value, the rough diamond production decrease by 5% to 8.7 million carats in the quarter ended Sept. 30. In December 2020, Anglo American reported that it will divest from its South African and Colombian thermal coal operations by mid-2023. The global miner said that a de-merger and listing on the Johannesburg Stock Exchange was the solution for its South African thermal coal assets, which include three mines, Goedehoop, Greenside, and Khwezela (https://www.mining.com/anglo-american-to-divest-from-thermal-coal-operations-by-2023/). In Colombia, Anglo American focused on Cerrejon, one of Colombia's biggest coal producers, as also BHP Group and Glencore did. Colombia is the fifth-largest coal exporter the world, and coal is the country's second top source of foreign exchange after oil (https://www.mining.com/web/coal-miner-cerrejon-union-fail-to-reach-agreement/). Iron ore markets have growth *due to a combination of unprecedented demand from China, which has embarked on a massive infrastructure build-out to stimulate the economy post-pandemic and worries about supply from Brazil and Australia* (https://www.mining.com/iron-ore-price-goes-parabolic-after-cyclone-warning/).
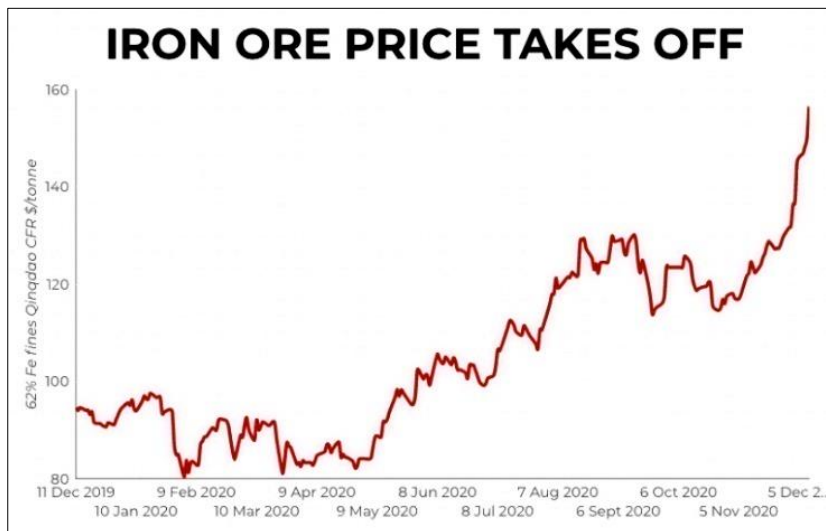
Fig. 23. The iron price evolution during 2020 (https://www.mining.com/iron-ore-price-goes-parabolic-after-cyclone-warning/)

Following the increase of Chinese and Indian demands, also expected in 2021, Rio Tinto and Fortescue announced that they maintain their outlooks on iron ore productions during 2020 (June 2020 PwC's *Mine*). Updating: according to Fastmarkets MB, benchmark 62% Fe fines imported into Northern China (CFR Qingdao) were for $164.39/ tonne on December 18, 2020, upped nearly 4% from prior day (https://www.mining.com/iron-ore-price-leaps-to-highest-since-2011/).

As Bloomberg analysis referring to December 2020, *copper-market cocktail means miners have rarely had it so good (…) copper reaches seven-year highs, currencies in major producing nations tumble, and low oil prices keep a lid on costs.*
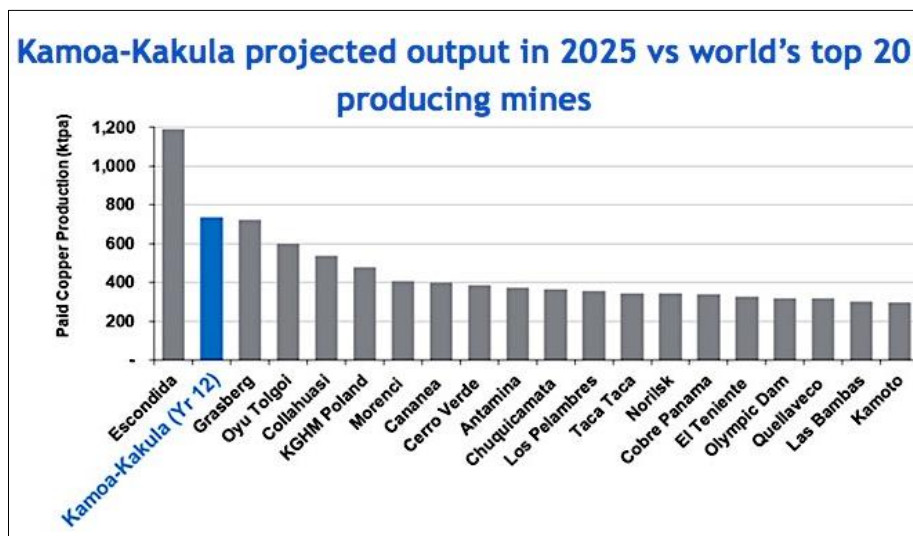
Fig. 24. The world's top 20 copper producing mines in 2025 (https://www.mining.com/ivanhoe-hails-progress-at-kamoa-kakula-platreef/)

An unusual combination of falling costs and rising prices allowed by the pandemic situation yielded Glencore the biggest dollar margin since it started releasing breakdowns in 2017, and possibly the highest since its takeover of Xstrata in 2013. Freeport-McMoRan, the world's largest listed copperminer and a top gold producer, has jumped almost 90% in 2020, after almost a decade of largely downbeat investor appraisal. Also it was announced a further 60% gain for First Quantum Minerals, following its 55% advance in 2020. An opposite situation happened in Chile, where copper prices were traded at record highs in local-currency terms, and miners wanted to get a share of the Antofagasta profits (https://www.mining.com/web/copper-market-cocktail-means-miners-have-rarely-had-it-so-good/).

In March 2020, Ivanhoe Mines/Canada informed that progress at its Kakula copper project, the first of multiple mining areas Kamoa-Kakula in the DRC, continues to move forward, with production slated for the third quarter of 2021. Being developed in partnership with China's Zijin Mining Group, Kamoa-Kakula would become the world's second-largest copper mine in 2025 (Fig. 24). The pre-feasibility study

(PFS) released in 2019 stated that the operation is expected to reach annual production of more than 700,000 tonnes of copper (https://www.mining.com/ivanhoe-hails-progress-at-kamoa-kakula-platreef/).

Dividends paid remain flat in 2020, with more liquidity offset by companies. If Glencore, Freeport − McMoRan and Sumimoto Metal Mining/Japan have already announced deferrals or reductions of declared dividends, others have so far increased dividends, such as Newmont (up 75%) and Kirkland Lake Gold (doubled) (June 2020 PwC's *Mine*).

Continuing the 2019 trend, in the first four months of 2020 the deal activity in gold fell by 33% compared to the same period of the prior year. The main deals of the global mining sector until June 2020 were the SSR Mining Inc./Canada (formerly Silver Standard Resources) merger with Alacer Gold Corp. (from Turkey) (effective in September 2020, acc. https://www.linkedin.com/company/alacer-gold-corporation), the Anglo American acquisition of fertilizer development company Sirius Minerals, and the A-Properti (from Russia) acquisition of the Elgaugol Coal Project (Elgaugol, a subsidiary of the Russian mining and steel, acc. https://www.nsenergybusiness.com/projects/elga-coal-complex/). Anglo American said that production across all minerals will increase by 14% in 2021, unit costs are expected to fall by 3%, and capital expenditure would be between $5.7 billion and $6.2 billion next year, reflecting deferred 2020 spending and new investments (https://www.mining.com/anglo-american-to-divest-from-thermal-coal-operations-by-2023/).

In December 2020, nickel-gold miner IGO Ltd acquired a 49% interest in Tianqi Lithium Energy Australia, which controls Greenbushes − the world's biggest hard-rock lithium mine, located about 250 km from Perth. The deal, which needs the approval of the Australian Foreign Investment Review Board, was presented to Tianqi shareholders on January 5, 2021. US-based lithium giant Albemarle holds a 49% stake in Talison Lithium, a partnership with Tianqi that operates Greenbushes mine. So, it is believed that the company have some form of pre-emptive rights over the project. Tianqi would use the proceeds from the deal with IGO to repay the $1.2 billion on a loan taken out 2018 to partially fund the acquisition of a 25% stake in Chilean miner SQM for $4.1 billion (https://www.mining.com/tianqi-lithium-sells-49-of-australian-unit-to-igo-in-1-4bn-deal/).

The most active movers in 2020 Top 40 were Fortescue Metals Group Ltd./Australia (iron ore) which rose 15 places to rank 10, and Mosaic Company/US (potash) which dropped 15 places to rank 32 (June 2020 PwC's *Mine*). The 2020 Top 3 in June is identical with those of prior year: BHP Group Ltd. Australia/UK, Rio Tinto Ltd. Australia/UK, Vale S.A./Brazil. Glencore dropped two places to rank 6, China Shenhua Energy and MMC Norilsk Nickel climbed one place to rank 5. The Top included 23 *traditional* companies (OECD's + Mexico + South Africa) and 16 companies from emerging countries (nine from China and Hong Kong, three from Russia, two from India, one from Brazil and one from Saudi Arabia).

4. Challenges in 2020 mining and beyond. A culture of involvement during the pandemic

Relatively frequent warnings referring to risks in mining industry are recorded since 2017 in all PwC' reports (Fig. 25). In South Africa for example, the perception about mining sector had been very subdued on the back of regulatory change − in particular the new version of Mining Charter, where the industry had termed as *sunset industry*. However, following consultations with industry, labour and mining communities, a revised version of the Charter had issued in September 2018. Re-emphasizing the role of mining as key to the future growth of the South African economy, President Ramaphosa stated his commitment *to prioritizing the restoration of a stable and predictable policy environment to ensure the realization of this potential*. Against this background, and based on three new investment projects totaling US$20 billion announced in October 2018 (https://www.pwc.co.tz/press-room/south-africa-mining.html), he claimed that South Africa's mining sector should be described not as *a sunset industry,* but *a sunrise industry*.

There are enough challenges in front of Top 40 actors of global mining industry: declining ore grades that make metals more costly to extract, declining exploration investment, that has already dropped 10% in 2020, acc. Bloomberg News (https://www.mining.com/web/copper-market-cocktail-means-miners-have-rarely-had-it-so-good/), declining in confidence if miners can capitalize further by increasing production, and the eternal story of environment negative impact.

Additionally, the Top 40 has continued to keep as major concern in 2019 and in 2020, at least in the pre-COVID period, the cybersecurity. If in 2018 21% of mining companies' CEO's were extremely concerned about cyber, their percentage dropped in 2019 at 14%, and in 2020 at just 12% (2020 PwC's *Mine*). Recently for example, because of environmental concerns, Chile's Environmental Court has finally pronounced in the coffin for Barrick Gold's giant Pascua − Lama gold-silver project, which had been on
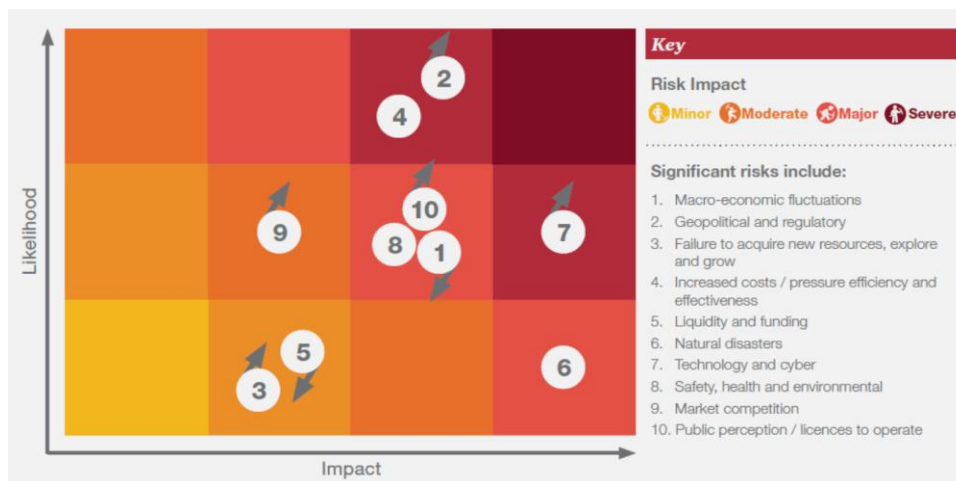
Fig. 25. Risks and uncertainties in mining, acc. PwC Analysis and Top 40 Annual reports. 2018 PwC's *Mine*

hold since 2013 (https://www.mining.com/chile-court-orders-total-and-definitive-closure-of-barricks-pascua-lama/). The world's no.1 iron ore producer Vale closely monitoring its Gongo Soco mine, in the southeastern Brazilian state of Minas Gerais, at almost two years after the collapse of a tailings dam belonging to the company's Córrego do Feijão mine in the town of Brumadinho, which killed more than 250 people (https://www.mining.com/vale-watching-gongo-soco-mine-as-wall-continues-to-erode/).

Another fear regards the China's rare earth element export policy amid its protracted trade war with the United States. After the US was launching sanctions against Chinese technology companies and threatening to punish Chinese financial institutions, some voices in China were asking countermeasures by restricting rare earth exports to the US. China's rare earth exports to the United States dropped 35.2% from 2019 to 5,184 tonnes in the first half of 2020, as reported the China Rare Earth Industry Association. The gap widened even more in July 2020, when China exported 1,620 tonnes of rare earth elements, a drop of 69.1% from a year earlier, and down 44% from June 2020. According to South China Morning Post from August 18, 2020, the deputy general secretary at the China Rare Earth Industry Association blamed pandemic, which led to weak external demand, also for rare earth minerals (https://www.scmp.com/economy/china-economy/article/3097847/chinas-rare-earth-export-plunge-caused-coronavirus-not).

Some important mining companies draw down additional credit lines to sustain their cash reserves during pandemic and post-pandemic growth strategies, as Vale ($ 5 billion), Agnico Eagle ($ 1 billion) and Kinross ($0.8 billion). Additionally, others have developed strategies to build resilience in local communities and support their needs because of the pandemic, as Anglo American, Nornickel and BHP (June 2020 Pwc's *Mine*). It seems therefore that the global mining sector can generate a culture of involvement during the pandemic through significant financial and human resources. In this respect, the Minerals Council of South Africa had decided that companies have to financial support employee education and health, and Indian companies have repurposed their medical facilities to treat Covid-19 patients. As of April 6, 2020, ALROSA and its CEO have provided financing to counter a spread of Covid-19 to the miner's main operations and headquarters in Mirny and Lensk districts, the Republic of Sakha (Yakutia) (http://eng.alrosa.ru/alrosa-and-its-management-join-efforts-to-support-local-communities-in-yakutia-against-covid-19/).

Conclusions

After an encouraging start to 2020, the global economy has been hit by the coronavirus pandemic. The global mining sector came under severe pressure of strong decline for raw materials in the early stages of the pandemic, without any strategy for regaining confidence. Several mines around the world were forced to slow or temporarily close their mining operations, as governments sought to contain the spread of the virus. Rio Tinto and BHP Group announces plans to review or lower capital spending, halting development projects to maximize cash, while Glencore reduces its capex forecast for the year by up to US$1.5 billion. In July 13, 2020 White&Case notified that *the world's biggest miners have been comparatively unscathed by the pandemic, given demand from China has held up and the most important mines continued to operate.* Indeed, *several major provinces in China announced plans to build or restart approx. $3.6 trillion of infrastructure projects in 2021.* That is why the percentage of generalist investors to remain wary of the mining industry downed from 36 to only 13% in mid-year

(https://www.whitecase.com/publications/insight/mining-metals-covid-19-world-underlying-resilience-masks-esg-concerns).

The future post-pandemic strategies have to focus on some priorities, such as those presented in Fig. 26. The major to severe risk impact in 2018 of the increased costs and cybersecurity (Fig. 25) was offset by other considerations. As expected, they are quite different from the pre-pandemic period, building resilience being the most important (27%), probably in connection with Environmental, Social and Governance (ESG) policies (13%), integrated into investment analysis and portfolio construction for offering investors potential long-term performance advantages and growth. The following priorities, productivity and efficiency in mining industry, had in fact always been constantly worrying, as shown in all *Mine* reports, and are also found on the second place (18%) for the near future period. The mining projects for new resources, explore and grow have also their importance (13%). Climate change (7%) and safety health and environmental (5%) have a more modest relevance in comparison with 2018 (Fig. 25), when they were analysed as consequences of major risk impact of mining.
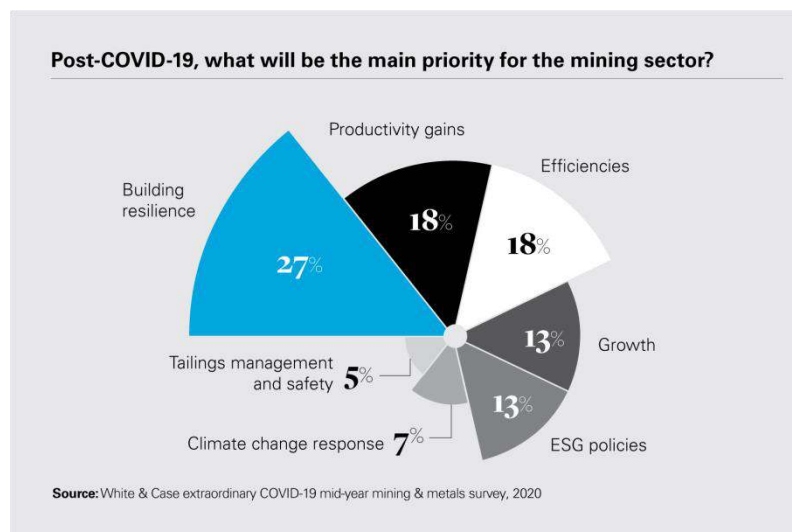
Fig. 26. The post-COVID-19 priorities for the mining sector, acc. White&Case mid-year mining & Metals Survey, 2020 (https://www.whitecase.com/publications/insight/mining-metals-covid-19-world-underlying-resilience-masks-esg-concerns).

According to woodmac.com editorial from July 2020, *we weren't expecting a global pandemic to shutter or disrupt nearly 80 gold mines around the world.* Maybe, but with a serious financial effort: $37 billion invested by 2025 to maintain the 2019 production level (https://www.woodmac.com/news/editorial/how-has-covid-19-changed-the-metals-and-mining-outlook/).

References

2016 PwC's *Mine.* https://www.pwc.com/gx/en/mining/pdf/mine-2016.pdf
2017 PwC's *Mine.* https://www.pwc.com/gx/en/mining/assets/mine-2017-pwc.pdf
2018 PwC's *Mine.* https://www.pwc.com/gx/en/mining/assets/pwc-mine-report-2018.pdf
2019 PwC's *Mine.* https://www.pwc.com/mx/es/publicaciones/archivo/2019/06/20190604-pwc-mx-mine-report- 2019.pdf
2020 PwC's *Mine.* https://www.pwc.com/gx/en/energy-utilities-mining/publications/pdf/pwc-mine-2020.pdf
Impunity Inc., 2012: Reflections of the super- rights and super – powers of corporate capital. https://www.tni.org/files/download/impunity_inc_0.pdf
https://www.scmp.com/economy/china-economy/article/3097847/chinas-rare-earth-export-plunge-caused- coronavirus-not
https://comtrade.un.org/data/
Mining Sector Performance Report 2006-2015. Energy and Mines Ministers' Conference Winnipeg, Manitoba, Aug. 2016. 67 p.

https://www.nrcan.gc.ca/sites/www.nrcan.gc.ca/files/mineralsmetals/pdf/mms-smm/MSRP_report_access_EN.pdf

White&Case, July 13, 2020. https://www.whitecase.com/publications/insight/mining-metals-covid-19-world-underlying-resilience-masks-esg-concerns

https://www.nsenergybusiness.com/features/six-largest-lithium-reserves-world

July 28, 2020 *Press Release:* Benchmark Mineral Intelligence. https://www.ewaste-expo.com/expect-to-pay-premiums-in-tighter-cobalt-spot-market-analyst-says/

https://www.arcgis.com/apps/Cascade/index.html?appid=3cedc4c7ef40422e9bbb1edbec5d83c6

https://www.worldbank.org/en/country/drc/overview

https://www.barrick.com/news/news-details/2018/Barrick-and-Randgold-Combine-to-Create-Industry-Leading-Gold-investment- Vehicle/default.aspx

Baker Steel's Investment Team, January 2020. http://www.bakersteelglobalfunds.com/wp-content/uploads/2020/01/The-Natural-Resources-Sector-in-2020-Baker-Steel-January-2020.pdf

https://www.mining.com/web/gold-slides-below-1700-as-investors-look-everywhere-for-cash/

https://www.mining.com/hasbrouck-gold-projects-operation-plan-approved/

https://www.mining.com/kirkland-lake-sets-1-3-1-4-moz-production-target-for-2021/

https://www.mining.com/barrick-boosts-inventory-of-key-commodities-due-to-coronavirus/

https://www.mining.com/iron-ore-price-leaps-to-highest-since-2011/

https://www.mining.com/anglo-american-to-divest-from-thermal-coal-operations-by-2023/).

https://www.mining.com/web/coal-miner-cerrejon-union-fail-to-reach-agreement/

https://www.mining.com/iron-ore-price-goes-parabolic-after-cyclone-warning/

https://www.mining.com/web/copper-market-cocktail-means-miners-have-rarely-had-it-so-good/

https://www.mining.com/ivanhoe-hails-progress-at-kamoa-kakula-platreef/

https://www.linkedin.com/company/alacer-gold-corporation

https://www.nsenergybusiness.com/projects/elga-coal-complex/

https://www.mining.com/anglo-american-to-divest-from-thermal-coal-operations-by-2023/

https://www.mining.com/tianqi-lithium-sells-49-of-australian-unit-to-igo-in-1-4bn-deal/

https://www.pwc.co.tz/press-room/south-africa-mining.html

https://www.mining.com/web/copper-market-cocktail-means-miners-have-rarely-had-it-so-good/

https://www.mining.com/chile-court-orders-total-and-definitive-closure-of-barricks-pascua-lama/

https://www.mining.com/vale-watching-gongo-soco-mine-as-wall-continues-to-erode/

https://www.scmp.com/economy/china-economy/article/3097847/chinas-rare-earth-export-plunge-caused-coronavirus-not

http://eng.alrosa.ru/alrosa-and-its-management-join-efforts-to-support-local-communities-in-yakutia-against-covid-19/

https://www.woodmac.com/news/editorial/how-has-covid-19-changed-the-metals-and-mining-outlook/

CONTENT

– continued from the front cover –